PARAMETRIC INVESTIGATION OF CATALYTIC DRY REFORMING OF GLYCEROL TO SYNTHESIS GAS

by

Pelin Su Bulutoğlu

B.S., Chemical Engineering, Boğaziçi University, 2015

Submitted to the Institute for Graduate Studies in
Science and Engineering in partial fulfillment of
the requirements for the degree of
Master of Science

Graduate Program in Chemical Engineering

Boğaziçi University

2017

ACKNOWLEDGEMENTS

I would like to express my deepest gratitude to my thesis supervisor, Prof. Ahmet Kerim Avcı. His guidance and support throughout my MSc studies is much appreciated. I consider myself lucky to have the opportunity to work with such a wise and considerate mentor.

I would also like to thank my thesis comittee, Prof. Ahmet Erhan Aksoylu and Prof. Ayşe Nilgün Akın for devoting their valuable time to read and comment on my thesis.

My special thanks go to members of KB-404, who made me feel like I am at my second home. I would like to thank Sinan Koç, who was always ready to help me by answering all my questions and sharing his valuable experiences with me. I am very happy to share a working environment with Hatice Merve Can, Amin Delparish, Selin Baç and Talha Ayar as well as former KB-404 members Begüm Koca and Özgür Yaşar Çağlar.

I am inexpressibly grateful for the friendship of Canberk Ozan, who has been there for me through my ups and downs. Thank you for the memories, these past two years would not have been the same without you.

I would like to express my special gratitude to Gizem Yumru and Ahmet Coşgun, members of the "grup". I cannot imagine my graduate years without you and the time outs we have taken together. I had so much fun with you. I would also like to thank İrem Teker for being such a good friend since the first days of my time in Boğaziçi.

Thanks to Tuğçe İlksoy, Doğa Fındık, Yiğit Ağanoğlu and Damla Üçkan for the good times. I learned so much about random things through the countless conversations. I will always be proud to order the kids' size!

A special gratitude goes to Cihat Öztepe, Ece Mutlu, Dilara Saadetnejad and all the design assistants whose names have been mentioned previously. It has been a pleasure and so much fun to work with them even at the toughest times of assistantship. I also would like to thank the members of CATREL team for their friendship and support.

I also want to thank Bilgi Dedeoğlu for the work he put into construction of my experimental system. Moreover, I appreciate the kindness of the departmental support staff Yakup Bal, Melike Gürbüz, Başak Ünen and Murat Düzgünoğlu.

Last but definitely not least, I would like to thank my family. This thesis would not have been possible without my parents, who were always by my side, whether it is to comfort me in my darkest times or to share my joy in my happiest. I also thank my brother, Fatoş and my little nephew Rüzgar, who brought joy to our lives in the past year.

Financial support provided by TÜBİTAK through project 113M962 is acknowledged.

ABSTRACT

PARAMETRIC INVESTIGATION OF CATALYTIC DRY REFORMING OF GLYCEROL TO SYNTHESIS GAS

Dry reforming of glycerol is a highly promising way for production of synthesis gas, as it involves catalytic conversion of CO_2, a greenhouse gas that hit threatening levels, with glycerol, which is a renewable hydrocarbon that is excessively available due to increasing bio-diesel production. The reaction has started to become the focus of experimental studies only recently, and there is still a huge lack of information in the literature regarding catalysis of glycerol dry reforming. In this study, it is aimed to test and compare the activities of Rh and Co based catalysts supported on ZrO_2 and CeO_2 in dry reforming conditions. It is also intended to observe the effects of two key operational parameters, namely temperature and CO_2-to-glycerol (CO_2/G) feed ratio, on reactant conversions and product distributions. 1 wt.% Rh/ZrO_2, 1 wt.% Rh/CeO_2, 5 wt.% Co/ZrO_2 and 5 wt.% Co/CeO_2 catalysts have been prepared and tested at temperatures between 600 and 750 °C and at CO_2/G ratios between 0 and 4. Characterizations of the prepared and spent catalysts were done by SEM and XRD analyses. At the studied conditions, activities of the tested catalysts were found to be decreasing in the order of Rh/ZrO_2 > Rh/CeO_2 > Co/ZrO_2 > Co/CeO_2. Rh was observed to be more active in CO_2 conversion and syngas production compared to Co. On the other hand, ZrO_2 supported catalysts were more selective towards H_2 and CO compared to CeO_2 supported catalysts. Blank tests showed glycerol conversion to some extent, suggesting that homogeneous glycerol decomposition takes place, especially at elevated temperatures. Positive effect of temperature on reactant conversions and syngas yields was also confirmed in the activity tests. Increasing the CO_2/G feed ratio resulted in inceased CO_2 conversions, but H_2 yields decreased with simultaneous increase in CO yields, which is attributed to reverse water gas shift reaction.

ÖZET

GLİSEROLÜN KURU REFORMLAMA REAKSİYONUYLA SENTEZ GAZINA DÖNÜŞÜMÜ ÜZERİNE PARAMETRİK ÇALIŞMA

Gliserolün kuru reformlama reaksiyonu; artan biodizel üretimi nedeniyle fazlaca bulunan gliserolü, atmosferde tehdit edici seviyelere ulaşmış bir sera gazı olan CO_2 ile dönüştürmesi nedeniyle sentez gazı üretimi için avantajlı bir yoldur. Reaksiyon, deneysel çalışmaların odağı olmaya yakın zamanda başlamıştır ve literatürde bu reaksiyonun katalizine dair hala büyük bir bilgi eksikliği bulunmaktadır. Bu çalışmada, ZrO_2 ve CeO_2 destekli Rh ve Co bazlı katalizörlerin aktivitelerinin gliserol kuru reformlama koşullarında test edilmesi ve karşılaştırılması amaçlanmıştır. Bunun yanı sıra, iki önemli parametrenin de (reaksiyon sıcaklığı ve CO_2-gliserol-oranı (CO_2/G)) tepken dönüşümü ve ürün dağılımına etkisi incelenmiştir. 1% Rh/ZrO_2, 1% Rh/CeO_2, 5% Co/ZrO_2 and 5% Co/CeO_2 katalizörler hazırlanmış ve 600-750 °C sıcaklıkta ve 0-4 CO_2/G oranlarında denenmiştir. Hazırlanmış ve harcanmış katalizörlerin karakterizasyonları SEM ve XRD analiz yöntemleriyle yapılmıştır. Çalışılan koşullarda katalizörlerin aktivitelerinin Rh/ZrO_2 > Rh/CeO_2 > Co/ZrO_2 > Co/CeO_2 sırasında azaldığı gözlemlenmiştir. Rodyumun kobalta göre CO_2 dönüşümü ve sentez gazı üretimi açısından daha aktif olduğu görülmüştür. Öte yandan, ZrO_2 ile desteklenen katalizörlerin CeO_2 ile desteklenenlere göre H_2 ve CO'ya karşı daha seçici olduğu sonucuna varılmıştır. Boş deneylerin belli miktarda gliserol dönüşümü göstermesi, gliserol parçalanmasının özellikle yüksek sıcaklıklarda homojen olarak gerçekleştiğine işaret etmektedir. Sıcaklığın tepken dönüşümlerine ve sentez gazı üretimine olan pozitif etkisi aktivite deneylerinde de gözlemlenmiştir. CO_2/G besleme oranındaki artış CO_2 dönüşümünde artış sağlamıştır. Bu durum, H_2 üretimindeki azalma ve CO üretimindeki artışın görülmesiyle birlikte ters su-gaz değişimi reaksiyonuna bağlanmıştır.

TABLE OF CONTENTS

LIST OF FIGURES

LIST OF TABLES

LIST OF SYMBOLS

A	Exponential factor
$d_{particle}$	Diameter of particle (mm)
d_{tube}	Diameter of tube (mm)
E_a	Activation energy (kJ mol^{-1})
F	Total volumetric flow rate (ml min^{-1})
F_i	Molar flow rate of species i (mol min^{-1})
K	Crystallite shape factor
L_{bed}	Length of bed (mm)
r_g	Glycerol consumption rate (mol g^{-1} s^{-1})
S_i	Selectivity of species i
T	Temperature ($^\circ$C)
W	Catalyst weight (mg)
X	Conversion
Y_i	Yield of species i
β	Full width at half maximum
γ	Reaction order with respect to glycerol
ΔH^0	Standard enthalpy of reaction (kJ mol^{-1})
θ	Bragg angle (rad)
λ	Wavelength of x-ray (Å)
τ	Average crystallite size (Å)
ϕ	Reaction order with respect to CO_2

LIST OF ACRONYMS/ABBREVIATIONS

BET	Brauner-Emmett-Teller
BJH	Barrett-Joyner-Halenda
DRE	Dry reforming of ethanol
EtOH	Ethanol
FWHM	Full width at half maximum
GC	Gas chromatograph
GDR	Glycerol dry reforming
GSR	Glycerol steam reforming
HPLC	High performance liquid chromatograph
MDR	Methane dry reforming
MFC	Mass flow controller
MSR	Methane steam reforming
PID	Proportional integral derivative
RWGS	Reverse water gas shift
SEM	Scanning electron microscopy
SRE	Steam reforming of ethanol
TEM	Transmission electron microscopy
TPD	Temperature programmed desorption
TPO	Temperature programmed oxidation
WGS	Water-gas shift

1. INTRODUCTION

With the increasing population and growing industries, the energy demand of the world is increasing continuously. Currently, a majority of the world energy demand is met by fossil fuels such as crude oil, coal and natural gas; with a consumption that accounts for 80% of total energy consumption [1]. However, there are two major drawbacks associated with fossil fuels. Due to their limited reserves, fossil fuels are not sustainable, and consumption of fossil fuels leads to a considerable increase in the emission of CO_2, which is a greenhouse gas. Current CO_2 level in the atmosphere is reported to be 30% higher than it was in the pre-industrial era [2]. Due to these drawbacks, it has become urgent to find alternative, sustainable fuels/energy sources that can replace the conventional, fossil-based ones.

Among a number of sustainable fuels, biodiesel is a promising alternative energy source because it is a fuel derived from renewable feedstocks such as animal or plant based fats [3]. Production of biodiesel has increased over the years as it became a major substitute for fossil diesel due to environmental concerns. Since 2005, biodiesel market grew by 23% per year, which corresponds to a seven-fold expansion of the market in the last decade [4]. The main by-product of biodiesel production is glycerol, a colorless, odorless trihydric alcohol. About 100 kg of glycerol/ton of biodiesel can be produced during the synthesis of biodiesel [5]. Along with the steady growth in biodiesel production, it is projected that 3 megatons of crude glycerol will be generated by 2020, whereas yearly use of glycerol in commercial applications is expected to be around 500 kilotons [6]. Even though glycerol of high purity is an important feedstock for many applications in food, cosmetic, pharmaceuticals and other industries, purification of crude glycerol is expensive. This situation yields a great surplus of crude glycerol, which is why researchers have focused on valorization of crude glycerol in novel processes such as reforming for H_2 and syngas production [7].

H_2 is a promising energy carrier due to its high energy density and zero carbon emission resulting from its combustion [8]. Furthermore, use of synthesis gas (syn-

gas), a gas mixture that consists of H_2 and CO, in Fischer-Tropsch (FT) synthesis to produce a variety of hydrocarbons generates an important demand for H_2 [9]. Ammonia, methanol, synthetic fuels and chemicals, fertilizers, synthetic plastic etc. are important materials produced by the utilization of syngas [10]. Steam reforming, dry reforming, auto-thermal reforming and aqueous phase reforming are the main methods for generation of syngas from glycerol. Though steam reforming is the most commonly researched method, dry reforming has recently become the focus of attention, as it has the advantage of removing CO_2 from the biosphere cycle by converting it into syngas or high value added carbon [9].

Glycerol dry reforming (GDR) is an endothermic reaction where one mole of glycerol reacts with one mole of CO_2 to produce H_2, CO and H_2O as given in Equation 1.1:

$$C_3H_8O_3 + CO_2 \rightleftharpoons 4CO + 3H_2 + H_2O \qquad \Delta H^0 = 292 \text{ kJ mol}^{-1} \tag{1.1}$$

The endothermic nature of the reaction requires operation at high temperatures in order to achieve high conversion of reactants, especially of CO_2 [9]. However, glycerol is a thermally unstable compound that decomposes at elevated temperatures, which renders the reaction mechanism complex due to presence of many side reactions. Accompanying side reactions include glycerol decomposition, water-gas shift, methanation, carbon deposition and carbon gasification reactions. At high temperatures, carbon gasification and methane reforming reactions take place, leading to an increase in the yield of H_2 and a decrease in carbon deposition [11]. A syngas ratio (H_2/CO) of 0.75 can theoretically be produced by GDR, which is suitable for use in FT synthesis for production of long chain hydrocarbons, carbonyls and carboxylic acids [12].

Though steam reforming of glycerol has been studied extensively [3,6,13,14], the available information in the literature regarding catalysis of glycerol dry reforming is rather scarce. Ni, Co, Rh, Ru, and Pt are the prevailing active metals used in dry reforming reactions, whereas oxides such as Al_2O_3, CeO_2, ZrO_2 and SiO_2 are among commonly used supports. Glycerol reforming catalysts suffer from two deactivation

mechanisms, namely coke formation and sintering. Coke formation is a major obstacle in glycerol reforming processes, as glycerol can easily decompose into coke precursors. Synthesis of active catalysts that are also resistant to carbon formation as well as sintering is thus of great importance for glycerol dry reforming. In this study, it is aimed to contribute to the present knowledge on GDR catalysis by synthesizing and testing the activities of Rh and Co based catalysts supported on two reducible oxides (ZrO_2 and CeO_2) in glycerol dry reforming conditions. Effect of several operational parameters, namely operating temperature and molar composition of the feed, which may provide some insight into the reaction mechanism, is also aimed to be observed.

The present work consists of 5 chapters. In Chapter 2, previous studies on catalysis and thermodynamics of dry reforming of several feedstocks have been summarized, with an emphasis on glycerol reforming. In Chapter 3, details on the experimental setup, catalyst preparation and operating parameters of the experiments have been provided. In Chapter 4, results of the experimental study has been given along with an interpretation of the outcomes. Finally, Chapter 5 consists of the conclusions that have been drawn from the study and recommendations for further improvements of the present work.

2. LITERATURE SURVEY

Synthesis gas (or syngas), which is a mixture of H_2, CO and CO_2, is an important intermediate in the chemical industry, used in the production of a number of key chemicals. Apart from its use as a source of hydrogen, it is also used for the production of ammonia, methanol and higher alcohols, and synthetic fuels via Fischer-Tropsch synthesis [15]. A big portion of industrialized syngas production is based on methane or natural gas as feedstock but other hydrocarbons such as liquid hydrocarbons, methanol, ethanol and glycerol are also considered as alternative feedstocks [16].

The four main routes for syngas production are steam reforming, dry reforming, partial oxidation and autothermal reforming. Among these, steam reforming is the established process for converting hydrocarbons to syngas and has been used industrially for several decades [17]. Steam reforming of hydrocarbons, especially methane, has been researched extensively and is optimized in terms of catalysis and reactor configurations. Depending on the desired syngas ratio, steam reforming reaction can be coupled with partial oxidation and/or dry reforming [16].

With increasing environmental concerns regarding the emission of greenhouse gases, dry reforming reaction started to receive much attention as a way of utilizing CO_2. Extensive research has been done on dry reforming of methane and propane since 1993, whereas reforming of biomass and bio-derived oxygenates (such as ethanol, dimethyl ether and glycerol) has become the focus of attention in more recent years [18]. This section will be focused on the recent developments regarding dry reforming of hydrocarbons, with an emphasis on dry reforming of glycerol, which is the subject of this study.

2.1. Methane Dry Reforming

As mentioned before, methane is the prominent feedstock of dry reforming reaction for the production of hydrogen and syngas. According to Gao *et al.*, more than

1800 relevant papers have been published until 2010 [18]. A brief summary of the available literature will be provided here in order to give an insight about the reaction mechanism and catalysis regarding dry reforming of methane.

2.1.1. Thermodynamics

Dry reforming of methane is the catalytic reaction of CO_2 with methane to produce H_2 and CO, as given in Equation 2.1.

$$CH_4 + CO_2 \rightleftharpoons 2CO + 2H_2 \qquad \Delta H^0 = 247 \text{ kJ mol}^{-1} \tag{2.1}$$

This reversible reaction is highly endothermic, therefore, high operating temperatures are needed in order to achieve high conversions of methane [19]. As can be seen in Equation 2.1, the reaction inherently produces syngas with H_2/CO ratio of 1, but the presence of reverse water-gas shift (RWGS, Equation 2.2), the accompanying side reaction, reduces the ratio to values less than 1:

$$CO_2 + H_2 \rightleftharpoons CO + H_2O \qquad \Delta H^0 = 41 \text{ kJ mol}^{-1} \tag{2.2}$$

Other side reactions accompanying MDR are methane decomposition (Equation 2.3) and the Boudouard reaction (Equation 2.4), which are both responsible for deactivation of the catalyst due to carbon formation [19]:

$$CH_4 \rightleftharpoons 2H_2 + C(s) \qquad \Delta H^0 = 75 \text{ kJ mol}^{-1} \tag{2.3}$$

$$2CO \rightleftharpoons CO_2 + C(s) \qquad \Delta H^0 = -171 \text{ kJ mol}^{-1} \tag{2.4}$$

It is inferred from the standard free energies of Reactions 2.3 and 2.4 that carbon formation can occur due to methane decomposition at temperatures above 557 °C and due to Boudouard reaction at temperatures below 700 °C [19]. Thermodynamic analysis done by Nikoo *et al.* shows that at CO_2/CH_4 ratio of 1, carbon deposition is negligible at temperatures above 900 °C. A decrease in carbon deposition is also observed with

increased CO_2 ratio in the feed [20]. Increased CO_2 feed drives the Boudouard reaction backwards, especially when combined with high temperatures, which enables gasification of deposited carbon. Increasing the CO_2 ratio in the feed results in an increase in methane conversion as well, but a decrease in the yield of H_2 is observed, due to reverse water gas shift reaction. Presence of RWGS is confirmed with the simultaneous increase in CO and H_2O yields [18–20]. It is also reported that increase in pressure leads to a decrease in both methane and CO_2 conversions, and a subsequent decrease in syngas yield. This is expected considering that dry reforming reactions are volume expansion processes [18].

2.1.2. Catalysis

A glance over the literature about catalysis for methane dry reforming shows that Ni, Co, Rh, Ru, Pd and Pt are the most frequently used active metals. On the other hand, Al_2O_3, CeO_2, ZrO_2, MgO, SiO_2 are the supports that are studied the most [18, 21, 22]. Among the active metals, noble metals (Rh, Ru, Pd and Pt) have been proven to be active in MDR and more resistant to sintering and coke formation compared to non-noble metals [22]. This statement is confirmed by the work of Hou *et al.* [23], in which a variety of noble and non-noble metals (Ru, Rh, Pt, Pd, Ir, Ni and Co) supported on α-Al_2O_3 are tested for dry reforming of methane. Their findings show that noble metals (5 wt.% loading) showed lower catalytic activity compared to non-noble metals (10 wt.% loading), but they exhibited excellent coke resistance abilities, as no coke deposition were observed on the used catalysts. However, while the stability of Rh and Ir was higher than Ni and Co on 240 min time-on-stream, Ru, Pd and Pt exhibited significant deactivation, which the authors attributed to sintering of these metals [23]. Tsyganok *et al.* prepared various noble metal catalysts supported on Mg-Al mixed oxide and tested their activity for DRM. They concluded that Ru, Rh and Ir based catalysts had the highest activity, Ru being the most active with 95% CH_4 and 97% CO_2 conversion. 2 wt% $Ru/MgAl_2O_4$ exhibited high stability and very little coke formation after 50 h time on stream. The high activity and stability of the catalyst was attributed to high dispersion of Ru on support, which created fine metal

particles less than 1.5 nm in size, as revealed by TEM images [24].

Despite their high activities and coke resistance abilities, implication of noble metal based catalysts in the industry is not feasible due to their high cost. Nickel is a good alternative to noble metals due to its high activity, availability and low cost and is reported frequently for dry reforming of methane [18]. However, easy deactivation of Ni based catalysts due to carbon deposition and sintering renders it unsuitable for industrial application without any measures to increase its stability. Inevitable coke formation on nickel based catalysts supported on Al_2O_3, TiO_2 and SiO_2 is observed in the work of Ruckenstein and Hu [25]. Coke formation was observed on all supported catalysts with different loadings (1 wt.% and 13.6 wt.% loading) and the sequence of carbon deposition was $Ni/Al_2O_3 > Ni/SiO_2 > Ni/TiO_2$. Moreover, the authors reported highest CO yields with the presence of Ni/Al_2O_3, with slightly less yields on Ni/SiO_2. Activity of Ni/TiO_2 was significantly lower, which was attributed to migration of TiO_x molecules over Ni particles during reduction. It was suggested that this was a consequence of strong metal-support interaction [25].

Cobalt is another non-noble metal frequently tested for DRM, due to its availability and low cost. Ruckenstein and Wang [26] tested Co based catalysts supported on alkaline earth metal oxides (MgO, CaO, SrO and BaO) as well as on γ-Al_2O_3 and SiO_2 for dry reforming of methane. Among the tested supports, MgO showed the highest activity with a CO yield of 93% and a H_2 yield of 90%, without any deactivation after 50 h of time on stream. Other samples either deactivated or showed low activity. For example, γ-Al_2O_3 provided a high initial CO yield, but a rapid decay was observed afterwards. Amount of carbon deposited on MgO supported sample was much lower than SiO_2, Al_2O_3 and CaO samples. Solid solution of MgO and CoO was detected on this sample, which may have enhanced the interaction between Mg and Co and eventually avoided metal sintering and coke formation by generating small Co clusters [26].

Activity and stability of Ni based catalysts can be improved in various ways such as selecting the right support or preparation method. Another possible way is addition of promoters. The work by Hou and Yashima [27] can be given as an example,

where small amounts of Rh-promoted Ni/α-Al_2O_3 catalysts were prepared to be tested for DRM and their activities were compared to monometallic Ni/α-Al_2O_3 and Rh/α-Al_2O_3 catalysts. Their results show that promoted catalysts possessed higher activity than both monometallic catalysts and the activity reached a maximum when rhodium constituted 5 wt.% of the loaded metal. Characterization of catalysts showed that dispersion of nickel improved and coke deposition was decreased with increasing amount of rhodium as promoter. An interesting result is that CO_2-TPD analysis showed the presence of dissociatively adsorbed CO_2 (in the form of CO + O) on Rh/α-Al_2O_3 and $Rh_{0.1}Ni/Al_2O_3$ samples. The authors suggested that Rh may be active in activating and dissociating CO_2, which helps gasification of deposited carbon [27]. Menegazzo *et al.* prepared Al_2O_3 and ZrO_2 supported Pd-(or Pt-)Ni catalysts and tested their activity for DRM. They concluded that the addition of Pt or Pd to Ni/ZrO_2 by co-impregnation method results in reduced coke deposition compared to monometallic Ni/ZrO_2 sample. Catalysts supported with ZrO_2 were more active than the ones supported with Al_2O_3, with Ni-Pd/ZrO_2 sample being the most active for DRM [28]. Another study showing the effect of promoters is published by Luna *et al.*, who studied CO_2 reforming of methane over Ni/Al_2O_3 catalysts modified with K, Sn, Mn, and Ca, prepared by sol-gel method. This time, highest activity was observed on unmodified Ni/Al_2O_3 catalysts and the activity was unchanged during 30 h of operation, but TPO analysis showed some amount of deposited carbon (60 mg/gcat) after 5 h time on stream at 750 °C. High activity and stability of the catalyst was attributed to the low Ni metal cluster size (5-7 nm) made possible by the preparation method. Modification of the catalyst with K resulted in a slight decrease in catalytic activity, but the amount of deposited carbon was significantly decreased (<10 mg/gcat). High carbon resistance of the K-promoted catalyst was believed to stem from increased reducibility and metal-support interaction caused by the promoter. Other promoters (Sn, Mg and Ca) caused significant decrease in activity and stability [29]. Wang *et al.* observed the effect of CeO_2 addition to Rh/Al_2O_3 for dry reforming of methane and showed that CeO_2 promoted catalyst gives higher CH_4 and CO_2 conversions, with lower coke deposition. CH_4 pulse experiments showed that CH_4 decomposition takes place on rhodium, since no CO and H_2 production was observed over CeO_2. However, CO production was observed over

CeO_2 in CO_2 pulse experiments, which showed that the oxygen vacancies of reduced CeO_2 enhanced CO_2 dissociation. Strong interaction between Rh-CeO_2 was observed, which favored the reduction of ceria near Rh. The authors concluded that CeO_2 can further improve the activity and coke resistance of Rh/Al_2O_3 catalyst due to the presence of Ce^{4+}/Ce^{3+} and $Rh^0/Rh^{\delta+}$ redox couples [30].

Selection of support is another significant parameter in the design of dry reforming catalysts. It is shown by a number of studies that in MDR, support is responsible for CO_2 activation, whereas CH_4 is activated on active metal sites [22]. Activation of CO_2 is important not only since CO_2 is a reactant, but also because dissociative adsorption of CO_2 to CO and O helps oxidation of the deposited surface carbon, through reverse Boudouard reaction (Equation 2.4). Van Keulen *et al.* observed that number of CO_2 molecules adsorbed on Pt/ZrO_2 was much greater than the number of Pt atoms on the catalyst. This result showed that CO_2 is adsorbed on ZrO_2 at a significant level, assuming that one Pt atom adsorbs one CO_2 atom. It is also concluded by the authors that an oxygen pool is present on the material and CO_2 acts as an oxygen supplier [31]. Moreover, as reported by Therdthianwong *et al.*, promotion of Ni/Al_2O_3 with ZrO_2 resulted in an increase in conversion of CO_2, suggesting enhanced CO_2 dissociation. A simultaneous decrease in coke deposition was also observed over ZrO_2-promoted Ni/Al_2O_3 compared to unpromoted Ni/Al_2O_3 (50% decrease) [32]. A similar effect of ZrO_2 on coke gasification was reported by Bradford and Vannice [33]. They compared the activities of ZrO_2, TiO_2, CrO_3 and SiO_2 supported Pt catalysts for dry reforming of methane. CrO_3 and SiO_2 supported catalysts were found to deactivate significantly after 5 to 15 h of reaction, whereas no significant deactivation was observed over ZrO_2 and TiO_2 supported catalysts even after 80 h of time on stream. Both supports suppressed carbon deposition, which was proven by temperature programmed hydrogenation results. The ability of Pt/TiO_2 catalysts to prevent carbon deposition was ascribed to the coverage of large Pt ensembles, where CO disproportionation takes place to produce C, with TiO_x species. The reasons behind the coke resistance ability of Pt/ZrO_2 catalyst was less clear, but it was suggested that due to strong Zr-Pt interaction, highly dispersed Pt particles blocked the Lewis acid sites on the support, which are active for carbon deposition. The ratio of deposited carbon

atoms to exposed Pt atoms ranged from 9 to 41 on the catalysts tested, which showed that carbon formation takes place significantly on the supports [33].

In order to have an understanding on the effect of support on catalytic activity of rhodium, Yokota *et al.* compared the activities of 0.5 wt.% Rh supported on various metal oxides prepared by impregnation method for dry reforming of methane. The turnover frequency of rhodium was in the order of: $TiO_2 > La_2O_3 \approx CeO_2 > ZrO_2 \approx MgO \approx SiO_2 \approx$ MCM-41 $> \gamma$-Al_2O_3. Dispersion of Rh on the supports were measured by CO adsorption and highest dispersion was observed on Al_2O_3 (102%), which had a high surface area (139 m^2/g), whereas lowest dispersion was observed on TiO_2 (6.8%) which had relatively lower surface area (38.9 m^2/g). XANES spectra results showed that Rh supported on TiO_2 had a spectrum similar to that of Rh coil, which showed that Rh remained at metallic phase during the reaction. However, Rh supported on Al_2O_3 had a spectrum similar to that of Rh_2O_3, which indicated the presence of cationic Rh, which explained the lower TOF observed on Al_2O_3 supported rhodium. It was concluded that the electronic interaction between Rh and support surface plays an important role on the activity of Rh in methane dry reforming reaction [34]. A similar study reported by Wang and Ruckenstein [35] provides a comparison of Rh supported on reducible (CeO_2, N_2O_5, Ta_2O_5 and ZrO_2) and irreducible oxides (γ-Al_2O_3, La_2O_3, MgO, SiO_2 and Y_2O_3) for the carbon dioxide reforming of methane. They concluded that irreducible oxides are more suitable supports for MDR, with MgO and Al_2O_3 showing the highest activity and stability, giving a CO yield of 83-85% and a H_2 yield of 76-79% at 800 °C and 60,000 ml/h/g space velocity. CO adsorption analysis showed that exposed Rh metal surface area was much higher over the irreducible supports compared to the reducible ones. A possible explanation for this given by the authors is that the Rh particles were covered by partially reduced oxide species. In terms of stability, γ-Al_2O_3, MgO and La_2O_3 provided stable activities over an extended period of reaction (100 h), whereas other irreducible supports showed various degrees of de-activation. Strong interactions between rhodium and magnesium or lanthanum oxides are confirmed with the formation of $LaRhO_3$ and $MgRh_2O_4$ species, which explained the high stability of Rh supported on MgO and La_2O_3. No information was given on coke deposition over the catalysts. All in all, it was concluded that activity of Rh for

MDR depended strictly on the type of support and structure [35].

2.2. Ethanol Dry Reforming

In the past decade, ethanol has become an attractive feedstock for hydrogen production due to its renewable nature [36]. Basically, almost any plant-based material can be a feedstock for bio-ethanol production. Currently, almost all of the produced ethanol is derived from starch and sugar based feedstocks, namely corn, sugar cane and potatoes. Rest of the ethanol is produced from energy crops and cellulosic feedstocks, which include residues from agriculture or forestry and parts of municipal waste [18,37]. Apart from its renewable nature, ethanol has several other advantages that render it a good candidate for H_2 source. First, ethanol is becoming increasingly available and it is easy to transport, biodegradable and non-toxic. Moreover, it is free of sulphur, which is a catalyst poison [38]. Steam reforming of ethanol has been researched extensively, whereas experimental work regarding dry reforming of ethanol is rather scarce. However, the resemblance of ethanol to glycerol (both are oxygenated hydrocarbons) makes any information on catalysis for dry reforming of ethanol (DRE) valuable. The published work on dry reforming of ethanol will be summarized in this section.

2.2.1. Thermodynamics

DRE is the reaction of ethanol with carbon dioxide to produce hydrogen and carbon monoxide as shown in Equation 2.5:

$$C_2H_5OH + CO_2 \rightleftharpoons 3CO + 3H_2 \qquad \Delta H^0 = 297 \text{ kJ mol}^{-1} \tag{2.5}$$

Compared to methane dry reforming, DRE is slightly more endothermic, which means that more energy input is needed. However, ethanol dry reforming is thermodynamically favorable at lower temperatures, typically below 500 °C, whereas methane dry reforming does not take place at temperatures below 650 °C [18].

Thermodynamic analyses of DRE have been carried out in a number of studies to determine the optimum reaction conditions. Wang and co-workers performed a thermodynamic analysis for reforming of ethanol with CO_2 using the Gibbs free energy minimization method. They provided a list of the possible reactions that take place in dry reforming conditions. The side reactions include ethanol dehydrogenation to acetaldehyde or ethanol dehydration to ethylene or ether, acetaldehyde decomposition to methane and carbon monoxide or acetaldehyde dry reforming, ethanol decomposition to carbon monoxide, methane and hydrogen, methanation reactions, WGS and RWGS and finally, carbon formation through Boudouard and methane decomposition reactions [39]. The proposed mechanism by Frusteri *et al.* [40] for ethanol steam reforming included ethanol dehydrogenation to acetaldehyde and subsequent decomposition of acetaldehyde into methane and carbon monoxide, which confirms the ethanol decomposition pathway proposed by Wang *et al.* [39]. It was concluded by Wang *et al.* that the optimum conditions for maximizing the H_2 yield were reaction temperatures between $927 - 1027\,^{\circ}C$, pressure at 1 atm and CO_2/EtOH ratios between 1.2 and 1.3. It was found that at these optimum conditions, ethanol was completely converted and H_2 yields of 94.75 - 94.86% were achieved. In addition, no carbon was formed at these operating conditions. Increase in pressure was found to have a negative effect on H_2 formation whereas the ratio of the inert N_2 in the feed had a positive effect. No carbon formation was observed at temperatures higher than $900\,^{\circ}C$, and no C_2H_4 and CH_3CHO were formed in the studied temperature range [39].

Tsiakaras and Demin performed a thermodynamic analysis of a solid oxide fuel cell system with ethanol as fuel. The fuel cell was assumed to be fed with the thermodynamic equilibrium products of ethanol steam reforming, dry reforming and partial oxidation reactions. For all three reactions, the analysis was done in the region which carbon formation was thermodynamically impossible ($527 - 927\,^{\circ}C$). It was found that highest efficiency was achieved with the products of dry reforming of ethanol at temperatures between $627\,^{\circ}C$ and $827\,^{\circ}C$, whereas at other temperatures steam reforming products gave rise to the highest efficiency. Maximum system efficiency with the products of DRE was found to be 83.6-89.9% [41].

Ortiz *et al.* [42] performed a thermodynamic analysis of dry reforming of ethanol with $CaCO_3$. What distinguishes this work from the former publications is the use of $CaCO_3$ as a source of carbon dioxide. The authors concluded that highest H_2 yield was achievable at 750 °C and carbon fee syngas could be produced at temperatures above 750 °C and $CaCO_3$/EtOH ratios above 2.2 [42].

Kale and Kulkarni conducted a research on the thermoneutral points of DRE and studied the variation of product yields at thermoneutral temperatures. DRE has a complex reaction mechanism with many side reactions. Even though the overall reaction is highly endothermic, the system can be thermoneutral at various temperatures (net $\Delta H=0$) due to the presence of side reactions. The authors found that thermoneutral temperatures ranged from 495.5 °C to 547.8 °C with CO_2/EtOH ratios from 1 to 5. They have concluded that complete conversion of ethanol was achieved at the thermoneutral points, and the thermoneutral temperature of 547.8 °C was the best operating temperature for value added product generation [43]. In a similar study by the same authors, thermoneutral point analysis of autothermal dry reforming of ethanol was conducted, with substoichiometric amount of O_2 introduced to the system. It was found that maximum moles of syngas with a ratio of 2.01 is obtained at a pressure of 1 atm, CO_2/EtOH ratio of 1, O_2/EtOH ratio of 0.5 for the thermoneutral temperature of 603.5 °C, which was selected to be the optimum point for valuable product generation. Along with 2.58 moles of syngas, 0.82 moles of carbon, 0.20 moles of methane and 0.89 moles of water was produced at this point [44].

2.2.2. Catalysis

Apart from the thermodynamic analyses, a number of experimental studies were conducted in order to assess the performances of various catalysts in DRE. Being an active and highly available reforming metal, nickel is tested for DRE by various groups. Hu and Lu [45] tested the performance of a conventional Ni/Al_2O_3 catalyst with a relatively high Ni loading (30 wt.%). Effect of temperature was investigated by changing the temperature between 500-800 °C while the CO_2/EtOH ratio was varied between 1 and 5. It was found that at 500 °C and CO_2/EtOH at 3, conversion of CO_2 was 5.2%

and significant formation of CH_4 and acetaldehyde was observed, which showed that decomposition of ethanol was dominant at lower temperatures. On the other hand, at 750 °C, full stoichiometric conversion of CO_2 was achieved. Coke formation was observed at all temperatures, but is found to decrease with increasing temperature and CO_2/EtOH ratio. Moreover, significant decrease in the BET surface area of the catalyst was observed in used samples, which was attributed to the blockage of some pores of the support due to coke deposition. The authors concluded that the reaction could selectively produce syngas at temperatures above 700 °C with a CO_2/EtOH ratio of 1 [45].

Zawadzki *et al.* also studied nickel as an active metal and tested the performance of 5 wt.% nickel supported on Al_2O_3, CeO_2, MgO and ZrO_2, prepared by wet impregnation with methanolic solution. It was found that NiAl and NiCe catalysts were the easiest ones to reduce and highest hydrogen selectivity and CO_2 conversion were achieved over NiCe. Thus, the authors concluded that ceria support showed the best performance in DRE. XRD analysis of NiCe showed no peaks ascribed to Ni, whereas Ni peaks were observed for other catalysts. This showed that Ni was finely dispersed on NiCe. Carbon formation was observed on all samples, but lowest carbon deposition was observed on NiMg. It was also found that coke deposition decreased when the temperature was increased from 700 °C to 750 °C, and most of the carbon formed was of filamentous form [46].

Like MDR catalysis, there are some studies to improve the activity and stability of nickel based catalysts for DRE with the use of promoters. Ni/Al_2O_3 catalyst was promoted with lanthanum by Bahari *et al.* [47] and the effect of promoter loading on the activity of catalysts for DRE was observed. 0-5 wt.% La was added on 10 wt.% Ni/Al_2O_3 with impregnation method. BET surface area of the samples decreased with increased promoter addition (108 m^2/g for unpromoted sample – 82 m^2/g for 3 wt.% La doped Ni/Al_2O_3). However, comparison of SEM images of promoted and unpromoted samples showed that La improved the dispersion of Ni on the support. Increased activity of promoted catalysts were verified by increased ethanol and CO_2 conversions. The improved catalytic activity was explained by excellent mobile oxygen storage and

redox properties of La_2O_3. Effect of CO_2 partial pressure was also observed in catalytic tests and it was found that conversion of both ethanol and CO_2 increased with increased CO_2 partial pressure. Moreover, a decrease in methane yield was observed as CO_2 partial pressure was increased, which the authors attributed to improved methane dry reforming [47].

Bellido *et al.* tested the performance of Ni/Y_2O_3-ZrO_2 catalyst for DRE, which was prepared in one step by the polymerization method and compared with a nickel catalyst prepared by wet impregnation. Additionally, effect of active metal loading was observed by testing 5 wt.% and 10 wt.% Ni/Y_2O_3-ZrO_2 (NiYZ) catalysts. It was found that polymerization led to more finely dispersed Ni particles compared to wet impregnation that resulted in higher catalyst activity. Maximum CO_2 conversion (61%) was achieved with 5 wt.% NiYZ catalyst at 800 °C and 1 atm, which was found to be the one with the lowest carbon deposition as well [48].

Proven to have good coke resistance abilities for dry reforming of methane, noble metals are promising active metals for DRE as well. Rhodium and iridium are the two noble metals tested for DRE up to this day. Da Silva *et al.* investigated the performance of ceria supported rhodium catalysts with high (275 m^2/g) and low (14 m^2/g) surface areas, prepared with two different methods, for steam (SRE) and dry reforming of ethanol. DRE was carried out in a fixed bed reactor at 1 atm, 500 °C and CO_2/EtOH = 1. At this temperature, ethanol conversion decreased from 97-98% to 60-50% in 6 h for both catalysts, indicating significant deactivation. This is expected considering the low reaction temperature. In addition, CO_2 conversion remained at 12%, showing that ethanol decomposition dominated at this temperature, which is in agreement with the findings of Hu and Lu [45]. At 800 °C, conversion of CO_2 increased to 88%, catalysts showed very good stability and the produced syngas had a ratio of 0.6. Another finding is that the catalyst with higher surface area showed better stability and catalyst deactivation in DRE came out to be more significant compared to SRE [49].

Hou *et al.* [50] tested the activity of CeO_2 supported iridium for dry reforming of ethanol. The catalytic reactions were carried out in a fixed bed reactor at 1 atm and at reaction temperatures between 450 and 700 °C. Similar to other studies described above, the authors found that ethanol conversion and selectivity of syngas (with $H_2/CO \approx 1$) increased with an increase in temperature, and complete conversion of ethanol was achieved at 700 °C. However, it was reported that at reaction temperatures below 600 °C, acetaldehyde, ethylene and methane formation was observed. Over a 70 h testing period, no deactivation of catalyst was observed, indicating that Ir/CeO_2 catalysts shows superior stability with DRE reaction. The authors explained that the stability of the catalyst was due to strong metal-support interaction and although a slight sintering was observed on ceria, this had no effect on the redox capability and Ir-ceria interaction [50].

Drif *et al.* [51] studied the performances of rhodium catalysts supported on alumina doped with various metal oxides (Zr, Mg, Ni, Ce and La), prepared by sol-gel method. After tests at 800 °C and 1 atm with a CO_2/EtOH ratio of 1, highest H_2 yields were obtained in the order of $NiO\text{-}Al_2O_3 \gg Al_2O_3 \approx MgO\text{-}Al_2O_3 \approx CeO_2\text{-}Al_2O_3 > ZrO_2\text{-}Al_2O_3 \approx La_2O_3\text{-}Al_2O_3$. Although the catalyst with the best performance was found to be $Rh/NiO\text{-}Al_2O_3$, some extent of deactivation was observed due to coke deposition, in the form of carbon nanotube as shown by TEM images. XRD results showed the presence of spinels for $Rh/MgO\text{-}Al_2O_3$ and $Rh/NiO\text{-}Al_2O_3$, which were reported to provide higher resistance to coking and to avoid migration of Rh in the support, increasing the stability. Higher activity of $NiO\text{-}Al_2O_3$ compared to $MgO\text{-}Al_2O_3$ was explained by higher content of spinal phase in the $NiO\text{-}Al_2O_3$ sample [51].

One of the interesting aspects of dry reforming reaction is the formation of carbon nanofilaments (CNF), which is a valuable product. There are a number of articles on CNF formation during methane dry reforming and recently, various authors published their work on the formation of CNF during ethanol dry reforming. For example, de Oliveira-Vigiel *et al.* [52] conducted the reactions in the presence of a 316 stainless steel catalyst. They have concluded that the catalyst was active since 98% of the theoretical value of H_2 yield was achieved. Moreover, CNF formation was observed, which could

easily be removed from the catalyst since it does not have a porous form. Abatzoglou *et al.* [53] used carbon steel 1008 as the catalyst and conducted the tests at a reaction temperature of 550 °C. They have reported that 25-29% of the CO_2 feed is sequestered as CNF at these conditions. They also performed a preliminary economic analysis and concluded that although the energetic efficiency of DRE is 50% lower than the steam reforming route, high value carbon product formed at low temperatures offsets this drawback [53].

2.3. Glycerol Dry Reforming

Glycerol, a by-product of biodiesel production, has been the focus of attention as a source of hydrogen and synthesis gas, mainly due to the increase in the production of bio-diesel. Glycerol steam reforming (GSR) is the main route to produce hydrogen from glycerol and extensive research is done on GSR from catalyst development to alternative reactor configurations [3, 6, 13, 14]. As in the case of ethanol and methane, dry reforming of glycerol is a promising alternative reaction for production of hydrogen and syngas. Dry reforming of glycerol (GDR) is the reaction of one mole of glycerol with one mole of CO_2 to produce H_2, CO and H_2O, as shown by Equation 2.6.

$$C_3H_8O_3 + CO_2 \rightleftharpoons 4CO + 3H_2 + H_2O \qquad \Delta H^0 = 292 \text{ kJ mol}^{-1} \tag{2.6}$$

2.3.1. Thermodynamics

Lin *et al.* [6] defines steam reforming of glycerol as the combination of glycerol decomposition and water gas shift (WGS) reactions. In dry reforming conditions (elevated temperature and CO_2 presence in the feed) reverse water gas shift is prevailing due to its endothermic nature [54]. Therefore, it is safe to say that dry reforming of glycerol is the combination of glycerol decomposition (Equation 2.7) and RWGS (Equation 2.8).

$$C_3H_8O_3 \rightleftharpoons 3CO + 4H_2 \qquad \Delta H^0 = 251 \text{ kJ mol}^{-1} \tag{2.7}$$

$$CO_2 + H_2 \rightleftharpoons CO + H_2O \qquad \Delta H^0 = 41 \text{ kJ mol}^{-1} \tag{2.8}$$

Unlike methane, glycerol is a thermally unstable material with three carbons, which renders the GDR system complex due to occurrence of many side reactions. Dehydration (Equation 2.9) and dehydrogenation (Equation 2.10) of glycerol are the two main pathways for glycerol decomposition:

$$C_3H_8O_3 \rightleftharpoons C_3H_6O_2 + H_2O \qquad \Delta H^0 = 450 \text{ kJ mol}^{-1} \tag{2.9}$$

$$C_3H_8O_3 \rightleftharpoons C_3H_6O_3 + H_2 \qquad \Delta H^0 = -15 \text{ kJ mol}^{-1} \tag{2.10}$$

3-hydroxypropanal, produced from Equation 2.9 can be further dehydrated to produce acrolein (Equation 2.11). $C_3H_6O_2$ can dehydrate to produce 2-oxopropanal via Equation 2.12:

$$C_3H_8O_2 \rightleftharpoons C_3H_4O_2 + H_2O \qquad \Delta H^0 = -36 \text{ kJ mol}^{-1} \tag{2.11}$$

$$C_3H_6O_3 \rightleftharpoons C_3H_4O_2 + H_2O \tag{2.12}$$

At high temperatures, decomposition reactions, such as decomposition of glycerol to ethylene, 2-oxopropanol decomposition and acetaldehyde decomposition reactions, (Equations 2.13, 2.14 and 2.15, respectively) are likely to occur [55]:

$$C_3H_8O_3 \rightleftharpoons C_2H_4 + CO + 2H_2O \tag{2.13}$$

$$C_3H_4O_2 \rightleftharpoons CH_3CHO + CO \tag{2.14}$$

$$CH_3CHO \rightleftharpoons CH_4 + CO \tag{2.15}$$

Valliyappan *et al.* [56] summarizes glycerol decomposition reactions with a scheme shown in Figure 2.1.

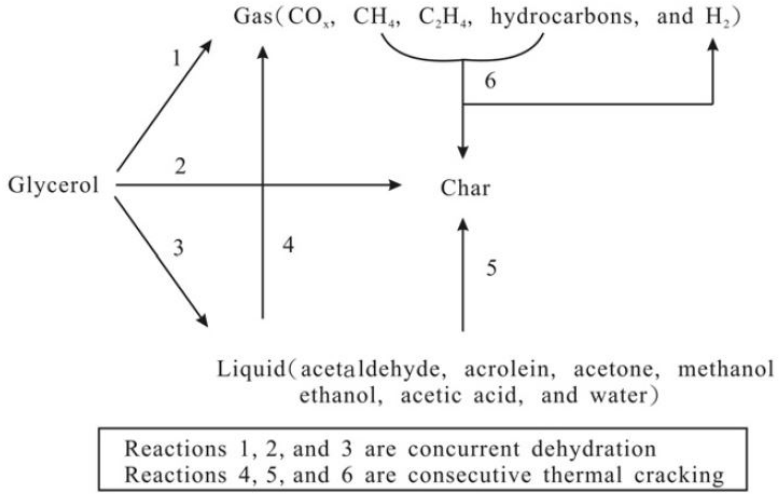

Figure 2.1. Glycerol decomposition scheme [56].

Other side reactions include methanation (Equations 2.16 and 2.17), methane dry reforming (Equation 2.18), and reactions that are responsible for coke formation (Equations 2.19-2.22), including methane decomposition and Boudouard reactions [9]:

$$CO + 3H_2 \rightleftharpoons CH_4 + H_2O \qquad \Delta H^0 = -251 \text{ kJ mol}^{-1} \tag{2.16}$$

$$CO_2 + 4H_2 \rightleftharpoons CH_4 + 2H_2O \qquad \Delta H^0 = -165 \text{ kJ mol}^{-1} \tag{2.17}$$

$$CH_4 + CO_2 \rightleftharpoons 2CO + 2H_2 \qquad \Delta H^0 = 247 \text{ kJ mol}^{-1} \tag{2.18}$$

$$C_{(s)} + H_2O \rightleftharpoons H_2 + CO \qquad \Delta H^0 = 131 \text{ kJ mol}^{-1} \tag{2.19}$$

$$C_{(s)} + 2H_2O \rightleftharpoons 2H_2 + CO_2 \qquad \Delta H^0 = 90 \text{ kJ mol}^{-1} \tag{2.20}$$

$$CH_4 \rightleftharpoons 2H_2 + C_{(s)} \qquad \Delta H^0 = 75 \text{ kJ mol}^{-1} \tag{2.21}$$

$$2CO \rightleftharpoons C_{(s)} + CO_2 \qquad \Delta H^0 = -172 \text{ kJ mol}^{-1} \tag{2.22}$$

Although there is a huge lack of information regarding catalysis of GDR in the literature, a number of thermodynamic analyses have been carried out in order to determine the optimum operating conditions. A thermodynamic analysis of the dry reforming

of glycerol was published by Wang *et al.* [9], where Gibbs free energy minimization method was utilized. It was concluded that the optimum condition for maximizing H_2 yield was at 727 °C and a carbon dioxide-to-glycerol ratio (CO_2/G) of 1. It was claimed that changing the operating conditions could alter the syngas ratio. No carbon formation was obtained thermodynamically above 677 °C with a CO_2/G ratio of 1. According to Equation 2.6, the syngas produced by dry reforming of glycerol has a ratio less than 1. However, depending on the operating conditions, produced syngas ratio may increase or decrease due to the extent of side reactions. According to the analysis done by Wang *et al.* [9], thermodynamic H_2/CO ratios produced by dry reforming of glycerol change between 1 and 2.15 at temperatures between $500 - 700$ °C and CO_2/G feed ratios between 1 and 5. The low H_2 content of the dry reforming product stream may not be suitable for direct use in fuel cells, but a low syngas ratio is required for the production of long chain hydrocarbons via Fischer-Tropsch synthesis by the Equations 2.23 and 2.24 [22]:

$$n\mathrm{CO} + (2n+1)\mathrm{H_2} \rightleftharpoons \mathrm{C}_n\mathrm{H}_{2n+2} + n\mathrm{H_2O} \tag{2.23}$$

When this reaction is combined with WGS to produce the needed hydrogen, the overall stoichiometry becomes:

$$2n\mathrm{CO} + (n+1)\mathrm{H_2} \rightleftharpoons \mathrm{C}_n\mathrm{H}_{2n+2} + n\mathrm{CO_2} \tag{2.24}$$

Moreover, production of carbonyls (Equation 2.25) and carboxylic acids (Equation 2.26) via Fischer-Tropsch also require syngas ratios close to 1 [12]:

$$n\mathrm{CO} + (2n-1)\mathrm{H_2} \rightleftharpoons (\mathrm{CH_2})_n\mathrm{O} + (n-1)\mathrm{H_2O} \tag{2.25}$$

$$n\mathrm{CO} + (2n-2)\mathrm{H_2} \rightleftharpoons (\mathrm{CH_2})_n\mathrm{O_2} + (n-2)\mathrm{H_2O} \tag{2.26}$$

Other than utilization of CO_2, this is another advantage of dry reforming reactions. Steam reforming reactions generate syngas with higher H_2/CO, which is not suitable for use in FT synthesis processes.

Another thermodynamic study on dry autothermal reforming of glycerol suggests that with a combination of dry reforming and partial oxidation of glycerol, thermoneutral conditions can be achieved where no external heat supply is needed [57]. From a temperature range of $327 - 727\,^{\circ}C$, O_2/C range of 0.1-0.5 and CO_2/G range of 1-5, the optimum thermoneutral point was detected at a temperature of $653\,^{\circ}C$, O_2/C ratio of 0.3 and CO_2/G ratio of 1. Additionally, carbon formation was found to be less in the case of autothermal dry reforming, compared to the cases where there is no oxygen feed [57]. Freitas and Guirardello [7] carried out a comparative study between several glycerol reforming methods (steam reforming, partial oxidation, autothermal reforming, dry reforming and supercritical water gasification) for H_2 and syngas production, via performing a thermodynamic analysis by the method of Gibbs energy minimization in combination with the virial equation of state. It is found that, for all methods, higher temperatures and lower pressures result in higher H_2 production. At $800\,^{\circ}C$, resulting syngas had a ratio of unity for dry reforming, whereas it was close to 2 for steam reforming, and molar fraction of produced syngas in the product stream was higher in DR compared to SR (92.7 and 88.4, respectively). Highest amount of coke formation was observed in dry reforming at a temperature of $600\,^{\circ}C$. In addition, increase in pressure resulted in significant coke formation in partial oxidation and dry reforming reactions, whereas no carbon formation was observed in any of the other methods [7]

2.3.2. Catalysis

Nickel based catalysts are the prevailing catalysts for reforming reactions, due to lower price of nickel compared to the noble metals. Thus, there are a number of publications regarding the use of nickel based catalysts in dry reforming of glycerol. Siew *et al.* [10] conducted several studies on nickel based catalysts promoted with lanthanum. In one of their studies, they tested the performance of 3 wt.% La promoted Ni/Al_2O_3 catalyst on dry reforming of glycerol. They have concluded that lanthanum provided better metal dispersion, thus finer crystallite size and higher BET surface area. Catalytic reaction tests were performed in a stainless steel fixed bed reactor at

temperatures between 650 and 850 °C and CO_2/G ratios between 0 and 5. Maximum glycerol conversion of 96% was achieved with a CO_2/G ratio of 1.67 and further increase of this ratio led to a decrease in H_2 production rate. They have reported that although nickel based catalysts were prone to carbon deposition, addition of lanthanum as a promoter significantly reduced carbon deposition. In 72 h long stability tests, no significant deactivation of the catalyst was observed. The authors also conducted a kinetic study and reported the rate of glycerol consumption in power-law form as given in Equation 2.27 [10]:

$$r_g = Ae^{\frac{-E_a}{RT}}(P_{C_3H_8O_3})^{\gamma}(P_{CO_2})^{\phi} \tag{2.27}$$

where r_g is the rate of glycerol consumption, A is the exponential factor which is calculated as 2.6×10^{-4}, E_a is the activation energy, calculated as 34.9 kj mol^{-1} and γ and ϕ are reaction orders calculated as 0.72 and 0.14, respectively [10].

In another study by the same authors, characterization of 2 wt.% La-promoted Ni/Al_2O_3 catalyst was done and compared with non-promoted nickel catalyst, both of which prepared by co-impregnation procedure. The authors found that promoted catalyst had a larger BET surface area compared to that of the non-promoted one (98 and 85 m^2/g, respectively) due to better dispersion. However, increasing the weight of lanthanum over 2 wt.% caused a decrease in the surface area. Dry reforming reaction was carried out with the promoted catalyst at 600 °C and glycerol conversion was found to be 24.5% [11]. Additionally, a longevity study for La-Ni/Al_2O_3 catalyst was carried out in another article by the same authors. In this study, 3 wt.% La-Ni/Al_2Ol_3 catalyst was found to have the largest BET specific surface area (97 m^2/g). Thus, this catalyst showed the best longevity performance, with a glycerol conversion of 90% even after 72 h of reaction time. Catalytic tests were performed in a fixed bed reactor, at 750 °C temperature and 1 atm pressure. Reduced CO generation was observed at lower CO_2/G ratios. In addition, they have concluded that presence of CO_2 was essential in reducing carbon deposition and attributed this to the gasification reaction [58].

Lee *et al.* [59] published a series of papers on the performance of nickel catalysts supported on cement clinker in glycerol dry reforming. This has been done with the intention of using the carbon dioxide emitted in the cement production process and thus, providing a solution to the environmental issues involved in the cement industry. It was reported that cement clinker (CC), an intermediate product of the cement industry, is rich in terms of CaO and MgO, which have improved resistance against carbon formation. In one of their studies, the authors prepared CC supported nickel with loadings of 5 wt.%, 10 wt.%, 15 wt.% and 20 wt.% and tested their performance in glycerol dry reforming. The results showed that addition of Ni significantly increased the BET specific surface area (from 0.55 to 17.83 m^2/g). The catalytic reactions were carried out in a fixed bed reactor at 750 °C and CO_2/G ratio of unity. It was found that 20 wt.% Ni/CC catalyst showed the best performance with the highest H_2 yield and least deactivation. The produced syngas was reported to have a ratio of ≈ 1.5, which was suitable for FT synthesis [60]. In another study by the same authors, a parametric study was conducted with 20% Ni/CC, which gave the best performance in GDR. Temperatures between 650 °C and 750 °C and CO_2/G ratios between 0.6 and 5 were tested. It was found that the optimum conditions for GDR with this catalyst was at 700 °C and at a CO_2/G ratio of unity. In addition, 70-80% glycerol conversions were reached, with produced syngas ratios below 2.0 [59].

Arif et al. [61] compared CaO and ZrO_2 supported Ni catalysts with different Ni loadings prepared by wet impregnation for dry reforming of glycerol. It was observed that at a temperature of 700 °C and a CO_2/G ratio of 1, Ni/CaO gave higher H_2 yield and glycerol conversion compared to Ni/ZrO_2. XRD patters of prepared samples showed that ZrO_2 supported samples had sharp and intense peaks, whereas CaO supported samples had shorter and broader diffraction peaks. The authors attributed this to fine dispersion of NiO on CaO, which also lead to higher surface area of the catalyst as revealed by BET analysis. Superiority of the CaO supported samples over ZrO_2 supported ones was attributed to higher metal dispersion and consequently, smaller NiO crystallite size. No information on deactivation or stability was provided.

Harun et al. [62] tested the activity of Ag- promoted Ni/SiO_2 catalysts for GDR and observed the effect of promoter loading by changing the Ag loading between 0-5 wt%. It was revealed by XRD analysis that addition of Ag does not change the metal size significantly. It was observed that the sample with the highest Ag loading (5 wt% Ag – 15 wt% Ni/SiO_2) gave the highest H_2 yield and glycerol conversion. The syngas produced had a H_2/CO molar ratio always less than 1. Two types of carbon was found to deposit on the catalysts upon SEM analysis of spent samples: solid carbon that covers the active sites of the catalyst and filamentous type carbon.

Dry reforming can also be coupled with steam reforming and partial oxidation for increased hydrogen yield and energy efficiency. Kumar *et al.* [63] performed a catalytic study for tri-reforming of glycerol for hydrogen generation. Tri-reforming reaction was carried out in the presence of CO_2, H_2O and O_2, so that dry reforming, steam reforming and partial oxidation could take place simultaneously. The reactions were carried out in the presence of CeO_2, ZrO_2 and CeO_2- ZrO_2 supported 10% Ni catalysts in a fixed bed microreactor at atmospheric pressure and temperatures between $400 - 800\,^{\circ}C$. BET surface areas of the prepared catalysts changed between 3.5 and 4.3 m^2/g. Complete conversion of glycerol and 95% of the theoretical H_2 yield was obtained. The authors found that at $600\,^{\circ}C$, CeO_2 - ZrO_2 supported catalyst gave the highest H_2 yield and CO_2 conversion. Moreover, lowest carbon deposition was observed on this catalyst (2.3 mg), whereas the highest amount of coke was found to deposit on Ni/CeO_2 [63].

It has been proposed by Mortensen *et al.* [54] that only the CO_2 adsorption and dissociation steps deviate when the mechanism of MDR is compared to that of MSR. The same can be proposed for GDR and GSR, since steps like glycerol decomposition, dehydration or dehydrogenation, H_2 and CO formation and methanation are seen in both cases. Moreover, RWGS takes place in dry reforming conditions, which results in the production of H_2O. Thus, dry reforming reactions can be considered as a combination of dry reforming and steam reforming to some extent. Catalysts that are active in glycerol steam reforming can be expected to perform well in GDR as well. Therefore, a short survey of GSR catalysis is made in order to identify catalysts that may have potential for high activity in GDR:

Nickel based catalysts supported on TiO_2, CeO_2 and MgO were prepared and tested for catalytic activity in dry reforming of glycerol by Adhikari *et al.* [64]. Catalytic tests showed that Ni/CeO_2 was by far the best performing catalyst for GSR with a maximum hydrogen selectivity of 74.7% at an S/C of 4 and a temperature of 600 °C, whereas Ni/MgO and Ni/TiO_2 gave hydrogen selectivities of 38.6% and 28.3%, respectively. Surface characterization revealed that Ni/CeO_2 had the highest BET surface area, metal dispersion and metal surface area. The authors suggested that the high metal surface area could be due to the better interaction of CeO_2 with nickel. Moreover, highest amount of coke deposition was observed on Ni/TiO_2, followed by Ni/MgO and Ni/CeO_2. Higher coke deposition on TiO_2 was attributed to the higher acidity of TiO_2 compared to MgO and CeO_2 supports [64].

A similar study was conducted by Nichele *et al.* [65], where Ni supported on TiO_2, ZrO_2 and SiO_2 (in the form of SBA-15 and amorphous dense nanoparticles) were prepared by impregnation and their catalytic activity in hydrogen production via GSR was observed. Extensive characterization on the samples were done in order to investigate the effect of structural and morphological properties on catalyst performance. It was concluded that activity of the Ni based catalysts were strongly dependent on the support. It was proposed that the reducibility of the sample is an important indicator of metal-support interaction and low reducibility of the active phase indicates a strong interaction with the support. The reducibility of the samples decreased in the order of $SiO_2 > ZrO_2 > TiO_2$. Moreover, results obtained from both XRD and TEM analyses suggested that metal dispersion increased in the order of $TiO_2 < SiO_2 < ZrO_2$. In the catalytic activity tests, Ni/ZrO_2 gave the best results without showing deactivation at 650 °C. It was revealed that the structure of zirconia was completely preserved after 20 h on stream and no change on the dispersion of Ni was observed among fresh and used catalysts. TGA results revealed that highest coke deposition was in fact on ZrO_2 supported sample, but coke formation occurred on the support and did not deactivate the active species both on TiO_2 and ZrO_2. It was observed that Ni/TiO_2 showed the highest CO selectivity and lowest CO_2 selectivity at both temperatures tested, which shows that TiO_2 supported sample has the lowest activity in WGS. SiO_2 supported sample suffered from severe deactivation, which was attributed to coke deposition since

this sample was characterized by the presence of silanols and Lewis acid sites. It was concluded that Ni/ZrO_2 was the most promising catalyst for GSR among the samples tested, metal-support interaction was very important for determination of catalytic activity and though carbon formation was observed on all samples, this led to poor access to the metal sites only in the case of Ni/SiO_2 samples [65, 66].

Cobalt is another active metal that is advantageous due to its low cost and high availability. There are a number of studies aiming to evaluate the activity of Co based catalyst in GSR processes. A 15 wt.% Co/Al_2O_3 catalyst prepared by impregnation method was tested by Cheng *et al.* [67]. They provided information on the physicochemical properties of the catalyst, which revealed the formation of Co_3O_4 and $CoAl_2O_3$ in the calcined catalyst. Moreover, TPD method showed that impregnation of Co resulted in an increase in the acid site concentration of the sample, whereas no significant change was observed in the basic site concentration. The acidic/basic site ratio was increased to 5.5 from 4.6 upon impregnation of cobalt. Parametric studies revealed that conversion of glycerol increased with increased steam partial pressure but decreased as the glycerol partial pressure increased. The produced syngas had a relatively high H_2/CO ratio (between 6 and 12) and high amount of CO_2 production was observed (H_2/CO_2 = 2-2.3). Inevitable carbon formation was observed even at excess steam-to-carbon ratios [67]. Zhang *et al.* compared the activities of ceria supported Ir, Co and Ni catalysts in ethanol steam reforming and glycerol steam reforming reactions. In both reactions, Ir/CeO_2 was the best performing catalyst, followed by Co/CeO_2 and Ni/CeO_2. Temperature programmed reduction studies on the prepared catalysts showed strong interaction between iridium and ceria, which is revealed by the decrease in the reduction temperature of CeO_2 in the presence of iridium. The strong interaction between Ir and ceria was shown previously by Hou *et al.* [50] as an Ir/CeO_2 catalyst was tested for DRE. As a result of the stability tests performed in ethanol steam reforming conditions, Ir/CeO_2 showed no deactivation, whereas Co and Ni based samples slightly deactivated [68].

Among noble metals, Ru, Pt, Rh and Ir are the prevailing metals for GSR. Suzuki *et al.* performed a catalyst screening and tested various La_2O_3 supported Group 8-10

metals for activity in GSR. At a reaction temperature of 600 °C, a S/C ratio of 3.3 and a W/F of 13.4 gcat h mol^{-1}, the order of activity was found to be as: Ru ≈ Rh > Ni > Ir > Co > Pd > Fe (activity is based on H_2 yield). It was observed that CO_2 selectivity was high over all catalysts, which was attributed to the use of basic supports that promote WGS. Finding that Ru is the most active metal in GSR among other tested metals, the authors prepared Ru on Y_2O_3, ZrO_2, CeO_2, La_2O_3, SiO_2, MgO and Al_2O_3 supports. The comparison of supports showed that Y_2O_3 and ZrO_2 supported catalysts were the most active with high glycerol conversions and H_2 yields, whereas Al_2O_3 and MgO supported catalysts showed the lowest glycerol conversions [69]. Chiodo *et al.* compared the activities of Al_2O_3, MgO and CeO_2 supported Ni catalysts to that of Rh/Al_2O_3. It was observed by the authors that Rh was more active and stable than Ni based catalysts. Ni loading was quite high (30 wt.%), whereas Rh loading was 5 wt.%. Before conducting catalytic tests, the authors performed a blank test to see the extent of homogeneous glycerol decomposition and observed the formation of CO, CO_2, olefins (ethylene and propylene), CH_4 and H_2. Glycerol conversion was around 65% at a temperature of 800 °C, which shows that glycerol decomposes significantly before reaching the catalyst surface. Coke formation was evident on all samples, but on Rh/Al_2O_3 lower rate of coke deposition was observed compared to Ni catalysts. It was discovered that hydrogen yield over Rh/Al_2O_3 increases with increasing temperature up to a temperature of 700 °C, but a further increase in temperature results in a sudden decrease in hydrogen yields, a trend not seen thermodynamically. This was attributed to sintering of Rh particles that took place at higher temperatures, as revealed by TEM analysis [70].

3. EXPERIMENTAL WORK

3.1. Materials

3.1.1. Chemicals

All chemicals used in the preparation of catalysts are listed in Table 3.1:

Table 3.1. Chemicals used for catalyst preparation.

Chemicals	**Specifications**	**Supplier**	**Molecular Weight (g/gmol)**
Cerium(III) nitrate hexahydrate	$Ce(NO_3)_3{\cdot}6H_2O$	Sigma-Aldrich	434.22
Cobalt(II) nitrate hexahydrate	$Co(NO_3)_2{\cdot}6H_2O$	Sigma-Aldrich	291.03
Rhodium(III) nitrate solution	$Rh(NO_3)_3$ 10 wt.% Rh	Sigma-Aldrich	288.92
Zirconium oxide, catalyst support	ZrO_2	Alfa-Aesar	123.22
Aluminum oxide, catalyst support	α-Al_2O_3 3/16" spheres	Alfa-Aesar	101.96

3.1.2. Gases and Liquids

The gaseous and liquid feeds that are used in the experimental system with their applications are listed in Table 3.2 and Table 3.3, respectively. All gases are of high purity and supplied by The Linde Group. From the gases listed in Table 3.2, N_2, CO_2, H_2, He and Ar are directly used in the experiments, whereas the others are used in the calibration of gas chromatographs. The deionized water is used in the preparation of precursor solutions and it is obtained from Zeneer Water Purification System with a

conductivity less than 0.1 μS cm^{-1}. Glycerol is fed to the reaction system as a reactant and is supplied by Sigma-Aldrich with 99.5% purity.

Table 3.2. Gases used in the experimental system.

Gas	**Specifications**	**Application**
Argon	99.998%	GC carrier gas
Carbon dioxide	99.995%	GC calibration, reactant
Carbon monoxide	99.90%	GC calibration
C_2 mixture	2% C_2H_6, 2% C_2H_4, 5% CH_4, balance N_2	GC calibration
Helium	99.99%	GC carrier gas
Hydrogen	99.99%	GC calibration, reducing agent
Methane	99.50%	GC calibration
Nitrogen	99.998%	GC calibration, inert

Table 3.3. Liquids used in the experimental system.

Liquid	**Specifications**	**Application**
Glycerol	$\geq$99.5%	Reactant
Deionized water	-	Catalyst preparation

3.2. Experimental System

The experimental system that is used in this study consists of four main parts:

- Catalyst Preparation System: The incipient-to-wetness impregnation system is used for the preparation of all catalysts tested in this study.
- Catalyst Characterization System: The structural properties of the catalysts that are prepared are analyzed by Scanning Electron Microscopy (SEM) integrated with Energy Dispersive X-ray Spectroscopy (EDX) and X-ray Diffraction (XRD).

Surface area characterization of the prepared supports are done by BET suface analysis method.

- Catalytic Reaction System: The prepared catalysts are tested for activity in a system consisting of mass flow controllers for gaseous feed, an HPLC pump for liquid glycerol feed, a three chambered furnace with programmable temperature controllers, a packed bed reactor and two cold traps.
- Product Analysis System: The composition of the product gas is analyzed by two on-line gas chromatographs.

3.2.1. Catalyst Preparation System

All catalysts used in this study are prepared by using the incipient-to-wetness impregnation system illustrated in Figure 3.1. The system is composed of a Retsch UR1 ultrasonic mixer for continuous mixing of the support, a Buchner flask for containing the support, a vacuum pump for evacuating the pores of the support and a peristaltic pump for controlled feed of the active metal solution. Details of catalyst preparation and pretreatment procedures will be provided in the coming sections.

3.2.2. Catalyst Characterization System

3.2.2.1. BET Surface Analysis. BET isotherms were obtained by using Quantachrome Nova 2200e automated gas adsorption system with liquid nitrogen at a temperature of 77 K. Specific surface areas of the samples were determined using multi-point BET analysis. Pore sizes and pore diameters were calculated by the BJH method of adsorption.

3.2.2.2. X-Ray Diffraction Analysis. X-ray Diffraction (XRD) analysis of the catalysts was carried out by Boğaziçi University Advanced Technologies R&D Center using a Rigaku D/Max-Ultima+/PC X-ray diffraction equipment having an X-ray generator with Cu target operated at 40 kV and 40 mA. The scan speed was 2° min^{-1}.

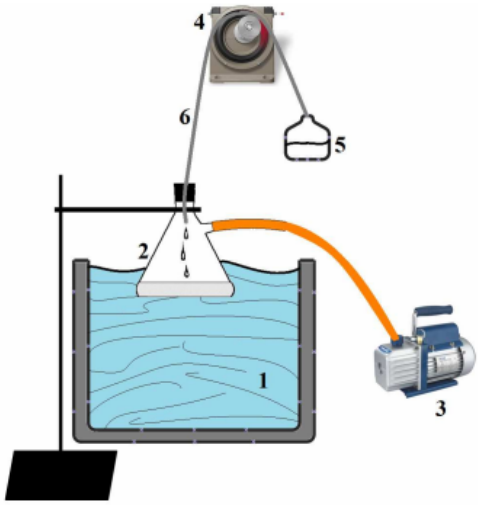

Figure 3.1. Schematic representation of the impregnation system. 1. Ultrasonic Mixer, 2. Buchner Flask, 3. Vacuum Pump, 4. Peristaltic Pump, 5. Aqueous Active Metal Solution, 6. Silicon Tubing [71].

3.2.2.3. SEM/EDX Analysis. SEM/EDX analysis was carried out in Koç University Surface Science and Technology Center (KUYTAM) by a Zeiss Evo LS 15 scanning electron microscope coupled with Bruker XFlash 5010 EDX detector with 123 eV resolution.

3.2.3. Catalytic Reaction System

The catalytic reaction system can be divided into three parts as feed, reaction and product analysis sections. A detailed schematic representation of the system is provided in Figure 3.2.

3.2.3.1. Feed Section. The feed section is composed of pressurized gas storage tanks containing purified Ar, He, dry air, H_2, N_2 and CO_2, Brooks Model 5850E Series Mass Flow Controllers and a Shimadzu LC-20AT HPLC pump, all of which are connected with Swagelok tubing and fitting of sizes 1/4", 1/8" and 1/16".

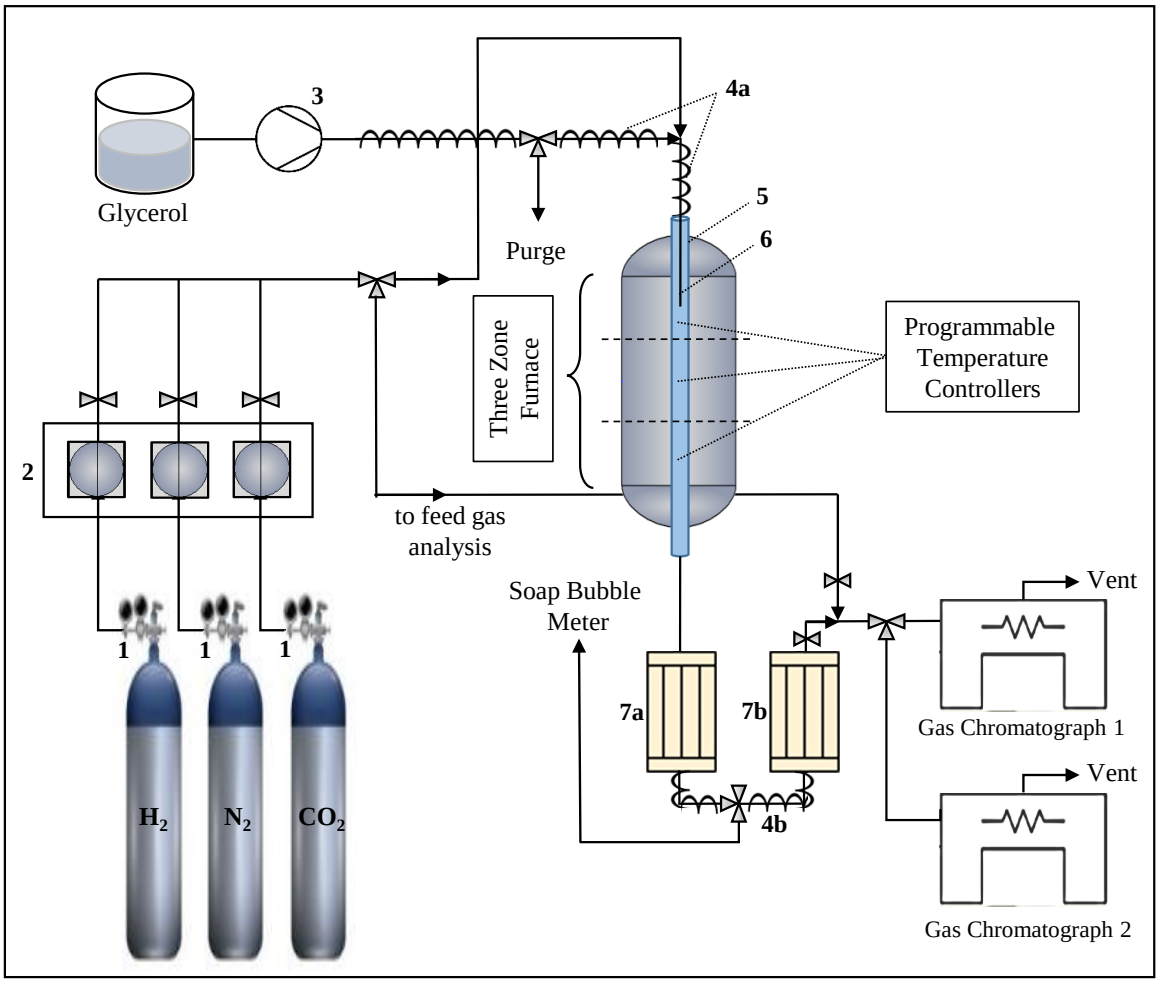

Figure 3.2. Schematic representation of the experimental system. 1. Gas regulators, 2. Mass flow controllers, 3. HPLC pump, 4. Heating lines, 5. Quartz reactor, 6.Injection nozzle, 7. Dewar flasks.

Gaseous feed leaves the pressurized gas tanks via regulators (marked as 1 in Figure 3.2), which keep the pressure at the outlet of the tanks at 2 atm. The gases then enter, via 1/8" tubing, their own individually calibrated mass flow controllers (MFC) where their volumetric flow rates are regulated in order to achieve desired feed ratios. Calibration curves for each mass flow controller can be found in Appendix A. On-off valves are installed to the outlets of the MFCs in order to prevent back flow and to decrease the dead volume caused by the unused gas lines. Downstream of the MFCs are connected as a single 1/8" line, where a 3-way valve is installed so that the feed gas can be directed either to the reactor or to a line which by-passes the reactor

and goes directly to the gas chromatographs for feed analysis.

Liquid glycerol is fed to the reactor by an HPLC pump through 1/16" tubing. Due to the high viscosity of glycerol at room temperature and the low inner diameter of the tubing, the pressure at the outlet of the pump tends to increase. At high flow rates, pressure exceeds the pressure limit of the pump, which leads to shut down. To avoid this situation, viscosity of glycerol is aimed to be decreased by increasing the temperature of the tubing to 100 °C with the use of heating lines and ENDA ET4420 type digital PID temperature controllers. The gaseous feed consisting of N_2 and CO_2 meets the liquid glycerol feed at a T-junction slightly above the reactor, and enters the reactor through 1/16" tubing. How the glycerol is fed to the reactor is of great importance in terms of maintaining the desired feed ratio. Two different feeding configurations that are tested are given in Figure 3.3 as configuration (a) and (b).

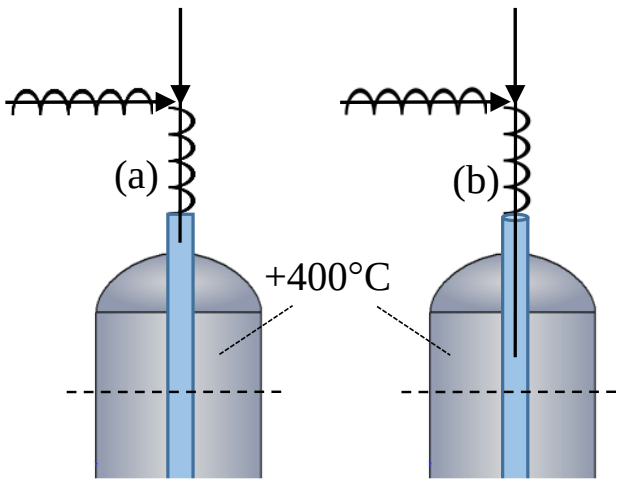

Figure 3.3. Different feeding configurations.

In configuration (a), glycerol leaves the 1/16" tubing slightly above the inlet of the reactor furnace, where the temperature is at room conditions. Thus, glycerol leaves the tubing in the form of liquid drops. As the liquid drop leaves the tubing, it starts falling down through the first zone of the furnace, where the temperature is above 400 °C, and it vaporizes before reaching the catalyst bed. This configuration is proven by our

group to be advantageous when there is any other condensable material in the feed, such as water. In that case, this configuration prevents the water from vaporizing before glycerol, and sustains the desired steam-to-carbon ratio over the catalyst bed [72]. Without the presence of water in the feed, however, this configuration turned out to be problematic. Low volumetric flow rate of the liquid feed combined with the high viscosity and surface tension of glycerol caused the accumulation of glycerol as a large drop around the tubing, while gaseous CO_2 flowed continuously and this created unsteady feed ratios throughout the experiment. Gaseous and liquid flow rates are altered in order to minimize the time between the drops as shown in Table 3.4, but even with the best conditions, the irregularity in the results could not be avoided. In some cases, it was observed that the gas-liquid feed mixture formed bubbles, which is unwanted since glycerol is lost on the sides of the reactor as the bubbles break.

Table 3.4. Time between glycerol drops with different feed flow rates.

Liquid Flow / **Gas Flow**	**3 NmL min^{-1}**	**4 NmL min^{-1}**
37 NmL min^{-1}	62 s*	-
47 NmL min^{-1}	52 s*	39 s*
57 NmL min^{-1}	52 s	50 s
67 NmL min^{-1}	62 s	55 s

*Cells marked with a star indicate bubble formation.

In the second configuration (configuration (b)), the 1/16" tubing extends until 10 cm below the furnace entry, where the temperature is above 400 °C. This enables complete evaporation of glycerol before leaving the tubing, preventing any drop formation. Both glycerol and CO_2 is fed continuously in gaseous form and the desired CO_2-to-glycerol (CO_2/G) ratio is sustained on the catalyst bed. Trials done with configuration (b) yielded steady results; thus, it is decided to move on with this configuration.

3.2.3.2. Reaction Section. The reaction section consists of a quartz reactor surrounded by a tube furnace, followed by two cold traps. The furnace used in the system is PROTHERM PZF 12/50/500, which includes three zones with PC442 type individual PID programmable temperature controllers. As explained in detail in Section 3.4, the quartz reactor is loaded with the catalyst bed, which is placed in the middle of the tube. The middle zone of the furnace is set to reaction temperature, whereas the upper and lower zones are set to 310 °C in order to ensure complete vaporization of glycerol and other condensable products throughout the furnace. However, due to the heat dissipation from the hot center of the furnace, the observed temperatures at the upper and lower zones are always above 400 °C.

The product stream leaves the reactor in 1/4" tubing, installed with a three-way valve that directs it either to the bubble meter connected to vent, or to two consecutive cold traps. The bubble meter can be used to measure the flow rate of the product stream or to check for any leakage in the reactor. It was also used for the calibration of mass flow controllers. The cold traps are placed in Dewar flasks filled with ice to ensure that all of the unreacted glycerol and other condensable products are separated from the gaseous products, which are sent to the product analysis system. A heating line is installed between the cold traps and the temperature is kept at 120 °C to make sure that any condensable materials that escape the first cold trap are brought to the second cold trap in gaseous form, and no condensables are left in the line in between.

3.2.3.3. Product Analysis Section. The product analysis section consists of two gas chromatographs equipped with Molecular Sieve 5A and Porapak Q type columns. The product and feed analysis lines are merged as a single line, where a three-way valve is installed to direct the stream either to the first or the second GC. Details of the analysis system will be provided in Section 3.2.4.

3.2.4. Product Analysis System

The feed and product stream compositions are analyzed by two online gas chromatograms equipped with different columns. Shimadzu GC-2014 is equipped with a Molecular Sieve 5A column, which detects hydrogen, nitrogen, methane and carbon monoxide. Agilent 6850N is equipped with Porapak Q type column, which detects carbon dioxide, ethane and ethlyene. Stream compositions are determined via calibration curves, provided in Appendix A, that convert peak areas to compositions. Calibrations are done for each gas with GC operating conditions specified in Table3.5. The product stream is sent continuously to GC-2 (Agilent) and diverted to GC-1 (Shimadzu) after each sampling.

Table 3.5. Operating parameters of gas chromatographs.

GC Parameter	**Shimadzu GC-2014**	**Agilent 6850N**
Detector Type	Thermal conductivity	Thermal conductivity
Column oven temperature	50 °C	40 °C
Injector temperature	80 °C	90 °C
Detector temperature	150 °C	80 °C
Carrier gas	Argon	Helium
Carrier gas flow rate	25 mL min^{-1}	20 mL min^{-1}
Detector current	50 mA	Set by GC
Column packing material	Molecular Sieve 5A (60-80 mesh)	Porapak Q (80-100 mesh)
Column tubing material	Stainless steel	Stainless steel
Column ID & length	2.1 mm & 2.0 m	2.1 mm & 1.82 m
Sampling loop	1 mL	1 mL

3.3. Catalyst Preparation and Pretreatment

Four different catalysts, namely Rh/ZrO_2, Rh/CeO_2, Co/ZrO_2 and Co/CeO_2 are prepared by incipient-to-wetness impregnation method. The steps of catalyst preparation include support preparation, active catalyst preparation and pretreatment.

3.3.1. Preparation of Support

3.3.1.1. Preparation of CeO_2. Ceria precursor cerium(III)nitrate ($Ce(NO_3)_3{\cdot}6H_2O$) is first calcined in air at 600 °C for 4 hours so that it thermally decomposes to ceria. The calcination temperature is selected based on the work of Zheng *et al.*. They performed the calcination at four different temperatures (400, 500, 600, and 700 °C) and concluded that 600 °C was the optimum temperature which enabled better dispersion of the active metal on ceria and increased catalytic activity [73].

After thermal decomposition, the obtained powder is again calcined at 800 °C in a muffle furnace for 4 hours. Thermal stability of the catalyst is an important property in dry reforming reactions due to the high temperatures required by the thermodynamics of the reaction (In this study, the maximum reaction temperature tested is 750 °C). It is reported that Hüttig and Tamman temperatures are good semi-empirical measures of the temperature at which sintering may occur. When $T_{Hüttig}$ (identified as $0.3T_{melting}$) is reached, atoms at defects become mobile; whereas when T_{Tamman} ($0.5T_{melting}$) is reached, atoms from the bulk become mobile [74]. CeO_2 has a relatively high melting point (2,400 °C), but its Hüttig temperature (720 °C) is still lower than our studied reaction conditions [75]. Thus, calcination is necessary to enhance the thermal stability of the support at studied reaction conditions.

3.3.1.2. Preparation of ZrO_2. ZrO_2 support is first sieved to get 45-60 mesh size (250-354 μm), which is the particle size used for packed bed configuration. Afterwards, sieved particles are calcined at 800 °C in a muffle furnace for 4 hours. ZrO_2 can be identified as a thermally stable material since it has high Hüttig and Tamman tem-

peratures (812.7 °C and 1,354.5 °C, respectively [75]), which are both higher than the operating temperatures. Nevertheless, the same calcination procedure is followed for both zirconia and ceria since a comparison between the supports is aimed to be done.

3.3.2. Preparation of Active Catalysts

All catalysts used in this study are prepared by the method of incipient-to-wetness impregnation.The basic steps of preparation are the same for all catalysts except for the preparation of precursor solutions. Thus, the impregnation procedure that will be described for 1 wt.% Rh/ZrO applies to all of the prepared catalysts.

For the preparation of 1 wt.% Rh/ZrO_2, a solution containing rhodium precursor is prepared. The precursor is available in the form of a 10 wt.% stock solution. The amount of stock solution that will provide the necessary amount of rhodium is first weighed (0.2 g of stock solution for preparing 2 g of catalyst), then the solution is diluted with deionized water to obtain approximately 0.6 mL of solution per gram of ZrO_2, which is the necessary amount to completely wet the support. 1.98 g of prepared ZrO_2 is placed in a Büchner flask and mixed ultrasonically under vacuum for 30 min. Then, the prepared precursor solution is impregnated on the support with the help of a peristaltic pump as shown in Figure 3.1. The resulting slurry is left in the ultrasonic mixer for 1.5 h under vacuum to ensure complete mixing. Afterwards, the catalyst is dried overnight in an oven at 110 °C. Lastly, the catalyst is calcined in a muffle furnace at 800 °C for 4 hours.

Same rhodium solution is prepared for the preparation of 1 wt.% Rh/CeO_2, except this time the solution is diluted with less water since CeO_2 can be completely wetted with approximately 0.55 mL g^{-1} of support. Then, the solution is impregnated on the support by following the same procedure described above.

For the preparation of 5 wt.% Co/ZrO_2, the necessary amount of cobalt precursor ($Co(NO_3)_2{\cdot}6H_2O$) is weighed (0.494 g for 2 g of catalyst) and dissolved in 0.6 mL water per gram of support. Lastly, same amount of cobalt precursor is dissolved in 0.55 mL

per gram of CeO_2 for the preparation of 5 wt.% Co/CeO_2.

3.3.3. Pretreatment

It is necessary to reduce the oxidized metal sites of the catalysts in order to activate the catalysts. All catalysts are reduced *in situ* in the presence of 40 NmL min^{-1} H_2 flow at 800 °C for 2 hours prior to the reaction tests. After reduction, N_2 is flowed over the catalyst bed until the reaction tests to prevent exposure to air.

3.4. Reaction Tests

The reaction tests are carried out in a quartz packed bed reactor (L = 80 cm, d_{in}=10 mm). As shown in Figure 3.4, approximately 1 cm in height quartz wool is placed in the middle of the reactor and catalyst bed is placed on the quartz wool. 20 mg of catalyst is used in the reactions and the catalyst bed is diluted with approximately 700 mg of α-alumina (45-60 mesh size) in order to achieve a bed length of 1 cm. This provides $L_{bed}/d_{particle}$ and $d_{tube}/d_{particle}$ ratios close to 35, which are acceptable for ignoring diffusive transport terms and assuming plug flow behavior, respectively [76].

3.4.1. Activity Tests

Activity tests are conducted in order to compare the catalytic activities of supported Rh and Co catalysts and to observe the effects of reaction temperature and molar CO_2/glycerol (CO_2/G) ratios in dry reforming of glycerol. All catalytic tests are conducted in gas phase with a total flow rate of 40 Nml min^{-1} and a fixed glycerol feed of 4 Nml min^{-1}. Nitrogen is used as an inert balance gas. Flow rate of N_2 is adjusted so that total flow rate and glycerol flow rate are fixed while changing CO_2/G ratios. At changing temperatures, CO_2/G ratio is kept at 1, which is observed to give the highest glycerol conversion and H_2 yields. At changing CO_2/G ratios, temperature is kept at 750 °C, at which coke formation is found to be negligible. Details of the experiments are given in Table 3.6.

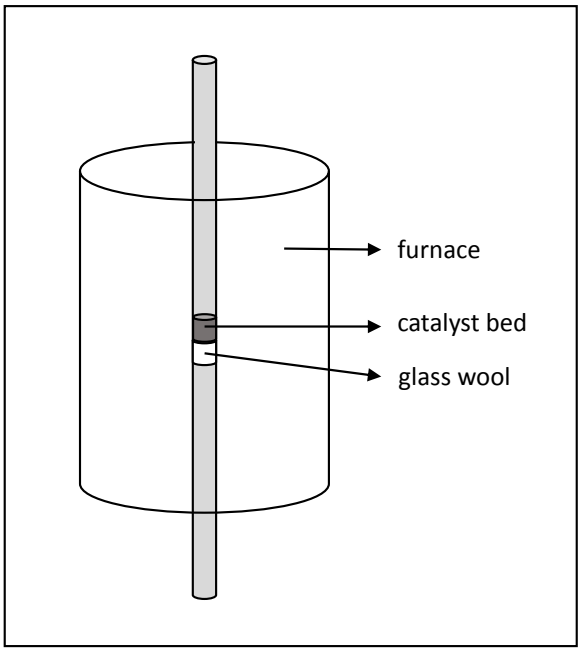

Figure 3.4. Diagram of the packed bed reactor.

Table 3.6. Reaction conditions for catalytic tests (Default values of reaction temperature and CO_2/G ratio are shown in boldface).

Parameter	**Value**
Reaction Temperature (°C)	600, 650, 700, **750**
Glycerol Flow Rate (Nml min^{-1})	4
CO_2/G	0,**1**,2,3,4
Catalyst Amount (mg)	20
Total Flow Rate (Nml min^{-1})	40
W/F (mg min Nml^{-1})	0.5

3.4.2. Blank Tests

Blank tests are carried out in order to observe the extent of homogeneous glycerol conversion and to verify that the glass wool, quartz reactor and the α-alumina used as bed diluent are inert towards the reaction. The tests were conducted at different temperatures (600, 650, 700 and 750 °C) and CO_2/G ratios (1,2,3,4) to observe the effects of these parameters on the homogeneous reaction. As done in the catalytic tests, total flow rate and glycerol feed flow rates are kept constant at 40 and 4 Nml min^{-1}, respectively.

3.4.3. Experimental Procedure

A step-by-step walk through of the experimental procedure is provided as follows:

- Catalyst bed is loaded into the reactor, which is then attached to the experimental system by the use of stainless steel couplings.
- After verifying that there is no leakage, the furnace is turned on and the reactor is brought to the reduction temperature (800 °C) in one hour under N_2 flow. Reactor effluent is sent to ventilation by utilizing the 3-way valve installed between the two cold traps.
- When the reactor reaches the reduction temperature, H_2 with a flow rate of 40 Nml min^{-1} is sent to the reactor and N_2 flow is turned off.
- About 25 minutes before the end of reduction, the carrier gases and the GCs are turned on consecutively. Temperatures of the ovens and detectors of the GCs are brought to the analysis conditions by turning the systems on.
- Reduction is stopped after two hours by turning the H_2 flow off and turning the N_2 flow back on. Furnace is turned off and the reactor is left to cool down to the reaction temperature. Furnace is set to the reaction temperature afterwards. Currents of the GCs are turned on provided that the analysis conditions are reached.
- Heating lines are turned on 30 minutes prior to the start of the experiment. N_2 flow is set to the value required by the experiment.

- The cold traps are packed with ice 10 minutes prior to the start of the experiment. The pump is turned on and glycerol is sent to purge by utilizing the 3-way valve installed on the glycerol line.
- Glycerol flow is directed to the reactor. After two minutes (the time that takes for glycerol to reach the injection nozzle), CO_2 feed is turned on and the experiment is started. The reactor effluent is sent to product analysis by utilizing the 3-way valve installed between the two cold traps. The flow is directed to GC-2 throughout the experiment, except for when sampling is done with GC-1.
- Product stream is analyzed by two GCs at the 30^{th}, 75^{th}, 120^{th}, 165^{th}, 210^{th}, 250^{th} and 300^{th} minutes of the experiment. The analysis is always done with GC-2 first, then the flow is directed to GC-1 and sampling is done after two minutes. Then, the product stream is directed back to GC-2.
- After the last sampling is done, the furnace, heating lines and the glycerol feed are turned off.
- N_2 flow rate is adjusted to feed analysis conditions and feed stream is sent to feed gas analysis.
- After feed gas data is taken, GC detectors are turned off and GCs are left to cool down. After the GC detector temperatures fall below 100 °C, GCs and carrier gases are turned off consecutively.
- N_2 is sent through all lines and then directed to the reactor, which is left to cool down to room conditions under N_2 flow.

3.4.4. Measurement of Catalytic Activities

Activities of the tested catalyst can be evaluated by looking at various parameters, namely glycerol conversion (X_G), CO_2 conversion (X_{CO_2}) and product yields and selectivities. Conversion of CO_2 is calculated using Equation 3.1.

$$X_{CO_2}(\%) = \frac{F_{CO_2,in} - F_{CO_2,out}}{F_{CO_2,in}} \times 100 \tag{3.1}$$

where $F_{CO_2,in}$ and $F_{CO_2,out}$ are molar inlet and outlet flow rates of CO_2, respectively in mol min^{-1}.

Since product analysis is done on the basis of gaseous products, it is not possible to calculate the conversion of glycerol by using the molar flow rate of glycerol in the product stream. In this case an atomic balance over hydrogen is conducted to calculate the amount of converted glycerol. In dry reforming conditions, it is not possible to make a carbon balance due to the presence of CO_2 in the feed, so hydrogen balance is utilized in various studies [10,11,47,58,60]. Molar flow rates of all gaseous products that contain H atoms are used in the calculation, as shown in Equation 3.2. It should be noted, however, that condensible species containing H atoms (water, acrolein, acetaldehyde, etc.) can not be included in the calculation. Thus, X_G is more correctly defined as conversion of glycerol into gaseous products.

$$X_G(\%) = \frac{2F_{H_2} + 4F_{CH_4} + 4F_{C_2H_4} + 6F_{C_2H_6}}{8F_{G,in}} \times 100 \tag{3.2}$$

where F_i is the molar flow rate of species i in the outlet stream and $F_{G,in}$ is the molar flow rate of species glycerol in the feed stream, both in mol min^{-1}.

In order to see the amount of condensed products that are not taken into account in the calculations, a mass balance is done over the inlet and outlet streams. Inlet and outlet mass flow rates of the gaseous components are calculated by multiplying the molar flow rates with their molecular weights. Mass flow rate of liquid glycerol is calculated by multiplying the volumetric flow rate of glycerol with its density ($\rho = 1.25$ g ml^{-1}). The resulting mass balance is defined as the ratio of the mass flow rate of the analyzed products stream over the mass flow rate of the inlet stream as shown in Equation 3.3:

$$\text{Mass balance } (\%) = \frac{\text{mass flow rate of product stream}}{\text{mass flow rate of inlet stream}} \times 100 \tag{3.3}$$

The mass balances change between 0.75% and 92.5% depending on the catalyst used and operating conditions. It is an important indicator of the amount of condensible products that are produced in the reactions. For example, mass balances are closer to 100% for the tests conducted at higher temperatures, which indicates that more glycerol is converted into gaseous products. Moreover, tests conducted at higher CO_2/G ratios give lower mass balances, since more H_2 is produced at these tests, which cannot be included in the mass balance.

Product yields and selectivities are other important measures of catalytic activity. Product yield (Y_i) and selectivity (S_i) are calculated by using Equations 3.4 and 3.5.

$$Y_i = \frac{\text{Moles of species } i \text{ in gaseous products}}{\text{moles of glycerol fed}} \tag{3.4}$$

$$S_i = \frac{\text{Moles of species } i \text{ in gaseous products}}{\text{moles of glycerol converted}} \tag{3.5}$$

4. RESULTS AND DISCUSSION

4.1. Effect of Temperature

Considering that dry reforming of glycerol is an endothermic reaction, temperature is an important parameter that affects the extent of the reaction. Effect of temperature on reactant conversions and product distributions were observed by conducting experiments at temperatures of 600, 650, 700 and 750 °C.

Effect of temperature on glycerol conversion over Rh/ZrO_2 (RhZr), Rh/CeO_2 (RhCe), Co/ZrO_2 (CoZr) and Co/CeO_2 (CoCe) catalyst samples as well as in the blank tests can be seen in Figure 4.1. Glycerol is a thermally unstable chemical, which decomposes at high temperatures. In order to see the extent of glycerol decomposition, a set of blank tests are conducted at four temperatures under dry reforming conditions ($CO_2/G = 1$). The results show that homogeneous thermal decomposition of glycerol takes place significantly at high temperatures. 9% of fed glycerol is decomposed at 600 °C, whereas glycerol conversion increases up to 48% at 750 °C. In the activity tests, it is observed that regardless of the catalyst used, glycerol conversion increases with increased temperature. This is expected since, as mentioned before, both glycerol decomposition (Equation 2.7) and dry reforming (Equation 2.7) reactions are endothermic, which are favored both kinetically and thermodynamically at elevated temperatures.

At lower temperatures, presence of catalyst does not have a significant effect on glycerol conversion compared to blank tests. At 600 °C, highest glycerol conversion is observed over RhZr, which differs from the blank test only by 5%. Similarly, at 650 °C, all samples yield similar glycerol conversions that change between 26-30%, whereas conversion from the blank test is ≈22%. However, at higher temperatures, a clear effect of catalyst on glycerol conversion can be seen. When the catalysts are examined individually, it is observed that samples that are supported on the same support exhibit similar glycerol conversion trends. Over ZrO_2 supported samples, there

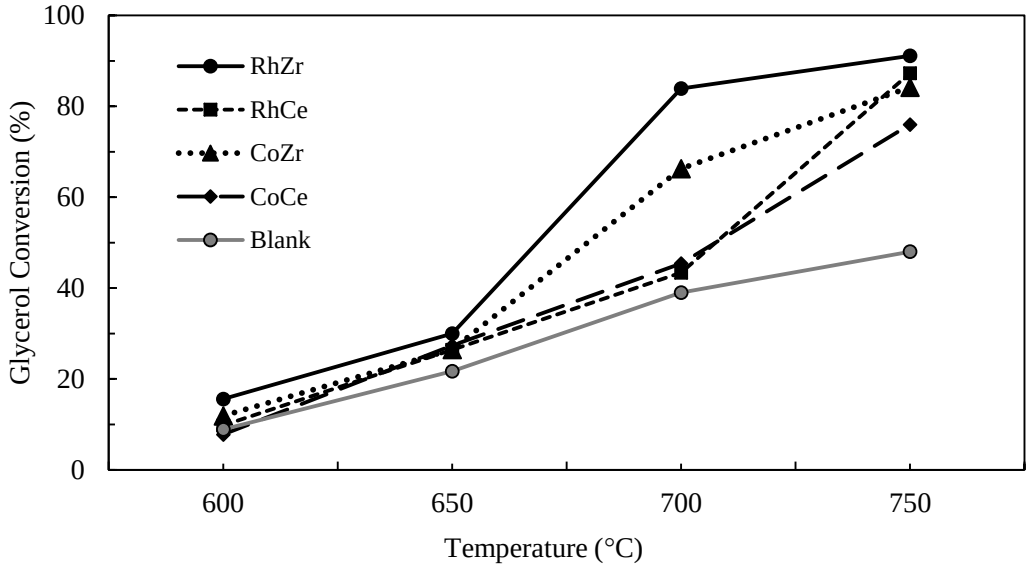

Figure 4.1. Glycerol conversions with respect to temperature at $CO_2/G = 1$.

is a sharp increase of glycerol conversion (54% and 40% increase over RhZr and CoZr, respectively) when the temperature increases from 650 to 700 °C. A jump in glycerol conversion with temperature is observed over CeO_2 supported samples as well, but unlike ZrO_2 supported samples, this jump is seen when the temperature increases from 700 to 750 °C. At 700 °C, CeO_2 supported samples exhibit glycerol conversions still comparable to the blank test (43% and 45% over RhCe and CoCe, respectively, 39% in the blank test) but almost 40% increase in glycerol conversion is observed over both samples at 750 °C. At the highest tested reaction temperature, all catalysts show glycerol conversions much higher than the blank test, which shows that catalytic activity is enhanced at elevated temperatures.

Figure 4.2 represents the changes in CO_2 conversions with increasing temperature over all samples. No CO_2 conversion is observed in the blank tests at any of the temperatures tested. In fact, CO_2 conversions are found to be negative and decreasing negatively with increased temperature, showing that CO_2 is a product of homogeneous glycerol decomposition. Other detected gaseous products of glycerol decomposition are H_2, CO, CH_4, C_2H_6 and C_2H_4. These results are in accordance with the results of Chiodo *et al.* [70], who additionally reported the presence of acetone, acetaldehyde,

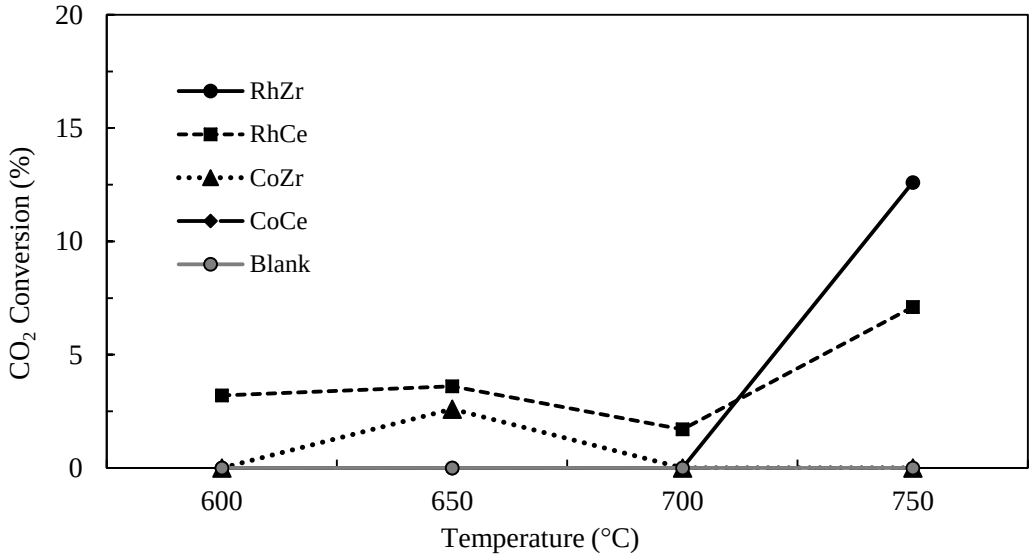

Figure 4.2. Carbon dioxide conversions with respect to temperature at $CO_2/G = 1$.

ethanol and propanol upon analyzing the condensed phase stream. In the activity tests, no CO_2 conversion is observed up to the temperature of 750 °C. At this temperature, RhZr and RhCe samples show CO_2 conversions of 12.6% and 7.1%, respectively, whereas no conversion is observed over Co based samples. It should be noted here that the default CO_2/G ratio is selected as 1 while reaction temperature is studied. However, CO_2 conversion is observed over these samples at increased CO_2/G ratios, which will be discussed in detail in Section 4.2. CO_2 conversions can occasionally be seen over RhCe and CoZr at temperatures below 700 °C (Figure 4.2), but these are very low (1-3%) and do not follow a trend with temperature, so they are neglected.

A thermodynamic analysis is done in order to determine the thermodynamic limits of reactant conversions and product distributions at studied reaction conditions. The thermodynamic analysis is done with the Gibbs Free Energy Reactor Unit-Op (GIBS) of CHEMCAD 7.1.0 chemical process simulation software. GIBS utilizes the Gibbs free energy minimization method provided that the inlet stream is identified. H_2, CH_4, CO, CO_2, glycerol, H_2O, C(s), N_2, C_2H_4 and C_2H_6 are the components that are taken into consideration in the thermodynamic calculations. Feed compositions and reaction temperatures tested in the activity tests are mimicked in the thermodynamic

analysis. Thermodynamic limits of CO_2 conversion at the studied reaction conditions are presented in Figure 4.3. It can be seen that at temperatures below 650 °C, CO_2 conversion cannot be achieved thermodynamically and CO_2 is produced. This is in accordance with the results of Wang *et al.* [9], who pointed out that conversion of CO_2 is possible at temperatures over 677 °C. It can be said that CO_2 producing reactions such as CO decomposition (Equation 2.22) or carbon gasification with steam (Equation 2.20) are dominating at lower temperatures, whereas CO_2 spending reactions such as RWGS (Equation 2.2) and methane dry reforming (Equation 2.1) are favored at higher temperatures owing to their endothermic nature. Even though it is thermodynamically possible to convert CO_2 at 700 °C, no CO_2 conversion is achieved experimentally at this temperature, which may be attributed to kinetic limitations, considering that CO_2 feed is also low (CO_2/G = 1).

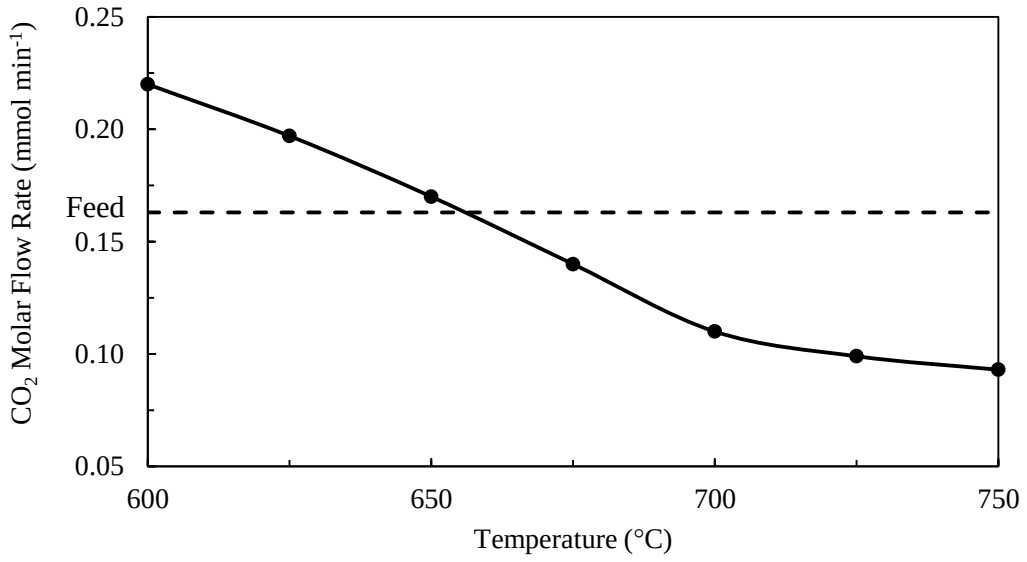

Figure 4.3. Thermodynamic limits of carbon dioxide flow rate in the product stream with respect to temperature (CO_2/G = 1).

Product distributions are important as much as reactant conversions when evaluating catalytic activity, since it is desired to maximize the yield of syngas while minimizing unwanted products such as methane, ethylene and ethane. Product distributions over the samples and in blank tests at four temperatures are tabulated in Tables 4.1 - 4.5. Analyzing the product distributions, it is observed that both H_2 and

CO production increases with increasing temperature, as their yields increase continuously with temperature over all samples and blank tests. The increase in syngas yields with temperature can be explained with favored decomposition (Equations 2.7-2.15), dry reforming (Equations 2.6 and 2.1) and steam reforming reactions (reverse of Equation 2.16) that produce H_2 and CO. Similar to glycerol conversion, it is noticed that H_2 yields increase drastically (almost quadruple) with a temperature increase from 650 to 700 °C over ZrO_2 supported samples. A similar jump in H_2 yields are observed over CeO_2 supported samples when the temperature is increased from 700 to 750 °C.

Syngas ratio (H_2/CO) is also an important parameter, since product selectivities of Fischer-Tropsch reactions depend on the H_2/CO ratio of the syngas used. As mentioned earlier, long chain hydrocarbons, carbonyls and carboxylic acids require low syngas ratios close to 1 [12,22]. In the blank tests, syngas ratios are not affected significantly by the temperature. At low temperatures, syngas ratio changes between 0.48 and 0.86 depending on the catalyst used. As the temperature increases, syngas ratio also increases and reaches 1 at 750 °C over all catalysts (Tables 4.1 - 4.5). Dry reforming of glycerol (Equation 2.6) inherently produces a syngas ratio of 0.75. Observation of syngas ratios that exceed this value suggest the presence of hydrogen producing side reactions, such as glycerol dehydration, methane steam reforming or methane decomposition. Moreover, low CO_2 conversions suggest that RWGS reaction does not take place to its full extent and this results in less H_2 converted to CO and H_2O.

Table 4.1. Product distributions over Rh/ZrO_2 at $CO_2/G = 1$.

T (°C)	**Product Yields (mol/(mol of glycerol fed))**					
	H_2	**CO**	**CH_4**	**C_2H_4**	**C_2H_6**	**H_2/CO**
600	0.42	0.49	0.082	0.018	0.0032	0.86
650	0.62	0.98	0.22	0.052	0.010	0.63
700	2.58	2.38	0.36	0.0067	0.013	1.08
750	2.82	2.79	0.40	0.0015	0.0036	1.01

Table 4.2. Product distributions over Rh/CeO_2 at $CO_2/G = 1$.

T (°C)	**Product Yields (mol/(mol of glycerol fed))**					
	H_2	**CO**	**CH_4**	**C_2H_4**	**C_2H_6**	**H_2/CO**
600	0.19	0.39	0.078	0.019	0.0034	0.48
650	0.44	0.99	0.24	0.053	0.012	0.44
700	0.70	1.44	0.42	0.073	0.016	0.49
750	2.51	2.51	0.48	0.0041	0.0069	1.00

Methane, ethane and ethylene are unwanted byproducts that decrease the syngas yield and may generate the need of separation processes that are costly in industrial production. Thus, their yields should be minimized by adjustment of operating conditions and employment of a selective catalyst. CH_4 yield increases with increasing temperature mainly due to the production of acetaldehyde that further decomposes to CH_4 by Equation 2.15. Since glycerol conversion increases with temperature, CH_4 yields also increase. However, when CH_4 selectivities are examined (Product selectivities over all catalysts and blank tests are presented in Table 4.6), it is observed that CH_4 selectivity increases up to a temperature of 650-700 °C, depending on the catalyst used, and then decreases upon further increase in temperature. This shows that at lower temperatures, CH_4 producing reactions such as acetaldehyde decomposition are dominant, whereas at higher temperatures, CH_4 is consumed by steam (MSR) and dry (MDR) reforming reactions as well as methane decomposition. Once methane is produced, high temperatures are needed for converting it due to its stable nature. Thermodynamically, MSR and MDR do not take place at temperatures below 620 and 650 °C, respectively [18]. Methane selectivity in the blank tests continue to increase at higher temperatures (Table 4.6), showing that MSR and MDR cannot take place homogeneously. Similarly, ethane and ethylene yields peak at 700 °C over all samples, but start to decrease at higher temperature due to further decomposition or reforming. The same trend is observed in the blank tests as well, which shows that unlike methane, decomposition of C_2H_4 and C_2H_6 can take place homogeneously.

Table 4.3. Product distributions over Co/ZrO_2 at $CO_2/G = 1$.

T (°C)	**Product Yields (mol/(mol of glycerol fed))**					
	H_2	**CO**	**CH_4**	**C_2H_4**	**C_2H_6**	**H_2/CO**
600	0.29	0.42	0.074	0.017	0.0032	0.67
650	0.53	0.91	0.20	0.048	0.010	0.58
700	1.66	1.91	0.42	0.050	0.017	0.87
750	2.33	2.31	0.49	0.016	0.012	1.01

Table 4.4. Product distributions over Co/CeO_2 at $CO_2/G = 1$.

T (°C)	**Product Yields (mol/(mol of glycerol fed))**					
	H_2	**CO**	**CH_4**	**C_2H_4**	**C_2H_6**	**H_2/CO**
600	0.17	0.31	0.054	0.016	0.0023	0.54
650	0.47	0.98	0.24	0.054	0.012	0.48
700	0.80	1.44	0.41	0.072	0.016	0.55
750	1.95	1.99	0.49	0.030	0.013	0.98

Table 4.5. Product distributions in the blank tests at $CO_2/G = 1$.

T (°C)	**Product Yields (mol/(mol of glycerol fed))**					
	H_2	**CO**	**CH_4**	**C_2H_4**	**C_2H_6**	**H_2/CO**
600	0.14	0.41	0.09	0.017	0.0034	0.34
650	0.37	0.81	0.19	0.044	0.0093	0.46
700	0.60	1.36	0.39	0.073	0.014	0.44
750	0.72	1.52	0.51	0.079	0.012	0.47

Table 4.6. Product selectivities over all samples and in the blank tests with varying temperature (CO_2/G = 1).

	T (°C)	Product Selectivities (mol/mol of glycerol converted)				
		H_2	CO	CH_4	C_2H_4	C_2H_6
Rh/ZrO_2	600	2.66	3.11	0.52	0.11	0.020
	650	2.08	3.27	0.74	0.17	0.035
	700	3.07	2.84	0.43	0.0080	0.015
	750	3.10	3.06	0.44	0.0016	0.0040
Rh/CeO_2	600	1.94	4.01	0.79	0.19	0.034
	650	1.67	3.75	0.90	0.20	0.045
	700	1.61	3.31	0.97	0.17	0.036
	750	2.87	2.87	0.55	0.0047	0.0079
Co/ZrO_2	600	2.39	3.55	0.62	0.14	0.027
	650	2.00	3.45	0.77	0.18	0.038
	700	2.50	2.87	0.64	0.075	0.025
	750	2.76	2.75	0.58	0.019	0.014
Co/CeO_2	600	2.13	3.95	0.69	0.20	0.030
	650	1.71	3.59	0.88	0.20	0.044
	700	1.76	3.18	0.91	0.16	0.035
	750	2.57	2.61	0.65	0.039	0.017
Blanks	600	1.58	4.60	0.96	0.19	0.038
	650	1.71	3.75	0.88	0.20	0.043
	700	1.53	3.48	0.99	0.19	0.036
	750	1.49	3.17	1.05	0.16	0.024

Reaction temperature is also an important factor for catalyst deactivation mechanisms. Thermodynamically, carbon formation is inhibited at high temperatures as shown in Figure 4.4. At CO_2/G ratio of 1, coke is thermodynamically not observed at temperatures over 700 °C, due to favored carbon gasification reactions (Equations 2.19, 2.20 and reverse of Equation 2.22), which are endothermic. A visual proof of decreased carbon formation is presented in Figure 4.5. Images of the catalyst beds including RhZr and α-Al_2O_3 as diluent were taken after testing at varied operating temperatures. It can be seen that as the operating temperature is increased amount of

coke deposited on the catalyst bed decreases as well, as verified by the lighter color of the bed at elevated temperatures. Moreover, activity loss of the tested samples were found to be less at higher temperatures as can be seen in Table 4.7, which may stem from decreased coke deposition. Activity loss is quantified by Equation 4.1, where $F_{H_2,0.5h}$ is the molar flow rate of H_2 at the first 0.5 hour of the reaction in mol min^{-1}, whereas $F_{H_2,5h}$ is the molar flow rate of H_2 after the 5^{th} hour of reaction.

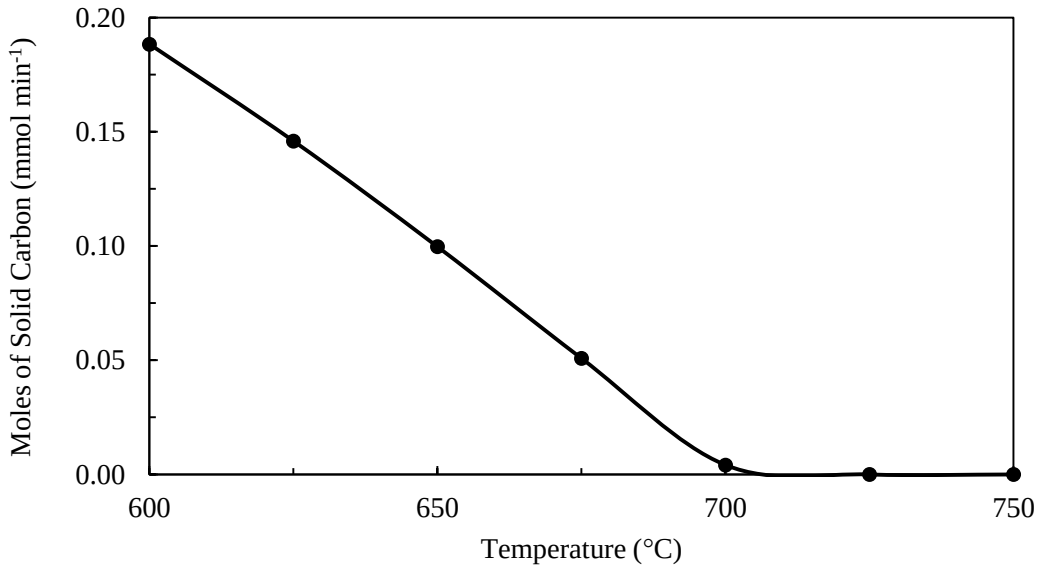

Figure 4.4. Thermodynamic limits of carbon production with respect to temperature (CO_2/G = 1).

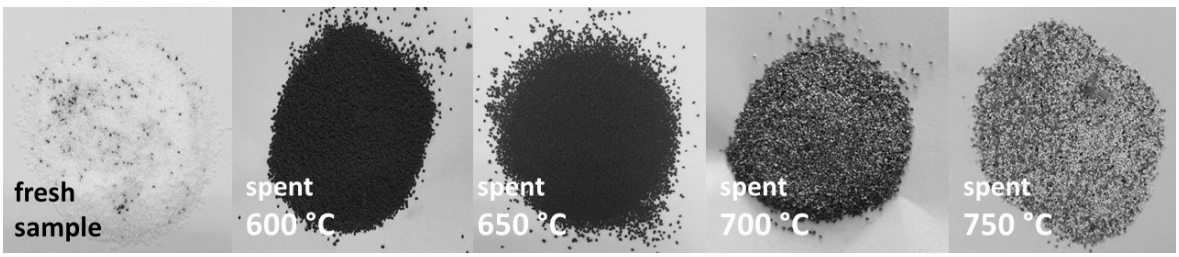

Figure 4.5. Visuals of the spent catalysts at varying reaction temperatures.

Analysis of Table 4.7 shows that acitivity loss of the tested catalysts decrease as the operating temperatures increase. For example, there is a 37.6% activity loss over RhZr at 600 °C, whereas no deactivation is observed at 700 °C. However, further increase of the temperature to 750 °C creates an activity loss of 11.7%, which may be

attributed to sintering of the active metal. Acitivity loss of RhCe also decreases as the operating temperature increases and at 750 °C, final activity is higher than the initial activity.

$$\text{Activity Loss}(\%) = \frac{F_{H_2,0.5h} - F_{H_2,5h}}{F_{H_2,0.5h}} \times 100 \tag{4.1}$$

Table 4.7. Activity losses observed over tested samples at varied operating temperatures (CO_2/G = 1).

	Activity Loss Based on H_2 production (%)			
T (°C) / Catalyst	**600**	**650**	**700**	**750**
RhZr	37.6	44.8	0.3	11.7
RhCe	32.5	17.5	7.4	-7.5
CoZr	61.7	53.5	39.4	-8.2
CoCe	54.1	28.3	45.6	-47.8

The aforementioned results suggest that higher temperatures are favorable for glycerol dry reforming. Among the temperatures tested, 750 °C is the optimum temperature both in terms of glycerol and CO_2 conversion and synthesis gas production.

4.2. Effect of CO_2/G Ratio

Feed composition is another important parameter that affects the reaction mechanism and consequently, product distributions. In order to observe the effect of CO_2 composition in the feed, different CO_2/G ratios between 1 and 4 have been tested at 750 °C, which is the optimum temperature for syngas production. Experiments with no CO_2 in the feed (CO_2/G = 0) were also conducted to see the extent of catalytic glycerol decomposition over all catalyst samples. Effect of CO_2/G ratio on glycerol conversions can be seen in Figure 4.6. A clear trend can be observed over all catalysts showing that glycerol conversion decreases with increased CO_2 in the feed. This finding is in contrast

with the published work on methane and ethanol dry reforming reactions that report an opposite effect [46, 77, 78]. On the other hand, Siew *et al.* [10, 79] worked on GDR and reported that glycerol conversion peaked at a CO_2/G ratio of 1.67 (98.7%), but then decreased with increasing CO_2/G ratio (68.8% at CO_2/G = 5), which is comparable to the results of this study. Interestingly, as shown in Figure 4.6, glycerol conversion is not affected by the CO_2 composition in the feed in the blank tests and remains at ≈48% at all CO_2/G ratios tested. Thus, the hindering effect of CO_2 presence in the feed on glycerol conversion is only seen in the presence of catalyst. This result may be attributed to two things: First, there may be a competition between glycerol and CO_2 on the active sites of the catalysts. Second, the decreasing trend of glycerol conversion with increasing CO_2/G may possibly stem from the definition of glycerol conversion (Equation 3.2). Conversion of glycerol is calculated by applying a hydrogen balance over the gaseous products, as described in Section 3.4.3 in detail. This definition is prone to be erroneous since condensable products cannot be included in the calculations. An increase in CO_2 composition in the feed results in less H_2 production, due to its conversion to H_2O via favored RWGS reaction (see Table 4.8). Since the flow rate of H_2O cannot be included in the calculation of glycerol conversion, this may result in decreased conversions. In order to offset this effect, it was assumed that all of the converted CO_2 is spent in RWGS reaction to produce H_2O and "corrected" glycerol conversions were calculated. Figure 4.7 shows the "corrected" vs. "original" glycerol conversions with respect to CO_2/G ratios over RhCe sample, which is selected as a representative of the behavior that is observed over all samples. As can been seen from the graph, there is a less steep but still decreasing trend of glycerol conversion with respect to CO_2/G ratio. Therefore, the second proposition is ruled out.

Effect of CO_2/G ratio on CO_2 conversion can be seen in Figure 4.8. Similar trends are observed over all samples, where there is a steep increase in CO_2 conversion up to a CO_2/G of 2, and then it flats out at higher CO_2/G ratios. A similar trend of CO_2 conversion with respect to CO_2/G ratio was obtained by Bej *et al.* [78], who studied EDR and reported that CO_2 conversion increased up to a CO_2/G of 1.4, and then decreased with increasing CO_2/G. According to thermodynamic calculations, thermodynamic limit of CO_2 conversion decreases continuously with increasing CO_2/G

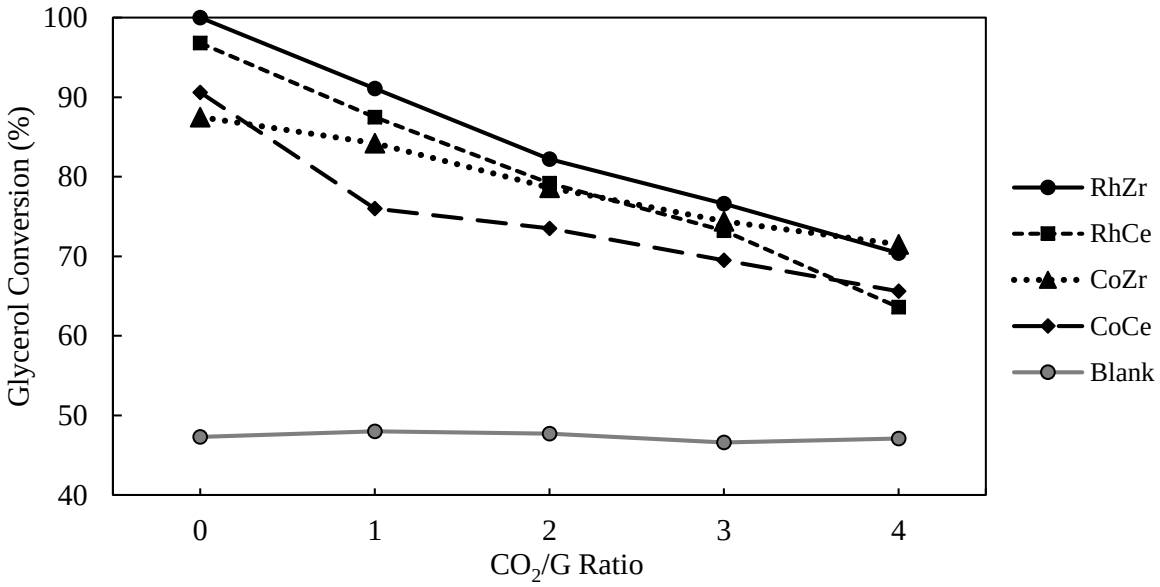

Figure 4.6. Glycerol conversions with respect to CO_2 ratio at T=750 °C.

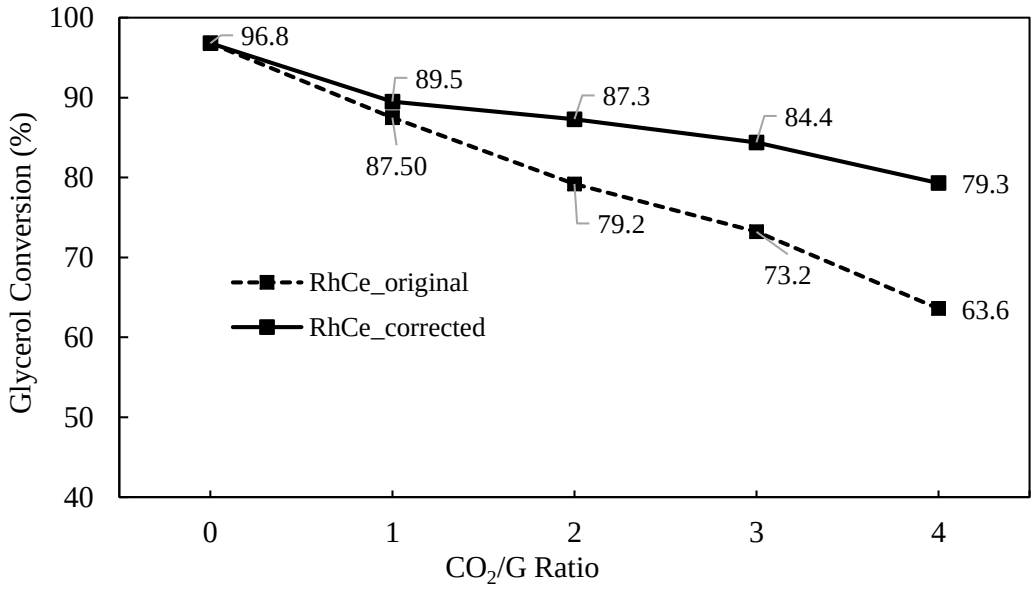

Figure 4.7. Corrected vs original glycerol conversions with respect to CO_2 ratio at T=750 °C.

ratios as shown in Fiugre 4.8. The increase in CO_2 conversion at lower ratios can be attributed to the elevated reaction rate due to increased concentration of CO_2. However, at higher ratios, CO_2 conversions approach the thermodynamic limit (especially in the case of RhZr), which slows down the reaction rate and CO_2 conversions cannot increase any further. In fact, a small decrease in CO_2 conversion over RhZr is visible as CO_2/G is increased from 3 to 4 (3% decrease) and it should be noted that RhZr gives CO_2 conversions closest to thermodynamic limits among the other samples. CoZr and CoCe give the lowest CO_2 conversions which are ca. 35% lower than the thermodynamic limit and CO_2 conversions continue to increase slightly (1% increase) at CO_2/G ratio of 4 over these samples.

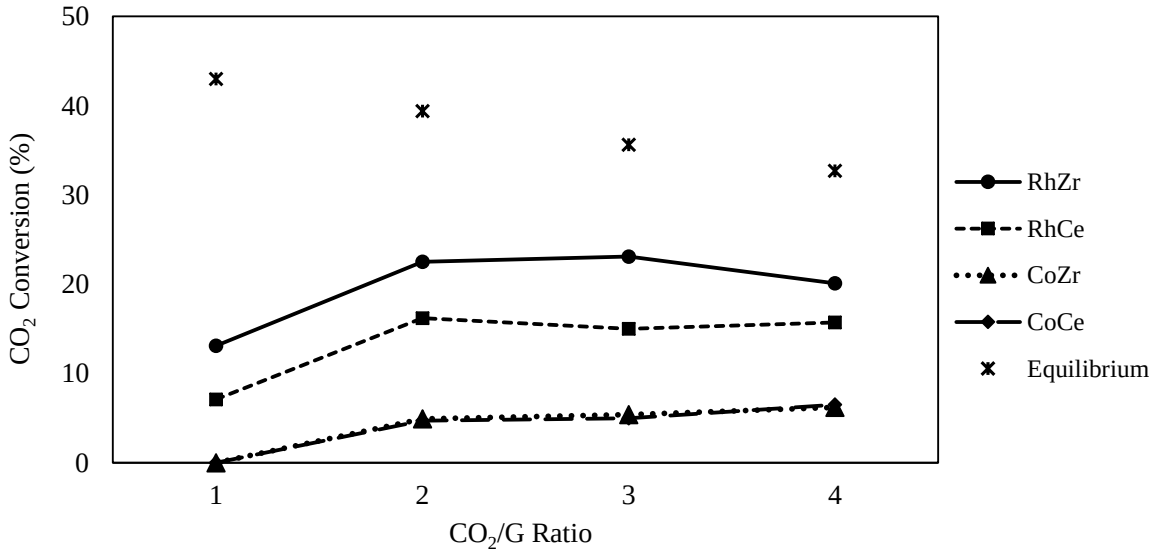

Figure 4.8. CO_2 conversions with respect to CO_2/G ratio at T=750 °C.

Product distributions with respect to CO_2/G ratios over RhZr, RhCe, CoZr and CoCe catalysts and results of the blank tests are presented in Tables 4.8-4.12, respectively. A decrease in hydrogen yields and an accompanying increase in CO yields are observed with increased CO_2 in the feed over all samples. This trend can be observed for RhZr sample in Figure 4.9. The simultaneous decrease in H_2 and increase in CO can be attributed to the presence of RWGS reaction, which shifts towards products side with increased CO_2 composition in the feed due to Le Chatelier's principle. It can be concluded that lower CO_2/G ratios are favorable for hydrogen production, whereas

higher CO_2/G ratios should be applied for CO production.

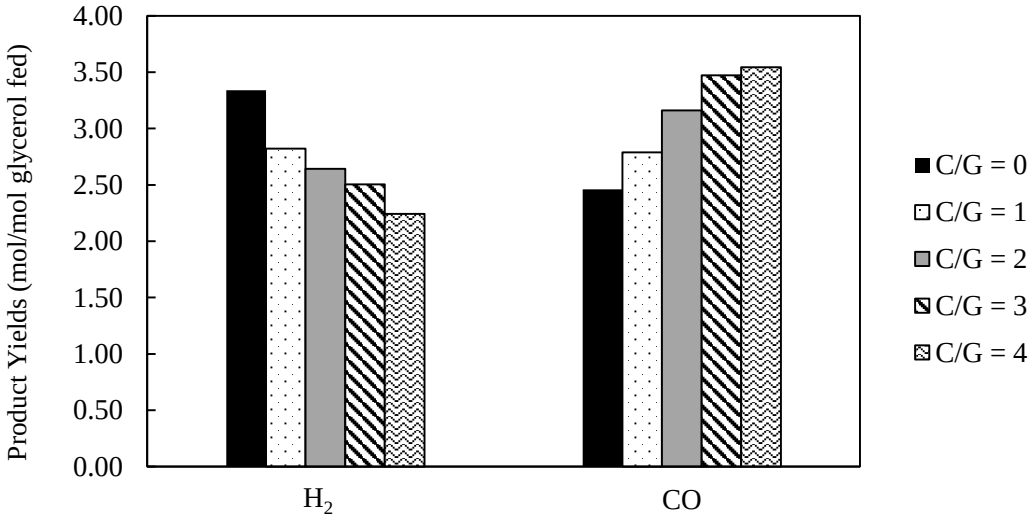

Figure 4.9. H_2 and CO yields over RhZr with respect to CO_2/G ratio at T=750 °C.

Behavior of methane and C_2 hydrocarbons depend on the catalyst that is employed. Over Rh based samples, it is observed that CH_4 and C_2 yields decrease as CO_2 feed increases. The decrease in CH_4 yields can be explained with favored MDR reaction (Equation 2.1). Similarly, C_2 hydrocarbons seem to be further decomposed into hydrogen and CO at higher CO_2 composition in the feed. This can be attributed to the increased oxygen in the system that is provided by CO_2. It has been shown by many studies that increased CO_2 in the feed helps gasification of deposited carbon, since CO_2 is reduced to CO and the released oxygen oxidizes the surface carbon [22]. Similarly, the released oxygen may help in the oxidation of C_2 hydrocarbons. On the other hand, yields of methane, ethane and ethylene does not show a clear decreasing trend over Co based catalysts. Moreover, CoZr and CoCe samples give methane yields that are always higher than RhZr and RhCe samples. This shows that Co based catalysts are not as active as Rh based catalysts in methane dry reforming. This result is in accordance with the findings of Ferreira-Aparicio *et al.* [80], who tested various transition metals including Rh and Co supported over alumina and silica, and reported that activity of Rh based samples were higher than Co based samples supported on both alumina and silica.

Table 4.8. Product distributions over Rh/ZrO_2 at T=750 °C.

CO_2/G	Product Yields (mol/(mol of glycerol fed))					
	H_2	CO	CH_4	C_2H_4	C_2H_6	C_2
0	3.34	2.46	0.33	0	0.0021	0.0021
1	2.82	2.79	0.40	0.0015	0.0036	0.0051
2	2.64	3.16	0.32	0.00018	0.0025	0.0027
3	2.50	3.47	0.28	0.00038	0.0012	0.0016
4	2.24	3.55	0.28	0.00063	0.0013	0.0020

Table 4.9. Product distributions over Rh/CeO_2 at T=750 °C.

CO_2/G	Product Yields (mol/(mol of glycerol fed))					
	H_2	CO	CH_4	C_2H_4	C_2H_6	C_2
0	2.91	2.09	0.47	0.0041	0.0070	0.011
1	2.51	2.51	0.48	0.0041	0.0069	0.011
2	2.24	2.74	0.45	0.0025	0.0072	0.0097
3	2.02	2.84	0.44	0.0023	0.0068	0.0091
4	1.77	2.93	0.38	0.0025	0.0046	0.0071

Table 4.10. Product distributions over Co/ZrO_2 at T=750 °C.

CO_2/G	Product Yields (mol/(mol of glycerol fed))					
	H_2	CO	CH_4	C_2H_4	C_2H_6	C_2
0	2.55	2.11	0.45	0.0090	0.0093	0.018
1	2.33	2.31	0.49	0.016	0.012	0.028
2	2.17	2.35	0.46	0.0081	0.0095	0.018
3	2.03	2.35	0.45	0.011	0.0089	0.020
4	1.93	2.44	0.44	0.0090	0.0094	0.018

Table 4.11. Product distributions over Co/CeO_2 at T=750 °C.

CO_2/G	**Product Yields (mol/(mol of glycerol fed))**					
	H_2	CO	CH_4	C_2H_4	C_2H_6	C_2
0	2.63	1.94	0.47	0.012	0.011	0.023
1	1.95	1.99	0.49	0.030	0.013	0.042
2	1.96	2.16	0.46	0.020	0.011	0.031
3	1.77	2.18	0.45	0.032	0.013	0.044
4	1.61	2.47	0.47	0.022	0.010	0.033

Table 4.12. Product distributions in the blank tests at T=750 °C.

CO_2/G	**Product Yields (mol/(mol of glycerol fed))**					
	H_2	CO	CH_4	C_2H_4	C_2H_6	C_2
0	0.73	1.55	0.48	0.081	0.012	0.092
1	0.72	1.52	0.51	0.079	0.012	0.091
2	0.75	1.60	0.48	0.082	0.012	0.095
3	0.73	1.54	0.46	0.081	0.012	0.094
4	0.74	1.54	0.47	0.079	0.012	0.091

4.3. Effect of Active Metal

Two active metals, namely rhodium and cobalt, are tested for their activity in glycerol dry reforming. Since highest CO_2 conversion is observed at the CO_2/G ratio of 4 and temperature of 750 °C, comparison of these catalysts are done at these conditions. Figures 4.10 and 4.11 give glycerol and CO_2 conversions over Rh and Co catalysts supported on ZrO_2 and CeO_2, respectively. When the figures are observed, an interesting trend stands out such that glycerol conversions stay almost unchanged regardless of the active metal, whereas CO_2 conversions change drastically. RhZr gives

a CO_2 conversion of 20.1%, whereas CO_2 conversion over CoZr is 6.2%. The same trend is observed on both supports. Thus, it can be suggested that glycerol conversion depends on the type of support, whereas CO_2 activation takes place on the active metal and Rh is better in CO_2 activation compared to Co. However, there is a strong agreement in the literature that activation of CO_2 occurs not only on the active metal, but rather on the support or the interfacial sites of the catalyst [81, 82]. It is possible that Rh is better dispersed on the studied supports compared to Co, which may result in increased number of interfacial sites between the active metal and support. In addition, CO_2 conversion capability of Rh has been proved by Puolakka *et al.* [83], who studied dry reforming of n-heptane over noble metal catalysts and reported the highest CO_2 conversions over Rh based samples compared to other noble metals.

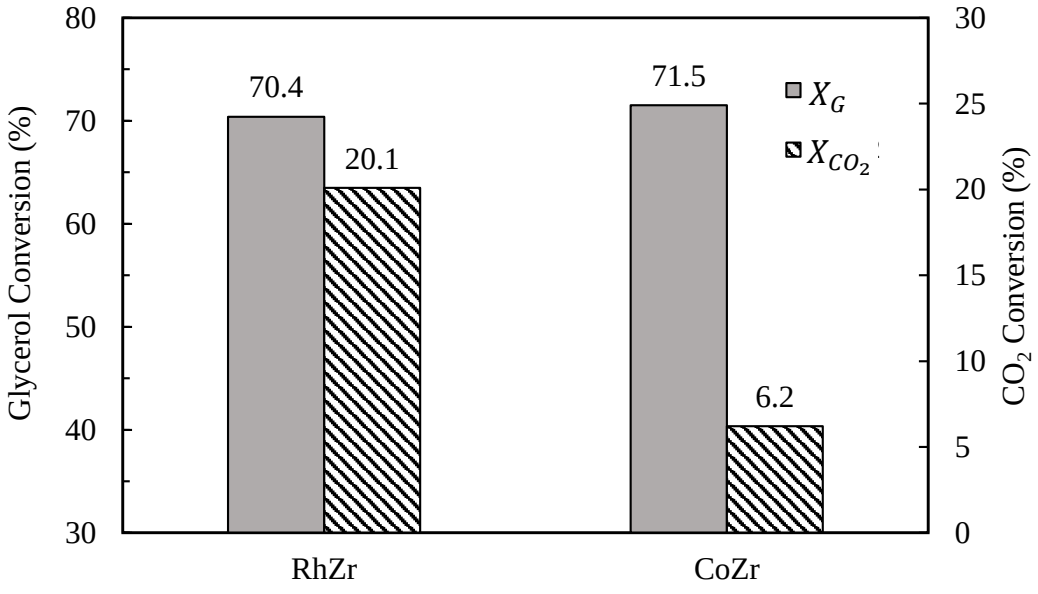

Figure 4.10. Glycerol and CO_2 conversions over Rh and Co supported on ZrO_2 (T=750 °C, CO_2/G = 4).

A comparison of product distributions over Rh and Co based samples can be seen in Table 4.13. At nearly same glycerol conversions, H_2 and CO yields observed over RhZr are greater compared to CoZr. On the contrary, CH_4 yields given by RhZr are remarkably lower. This is an indication of higher performance of Rh in methane activation, either by dry reforming or steam reforming reactions. Superior activity of

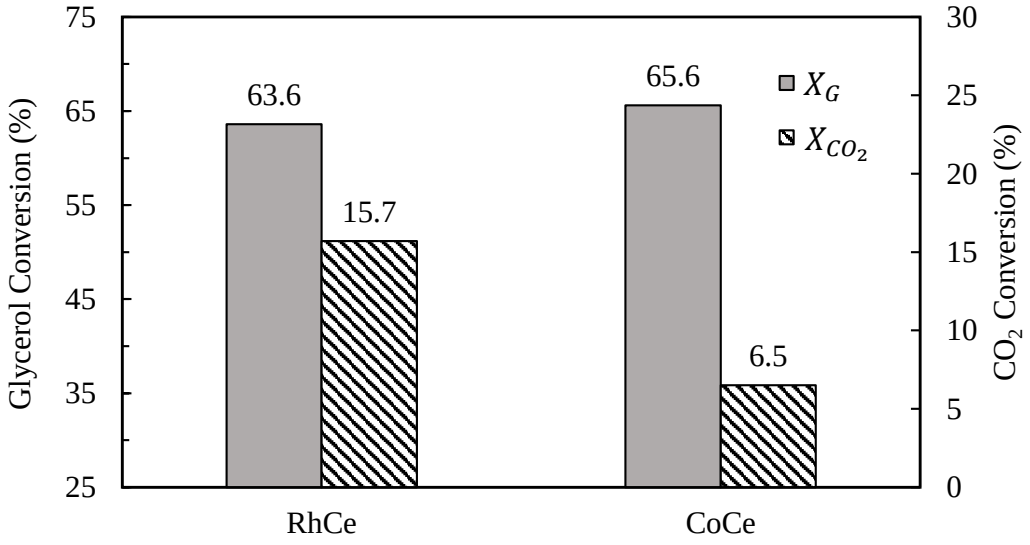

Figure 4.11. Glycerol and CO_2 conversions over Rh and Co supported on CeO_2 (T=750 °C, CO_2/G = 4).

Rh in MDR was also mentioned in Section 4.2. It has also been reported that Rh is more active compared to Co in methane steam reforming and glycerol steam reforming reactions [69]. Moreover, Liao *et al.* [84] studied the total dissociation enthalpy of methane on various metals and reported that total dissociation enthalpy of methane was the lowest on Rh compared to other noble metals. It is also noticeable that formation of C_2 hydrocarbons are much less over Rh supported samples compared to Co supported samples (tenfold difference between RhZr and CoZr). This is an expected result considering the C-C and C=C bond breaking capacity of Rh [70]. Both methane and C_2 hydrocarbons are actively converted over Rh based catalysts, which results in higher H_2 and CO yields. Although total moles of syngas are higher over Rh based catalysts, syngas ratios are lower over these samples compared to Co based catalysts. This is due to lower CO_2 conversions observed over Co based samples, which indicates that RWGS took place at a lower extent and less H_2 is converted CO.

In the light of these findings, it can be concluded that Rh is superior to Co in glycerol dry reforming reaction both in terms of CO_2 conversion and syngas yield.

Table 4.13. Product distributions over tested catalysts (T=750 °C, CO_2/G = 4).

Catalyst	**Product Yields (mol/(mol of glycerol fed))**						
	H_2	**CO**	**CH_4**	**C_2H_4**	**C_2H_6**	**C_2**	**H_2/CO**
RhZr	2.24	3.55	0.28	0.00063	0.0013	0.0020	0.63
CoZr	1.93	2.44	0.44	0.0090	0.0094	0.018	0.79
RhCe	1.77	2.93	0.38	0.0025	0.0046	0.0071	0.60
CoCe	1.61	2.47	0.47	0.022	0.010	0.033	0.65

4.4. Effect of Support

Rh and Co metals are supported on two different supports, namely ZrO_2 and CeO_2 in order to compare the effects of these supports on catalytic activity. Glycerol and CO_2 conversions given by ZrO_2 supported and CeO_2 supported samples are presented in Figures 4.12 and 4.13, respectively. It is observed that both glycerol and CO_2 conversions are higher over Rh supported on ZrO_2, compared to RhCe. As mentioned earlier, glycerol conversions are not affected significantly by the type of active metal, but the type of support has a significant effect on glycerol conversion as X_G decreases from 70.4 to 63.6% over RhZr and RhCe, respectively. Observing Co based samples, Figure 4.13, the same can be said about glycerol conversions. However, changing the support has no effect on CO_2 conversions over these samples. Combined with the fact that effect of temperature on glycerol conversion changed based on the type of support as mentioned in Section 4.1 (Figure 4.1), these findings suggest that activation of glycerol is affected significantly by the type of support, whereas CO_2 conversions depend on the type of active metal.

A glance over the product distributions given in Table 4.13 confirms the superiority of ZrO_2 over CeO_2. It can be seen that, regardless of the active metal, both H_2 and CO yields are higher over samples supported on ZrO_2. This may be attributed to higher glycerol conversion over these samples. Additionally, yields of CH_4 and C_2 hydrocarbons are lower over ZrO_2 supported samples although glycerol conversion is

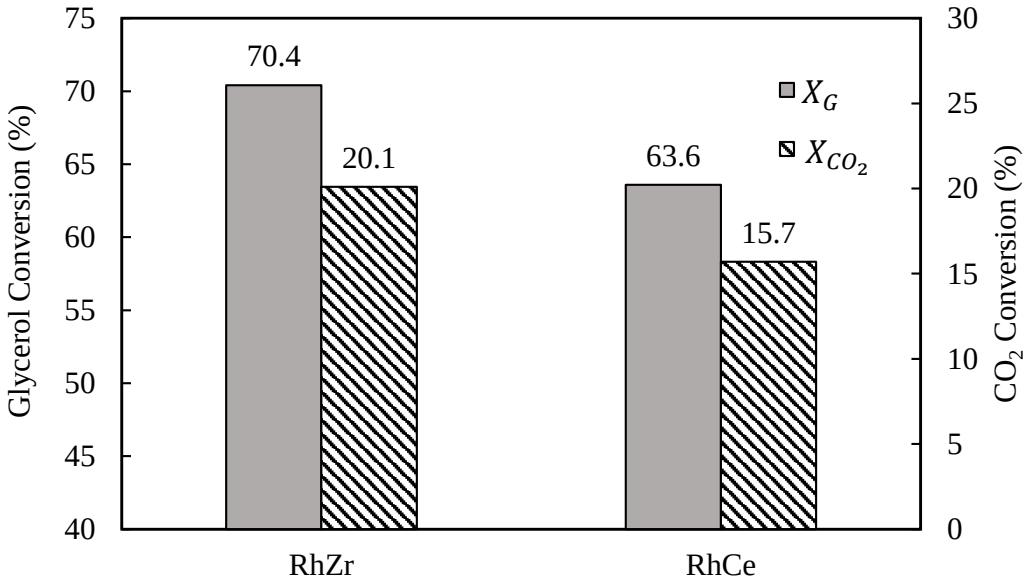

Figure 4.12. Glycerol and CO_2 conversions over Rh catalysts supported on ZrO_2 and CeO_2 (T=750 °C, CO_2/G = 4).

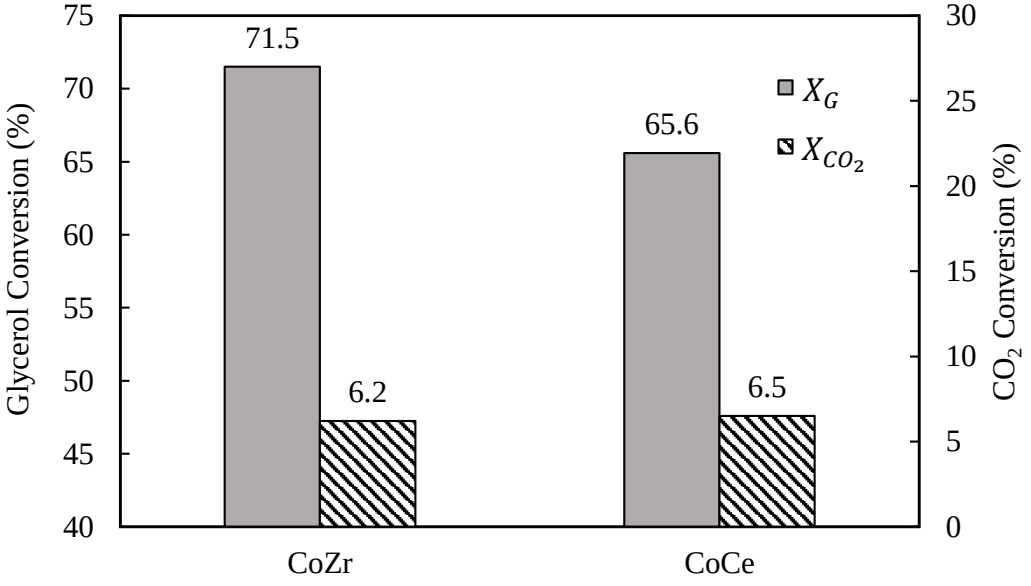

Figure 4.13. Glycerol and CO_2 conversions over Co catalysts supported on ZrO_2 and CeO_2 (T=750 °C, CO_2/G = 4).

higher, which suggests that conversion of these products into H_2 and CO is promoted over these samples.

Both ZrO_2 and CeO_2 are promising supports for dry reforming reactions, due to their good O-transfer properties. The oxygen deficiencies on ZrO_2 helps dissociation of CO_2 into CO and O, which oxidizes the surface carbon [31–33]. Moreover, monoclinic phase of ZrO_2 is thermally stable up to a temperature of 1200 °C [85]. CeO_2 is a support with excellent oxygen storage capacity, which creates an oxygen reservoir that helps gasification of deposited carbon [30, 86]. The difference between the activities of the supports may be attributed to the difference in the level of dispersion of the active phase. It has been reported by Yokota et al. [34] that dispersion of Rh on ZrO_2 was higher compared to Rh/CeO_2. Similarly, it was reported by Wang and Ruckenstein that for the same metal loading, metal surface area of Rh on ZrO_2 was [35] higher compared to Rh on CeO_2, which also resulted in higher conversions and yields obtained over Rh/ZrO_2.

4.5. Stability Tests

Dry reforming reactions typically operate at harsh conditions (like high temperatures to overcome thermodynamic restrictions and high carbon content in the feed). Therefore, catalyst deactivation due to carbon deposition and sintering is a major issue in dry reforming reactions. Coke deposition is the primary challenge in glycerol dry reforming reaction, since glycerol decomposition, dehydration and dehydrogenation as well as CO disproportionation and CH_4 decomposition can all be responsible for coke accumulation on the catalyst. It is shown by thermodynamic calculations that carbon formation decreases at increased temperatures (Figure 4.4). Amount of carbon deposition can also depend on the characteristics of support and active metal. To observe the extent of deactivation on the catalysts in an extended reaction period, 24 h time-on-stream (ToS) tests have been performed over RhZr, RhCe, CoZr and CoCe samples. The tests have been conducted at the harshest conditions (T=750 °C, CO_2/G = 4). Higher CO_2/G ratios may be good for gasification of the deposited carbon, but higher amount of CO_2 in the feed results in more H_2O production due

to RWGS and presence of H_2O is known to promote metal sintering. The change in CO_2 conversions with respect to TOS is presented in Figure 4.14. Conversion of CO_2 drops significantly over the first 5 hours over RhZr where it decreases from 29% to 20%, but then remains constant throughout the reaction period. A similar initial drop is apparent over CoZr, where conversion changes from 9.7% to 6.5% over the first 3.5 hours. No such initial deactivation is observed over the CeO_2 supported samples. It is possible that the active metal is getting partly encapsulated by ZrO_2 in the first few hours. It has been reported that partial encapsulation of the metal is observed over highly reducible supports such as TiO_2, ZrO_2 and La_2O_3, especially when the metal is highly dispersed [87]. Another possibility is metal sintering, which is promoted at high temperatures. Going back to Table 4.7, it can be seen that RhZr suffers from some activity loss at 750 °C with a CO_2/G of 1, whereas no deactivation is observed at 700 °C. The degree of initial deactivation is higher in the stability test, in which the CO_2/G ratio is also higher. The initial deactivation can also be attributed to coke deposition, but this is unlikely considering that there is no significant change in CO_2 conversions after the initial deactivation period over RhZr sample.

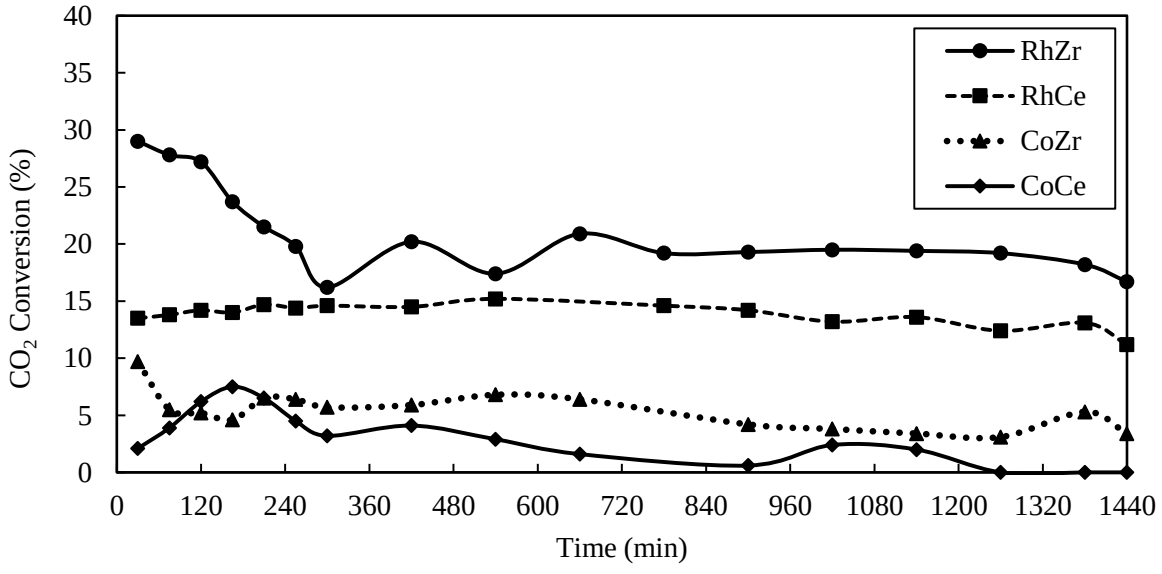

Figure 4.14. CO_2 conversions over tested samples with respect to ToS. (T=750 °C, CO_2/G = 4).

Table 4.14. Resuts of time-on-stream tests over the tested samples (T=750 °C, CO_2/G = 4).

	Time (h)	Product Yields (mol/(mol glycerol fed))				X_{CO_2}	X_G
		H_2	CO	CH_4	C_2		
RhZr	0.5	2.61	3.94	0.11	0.00	29.0	69.7
	7	2.12	3.41	0.34	0.0024	20.2	69.8
	23	2.11	3.37	0.34	0.0024	18.2	69.9
RhCe	0.5	1.79	2.99	0.45	0.011	13.5	67.7
	7	1.90	3.21	0.45	0.0088	14.5	70.4
	23	1.94	3.02	0.45	0.010	13.1	71.7
CoZr	0.5	1.86	2.72	0.42	0.012	9.7	68.1
	7	2.12	2.74	0.47	0.016	5.9	77.4
	23	2.01	2.49	0.46	0.024	5.3	74.5
CoCe	0.5	1.48	2.27	0.43	0.044	2.1	52.6
	7	1.64	2.28	0.46	0.046	4.1	69.2
	23	1.44	2.07	0.46	0.059	0	62.2

It can be seen from the CO_2 conversion trends that Rh based samples show higher stability compared to Co based samples. Approximately 2% drop in CO_2 conversion is observed over CoZr after the initial deactivation period. A more significant deactivation is observed over CoCe sample, where CO_2 conversion drops from 4.2% to 0 in the last 14 hours of the reaction. Similarly, glycerol conversions show a 3% and 7% decrease over CoZr and CoCe, respectively, in the last 16 hours of the reaction, whereas no change is observed over Rh based samples. The deactivation of Co based samples can be attributed to coke formation or sintering of the metal particles. It is known that noble metals are more resistant to carbon deposition than non-noble metals. It has been shown by Hou *et al.* [23] that significant amount of coke was observed on Co/Al_2O_3 catalyst, whereas there was no carbon deposition on Rh/Al_2O_3 DRM at 800 °C. Moreover, Cheng *et al.* [67] reported that acidic/basic site ratio of the catalyst increased upon impregnation of cobalt on Al_2O_2. Acidity can be a cause of carbon formation, since it is known that carbon formation is favored on the acid cites of the catalyst [22]. Another possibility is sintering of the active metal, which is

likely considering that operating temperature is high. Table 4.14 shows the product yields and reactant conversions over the samples at the 0.5^{th}, 7^{th} and 23^{rd} hours of the reaction. It is evident from the table that, both in terms of H_2 and CO yields and reactant conversions, highest deactivation is observed over CoCe sample.

4.6. Catalyst Characterizations

Fresh reduced and spent catalysts are characterized with SEM and XRD analyses in order to have an insight on the physical and chemical characteristics of the samples. Moreover, surface areas of the supports have been determined via BET analysis.

4.6.1. Results of BET Analysis

Results of the BET analysis on prepared supports are given in Table 4.15. It is revealed that both ZrO_2 and CeO_2 have low surface area, which is expected considering the high calcination temperature (800 °C). Our results are similar to the results published by Zhao *et al.* [88], who reported that surface area of ZrO_2 depended significantly on the calcination temperature. According to their results, ZrO_2 calcined at 800 °C had a BET surface area of 15 m^2/g [88]. Moreover, da Silva *et al.* [49] used the same method for preparing CeO_2 that is used in this study and reported the surface area of the support as 14 m^2/g. The results show that ZrO_2 has a higher surface area, though slightly higher, compared to CeO_2, which may result in enhanced dispersion of the active metal on ZrO_2.

Table 4.15. Results of BET analysis on prepared supports.

Support	**Surface Area (m^2/g)**	**Pore Volume (cc/g)**	**Average Pore Size ($\AA$)**
ZrO_2	16.3	2.59×10^{-2}	16.2
CeO_2	10.2	1.76×10^{-2}	15.0

4.6.2. Results of SEM Analysis

SEM images of reduced and spent samples are taken to observe any physical changes that may occur during the course of reaction. The active metal could not be detected in the reduced and spent samples of RhZr, RhCe and CoZr. Moreover, no visible change on the surface of the catalysts is observed between reduced and spent samples, such as coke deposition, as shown in Figure 4.15. Co particles, however, can be observed on both reduced and spent samples when supported on ceria, as can be seen in Figure 4.16. Particle diameters are measured as 47.01 and 47.40 nm in reduced and spent samples, respectively, which suggests that no apparent sintering or agglomeration of the active phase took place during the tests.

4.6.3. Results of XRD Analysis

X-ray diffraction analysis is performed on fresh and reduced samples of CoZr and CoCe and the diffraction peaks of the samples are given in Figures 4.17 and 4.18. Rh based samples are not objected to XRD analysis since the low lading of Rh (1 wt.%) results in very small particle sizes that are invisible to XRD [86, 89, 90].

The zirconia used in this study exhibited peak characteristics of monoclinic structure, whereas ceria exhibited peak characteristics of cerianite structure. The diffraction peaks at 2θ of 44.2°, 51.5° and 75.9° belong to metallic cobalt, and other peaks belong to supports. No additional peaks are observed on the spent samples, which shows that no new phases appeared during the reaction. Moreover, it is observed that cobalt stayed in metallic phase and was not oxidized throughout the reaction, as no peaks that belong to Co_3O_4 is observed on the spent samples.

Crystallite sizes (τ) of the detected cobalt phase is calculated by using Scherrer Equation as given in Equation 4.2, where K is the shape factor (0.9 for spherical crystals), λ is the wavelength of the x-ray (1.54 $\mathring{A}$), β is the full width at half maximum (FWHM) and θ is the angle in radians. Calculated average crystallite sizes for Co from the diffraction peaks of the (1 1 1) plane are presented in Table 4.16. The results suggest

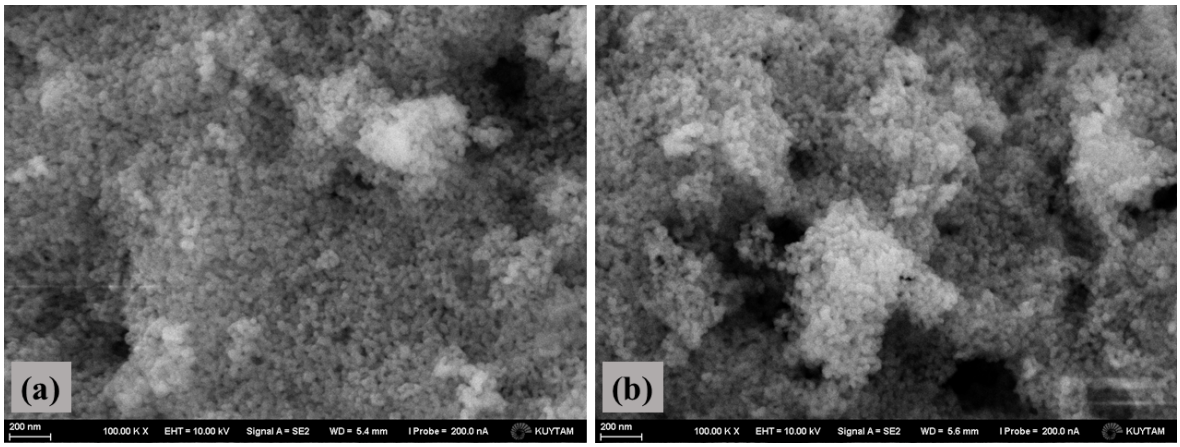

Figure 4.15. SEM images of reduced (a) and spent (b) Rh/ZrO_2 samples.

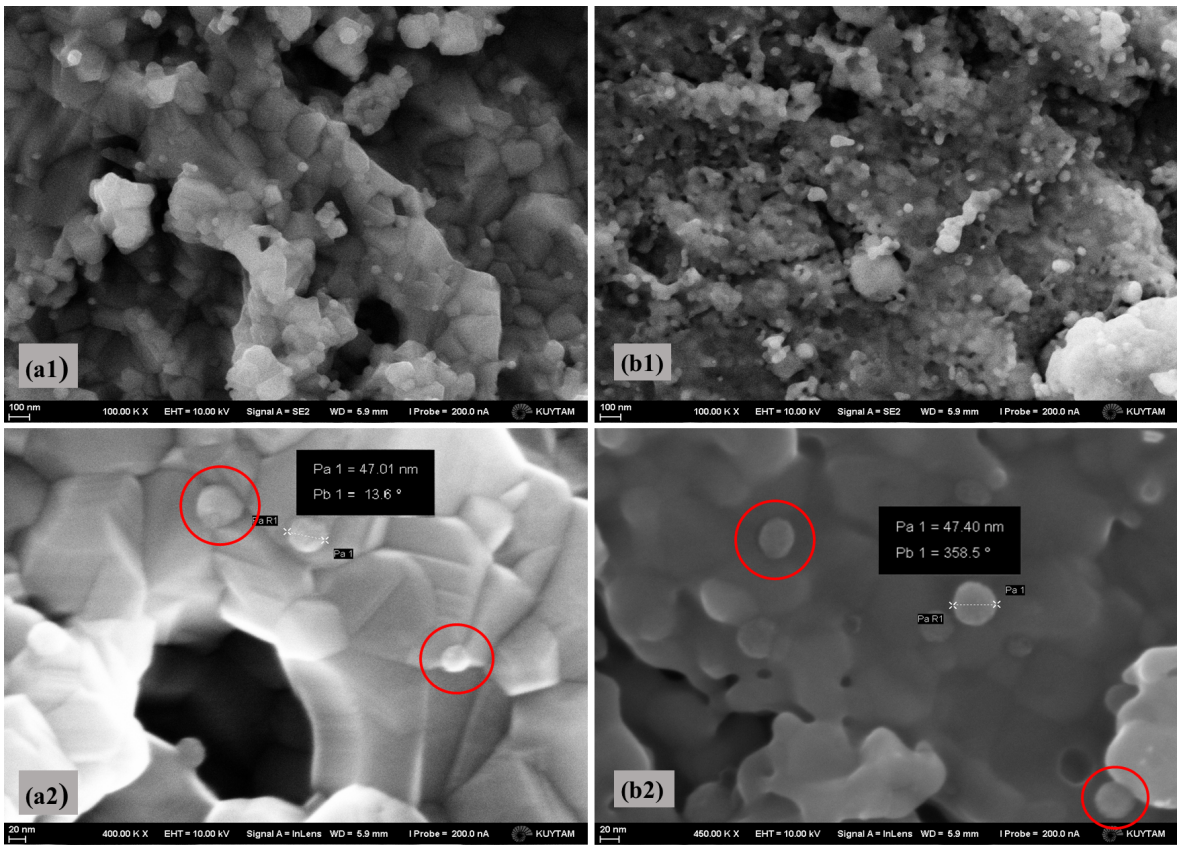

Figure 4.16. SEM images of reduced (a1) and spent (b1) Co/CeO_2 samples ((a2) and (b2) are close-ups of reduced and spent samples, respectively).

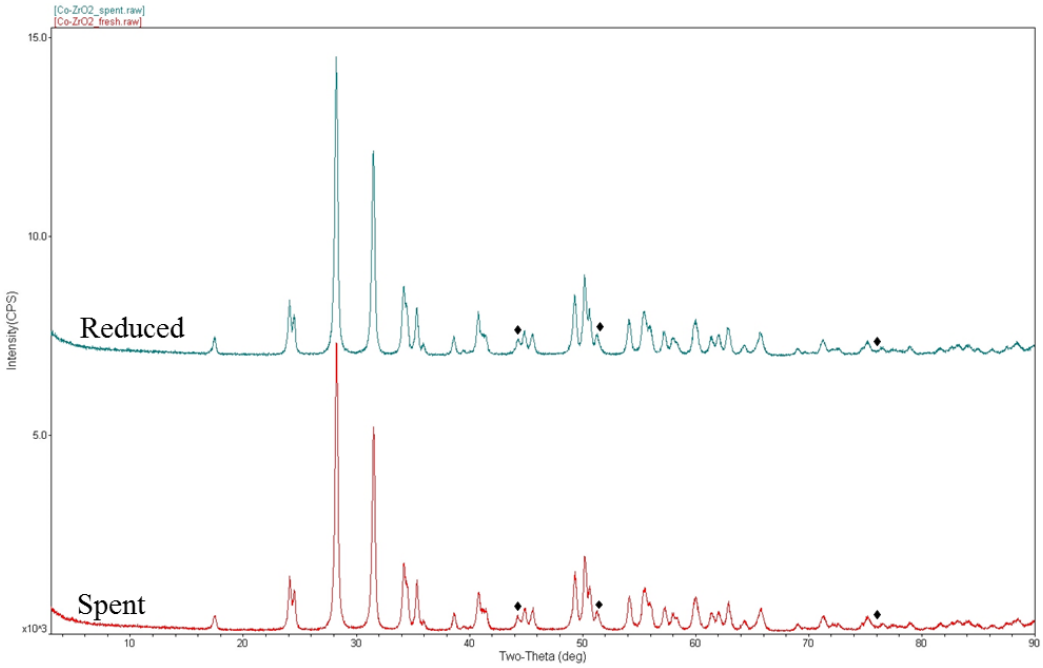

Figure 4.17. X-ray diffraction peaks of reduced and spent Co/ZrO_2 samples (Peaks marked with ♦ are diffraction peaks associated with metallic cobalt).

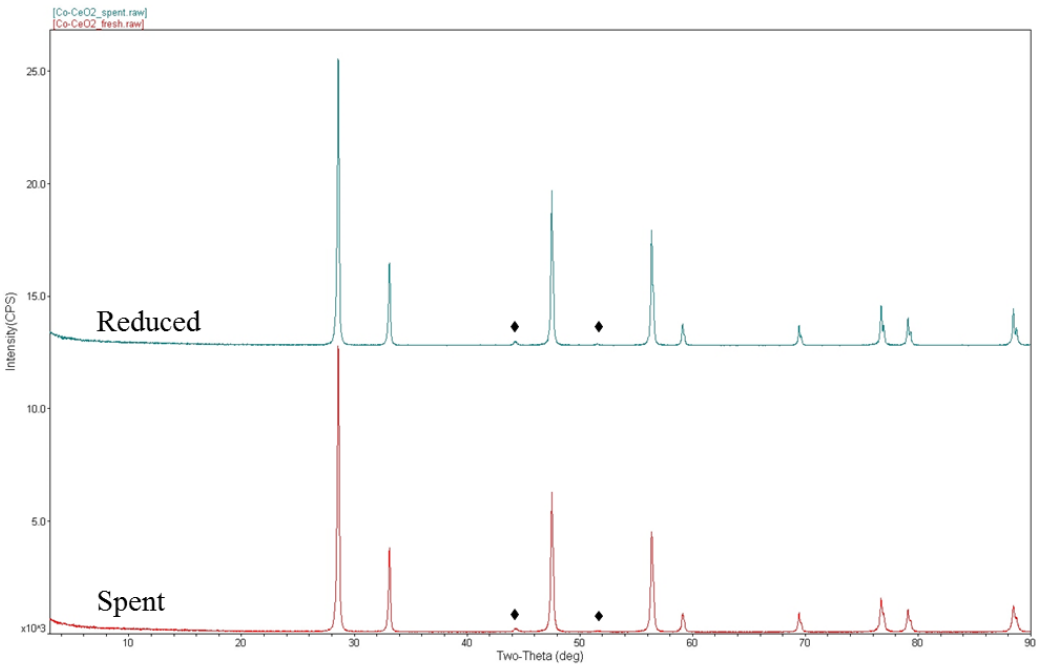

Figure 4.18. X-ray diffraction peaks of reduced and spent Co/CeO_2 samples (Peaks marked with ♦ are diffraction peaks associated with metallic cobalt).

that average crystallite size of cobalt supported on zirconia is lower compared to ceria suported samples. This may indicate some sort of interaction between Co and ZrO_2, leading to smaller crystallite size. Xiong *et al.* [91] studied the effect of metal loading of Co on the dispersion and crystallite size of Co/Al_2O_3 catalysts and reported that increasing Co loading resulted in increased crystallite size. A simultaneous decrease in dispersion was observed in the study with increased metal loading. Their findings suggest that there may be a relationship between metal crystallite size and metal dispersion.

$$\tau = \frac{K\lambda}{\beta cos(\theta)} \times \frac{180^\circ}{\pi} \tag{4.2}$$

Table 4.16. Results of XRD analysis on Co based samples.

Sample	2θ	**Crystallite Size** ($\AA$)
Co/ZrO_2, reduced	44.26°	175
Co/ZrO_2, spent	44.32°	152
Co/CeO_2, reduced	44.26°	217
Co/CeO_2, spent	44.30°	277

5. CONCLUSION

5.1. Conclusions

The objective of this study is to synthesize and test the activity of Rh and Co based catalysts supported on ZrO_2 and CeO_2 in glycerol dry reforming. 1 wt.% Rh/ZrO_2 (RhZr) and, 1 wt.% Rh/CeO_2 (RhCe), 5 wt.% Co/ZrO_2 (CoZr) and 5 wt.% Co/CeO_2 (CoCe) catalysts have been prepared by the incipient-to-wetness impregnation method. An experimental system has been constructed in order to test the synthesized catalysts at varying temperatures and CO_2/G ratios. The effect of operational parameters as well as type of active metals and supports has thus been observed. The main conclusions drawn from the results of the study are listed as follows:

- Rh/ZrO_2 shows the best performance among the prepared catalysts, both in terms of reactant conversions and syngas yield.
- Maximum CO_2 conversion (23.1%) is observed over Rh/ZrO_2 at 750 °C with a CO_2/G ratio of 3. Maximum H_2 yield (2.82 mol of H_2 per mol of glycerol fed) in dry reforming conditions is observed over the same catalyst at 750 °C with a CO_2/G ratio of 1.
- Activities of the tested catalysts based on CO_2 conversion are decreasing in the order of: RhZr > RhCe > CoZr ≈ CoCe. If syngas production is taken as the basis, CoZr is more selective towards syngas than CoCe and the order becomes: RhZr > RhCe > CoZr > CoCe.
- Rh based catalysts show considerably higher CO_2 conversions, while glycerol conversions do not change significantly upon changing the active metal.
- Over the same support, Rh based catalysts are more selective towards H_2 and CO but less selective towards CH_4 and C_2 hydrocarbons compared to Co based catalysts.
- Changing the support does not have a significant effect on CO_2 conversions, but glycerol conversions change based on the type of support. Higher glycerol conversion are observed over ZrO_2 compared to CeO_2. The effect of support on

glycerol conversion is also observed upon examining the temperature trends. A jump in glycerol conversion is observed at 700 °C over ZrO_2 supported samples, whereas a similar jump is observed over CeO_2 supported samples at 750 °C.

- ZrO_2 supported samples are more selective towards H_2 and CO compared to CeO_2 support samples if the same active metal is used.
- Reaction temperature has a significant effect on the extent of reaction. Both glycerol and CO_2 conversions increase with increasing temperature.
- Conversion of glycerol is observed in the blank tests, reaching 48% at a temperature of 750 °C. This shows that homogeneous glycerol decomposition takes place to a significant extent. Detected products of glycerol decomposition are H_2, CO, CH_4, C_2H_4 and C_2H_6.
- No CO_2 conversion is observed over any catalysts at temperatures below 750 °C at a CO_2/G ratio of 1. CO_2 conversion is not observed over Co based samples at any of the temperatures tested at a CO_2/G ratio of 1.
- Syngas yields increase with increasing temperature over all catalysts and in the blank tests.
- CH_4 yields increase with increasing temperature over all catalysts and in the blank tests. However, selectivity towards CH_4 first increases, then decreases with increasing temperature. This shows that methane is converted via MDR or MSR at elevated temperatures.
- Both thermodynamic studies and visuals of the spent catalysts show that coke deposition decreases with an increase in the reaction temperature. Moreover, percent activity loss of the catalysts commonly decrease at higher temperatures.
- Molar H_2/CO ratio of the produced syngas changes between 0.5 and 1. It is observed that syngas ratio increases with increasing temperature and decreases with increased CO_2/G.
- Increasing the CO_2 content in the feed by increasing the CO_2/G ratio results in a decrease in glycerol conversions.
- CO_2 conversion increases with CO_2/G ratios up to 2 over all samples. At higher ratios, CO_2 conversion plateaus and a slight decrease in CO_2 conversion is observed over RhZr catalyst as the CO_2/G is increased to 4.

- As the CO_2/G ratio increases, H_2 yields decrease, whereas CO yields increase. This suggests that RWGS reaction is favored with increased CO_2 content in the feed.
- CH_4 yields decrease as CO_2/G increases over RhZr and RhCe samples. However, no such trend is observed over CoZr and CoCe samples. This suggests that MDR is catalyzed by Rh based catalysts, whereas activity of Co for MDR is low.
- BET analysis revealed that surface area of the prepared supports are 16.3 and 10.2 m^2/g for ZrO_2 and CeO_2, respectively.
- 24 h time-on-stream tests revealed that Rh based samples do not lose their activity after an initial deactivation period. Co based samples are less stable compared to Rh based samples, but no significant deactivation is observed on any of the samples.

5.2. Recommendations

- Effect of CO_2/G ratios can be observed at lower temperatures (such as 700 °C) to see if CO_2 conversion is possible at lower temperatures.
- Metal loadings of the prepared catalysts can be varied to see its effect on catalytic activity.
- Effect of catalyst preparation parameters such as preparation method or calcination temperature can be studied to find the optimum parameters for catalytic activity.
- Nickel is known to be a good reforming catalyst, which is also cost effective. Ni can be used as an active metal and its activity can be compared with the tested catalysts. Among noble metals, ruthenium is a promising active metal for reforming reactions. Ru can also be tested as an active metal.
- Effect of a promoter can be evaluated by addition of small amount of various promoters on the tested catalysts. K, Mn, Ca, Mg, La are commonly added promoters in dry reforming reactions. Besides, Rh can be used as a promoter on the supported Co catalysts and their activity can be compared with monometallic Rh catalysts.

- More characterizations can be done in order to gain more insight about physical and chemical properties of the prepared and tested samples. TEM analysis can be done to measure the metal particle sizes before and after the reaction, which could not be detected with SEM analysis except for Co/CeO_2. Moreover, TGA analysis can be done to quantify the amount of coke deposited on the samples during the reaction.
- Effect of reactor configuration can be observed by conducting tests with packed and coated microchannel reactors.

REFERENCES

1. IEA, *Annual Energy Outlook 2015 with Projections to 2040*, 2015, `https://www.eia.gov/forecasts/aeo/pdf/0383(2015).pdf`, accessed January 2016.

2. Marbán, G. and T. Valdés-Solís, "Towards the hydrogen economy?", *International Journal of Hydrogen Energy*, Vol. 32, No. 12, pp. 1625–1637, 2007.

3. Silva, J. M., M. Soria and L. M. Madeira, "Challenges and strategies for optimization of glycerol steam reforming process", *Renewable and Sustainable Energy Reviews*, Vol. 42, pp. 1187–1213, 2015.

4. Naylor, R. L. and M. M. Higgins, "The political economy of biodiesel in an era of low oil prices", *Renewable and Sustainable Energy Reviews*, Vol. 77, pp. 695–705, 2017.

5. Dou, B., C. Wang, H. Chen, Y. Song and B. Xie, "Continuous sorption-enhanced steam reforming of glycerol to high-purity hydrogen production", *International Journal of Hydrogen Energy*, Vol. 38, No. 27, pp. 11902–11909, 2013.

6. Lin, Y.-C., "Catalytic valorization of glycerol to hydrogen and syngas", *International journal of hydrogen energy*, Vol. 38, pp. 2678–2700, 2013.

7. Freitas, A. C. and R. Guirardello, "Comparison of several glycerol reforming methods for hydrogen and syngas production using Gibbs energy minimization", *International Journal of Hydrogen Energy*, Vol. 39, No. 31, pp. 17969–17984, 2014.

8. Kalinci, Y., A. Hepbasli and I. Dincer, "Biomass-based hydrogen production: a review and analysis", *International journal of hydrogen energy*, Vol. 34, No. 21, pp. 8799–8817, 2009.

9. Wang, X., M. Li, M. Wang, H. Wang, S. Li, S. Wang and X. Ma, "Thermodynamic analysis of glycerol dry reforming for hydrogen and synthesis gas production", *Fuel*, Vol. 88, No. 11, pp. 2148–2153, 2009.

10. Siew, K. W., H. C. Lee, J. Gimbun, S. Y. Chin, M. R. Khan, Y. H. Taufiq-Yap and C. K. Cheng, "Syngas production from glycerol-dry (CO_2) reforming over La-promoted Ni/Al_2O_3 catalyst", *Renewable Energy*, Vol. 74, pp. 441–447, 2015.

11. Siew, K. W., H. C. Lee, J. Gimbun and C. K. Cheng, "Characterization of La-promoted Ni/Al_2O_3 catalysts for hydrogen production from glycerol dry reforming", *Journal of Energy Chemistry*, Vol. 23, No. 1, pp. 15–21, 2014.

12. De Klerk, A., *Fischer-Tropsch Refining*, John Wiley & Sons, 2012.

13. Delparish, A. and A. K. Avci, "Intensified catalytic reactors for Fischer-Tropsch synthesis and for reforming of renewable fuels to hydrogen and synthesis gas", *Fuel Processing Technology*, Vol. 151, pp. 72–100, 2016.

14. Abatzoglou, N. and C. Fauteux-Lefebvre, "Review of catalytic syngas production through steam or dry reforming and partial oxidation of studied liquid compounds", *Wiley Interdisciplinary Reviews: Energy and Environment*, Vol. 5, No. 2, pp. 169–187, 2016.

15. Rostrup-Nielsen, J., J. Sehested and J. K. Nørskov, "Hydrogen and synthesis gas by steam-and CO_2 reforming", *Advances in Catalysis*, Vol. 47, pp. 65–139, 2002.

16. Rostrup-Nielsen, J. and J. B. Hansen, "Steam Reforming for Fuel Cells - Chapter 4", pp. 49–71, 2011.

17. Pen, M., J. Gomez, J. G. Fierro *et al.*, "New catalytic routes for syngas and hydrogen production", *Applied Catalysis A: General*, Vol. 144, No. 1-2, pp. 7–57, 1996.

18. Gao, J., Z. Hou, H. Lou and X. Zheng, "Dry (CO_2) Reforming - Chapter 7", pp. 191–221, 2011.

19. Wang, S., G. Lu and G. J. Millar, "Carbon dioxide reforming of methane to produce synthesis gas over metal-supported catalysts: state of the art", *Energy & Fuels*, Vol. 10, No. 4, pp. 896–904, 1996.

20. Nikoo, M. K. and N. Amin, "Thermodynamic analysis of carbon dioxide reforming of methane in view of solid carbon formation", *Fuel Processing Technology*, Vol. 92, No. 3, pp. 678–691, 2011.

21. Usman, M., W. W. Daud and H. F. Abbas, "Dry reforming of methane: influence of process parameters—a review", *Renewable and Sustainable Energy Reviews*, Vol. 45, pp. 710–744, 2015.

22. Pakhare, D. and J. Spivey, "A review of dry (CO_2) reforming of methane over noble metal catalysts", *Chemical Society Reviews*, Vol. 43, No. 22, pp. 7813–7837, 2014.

23. Hou, Z., P. Chen, H. Fang, X. Zheng and T. Yashima, "Production of synthesis gas via methane reforming with CO_2 on noble metals and small amount of noble-(Rh-) promoted Ni catalysts", *International journal of hydrogen energy*, Vol. 31, No. 5, pp. 555–561, 2006.

24. Tsyganok, A. I., M. Inaba, T. Tsunoda, S. Hamakawa, K. Suzuki and T. Hayakawa, "Dry reforming of methane over supported noble metals: a novel approach to preparing catalysts", *Catalysis Communications*, Vol. 4, No. 9, pp. 493–498, 2003.

25. Ruckenstein, E. and Y. H. Hu, "Role of Support in CO_2 Reforming of CH_4 to Syngas over Ni Catalysts", *Journal of Catalysis*, Vol. 162, No. 2, pp. 230–238, 1996.

26. Ruckenstein, E. and H. Wang, "Carbon dioxide reforming of methane to synthesis

gas over supported cobalt catalysts", *Applied Catalysis A: General*, Vol. 204, No. 2, pp. 257–263, 2000.

27. Hou, Z. and T. Yashima, "Small amounts of Rh-promoted Ni catalysts for methane reforming with CO_2", *Catalysis letters*, Vol. 89, No. 3, pp. 193–197, 2003.

28. Menegazzo, F., M. Signoretto, F. Pinna, P. Canton and N. Pernicone, "Optimization of bimetallic dry reforming catalysts by temperature programmed reaction", *Applied Catalysis A: General*, Vol. 439, pp. 80–87, 2012.

29. Luna, A. E. C. and M. E. Iriarte, "Carbon dioxide reforming of methane over a metal modified Ni-Al_2O_3 catalyst", *Applied Catalysis A: General*, Vol. 343, No. 1, pp. 10–15, 2008.

30. Wang, R., H. Xu, X. Liu, Q. Ge and W. Li, "Role of redox couples of Rh0/Rh+ and Ce4+/Ce3+ in CH_4/CO_2 reforming over Rh-CeO_2/Al_2O_3 catalyst", *Applied Catalysis A: General*, Vol. 305, pp. 204–210, 2006.

31. Van Keulen, A., K. Seshan, J. Hoebink and J. Ross, "TAP investigations of the CO_2 reforming of CH_4 over Pt/ZrO_2", *Journal of Catalysis*, Vol. 166, No. 2, pp. 306–314, 1997.

32. Therdthianwong, S., C. Siangchin and A. Therdthianwong, "Improvement of coke resistance of Ni/Al_2O_3 catalyst in CH_4/CO_2 reforming by ZrO_2 addition", *Fuel Processing Technology*, Vol. 89, No. 2, pp. 160–168, 2008.

33. Bradford, M. C. and M. A. Vannice, "CO_2 reforming of CH_4 over supported Pt catalysts", *Journal of Catalysis*, Vol. 173, No. 1, pp. 157–171, 1998.

34. Yokota, S., K. Okumura and M. Niwa, "Support effect of metal oxide on Rh catalysts in the CH_4-CO_2 reforming reaction", *Catalysis letters*, Vol. 84, No. 1, pp. 131–134, 2002.

35. Wang, H. and E. Ruckenstein, "Carbon dioxide reforming of methane to synthesis gas over supported rhodium catalysts: the effect of support", *Applied Catalysis A: General*, Vol. 204, No. 1, pp. 143–152, 2000.

36. Sharma, Y. C., A. Kumar, R. Prasad and S. N. Upadhyay, "Ethanol steam reforming for hydrogen production: Latest and effective catalyst modification strategies to minimize carbonaceous deactivation", *Renewable and Sustainable Energy Reviews*, Vol. 74, pp. 89–103, 2017.

37. AFDC, *Ethanol Feedstocks*, 2017, `https://www.afdc.energy.gov/fuels/ethanol_feedstocks.html`, accessed May 2017.

38. Haryanto, A., S. Fernando, N. Murali and S. Adhikari, "Current status of hydrogen production techniques by steam reforming of ethanol: a review", *Energy & Fuels*, Vol. 19, No. 5, pp. 2098–2106, 2005.

39. Wang, W. and Y. Wang, "Dry reforming of ethanol for hydrogen production: thermodynamic investigation", *International Journal of Hydrogen Energy*, Vol. 34, No. 13, pp. 5382–5389, 2009.

40. Frusteri, F., S. Freni, L. Spadaro, V. Chiodo, G. Bonura, S. Donato and S. Cavallaro, "H_2 production for MC fuel cell by steam reforming of ethanol over MgO supported Pd, Rh, Ni and Co catalysts", *Catalysis Communications*, Vol. 5, No. 10, pp. 611–615, 2004.

41. Tsiakaras, P. and A. Demin, "Thermodynamic analysis of a solid oxide fuel cell system fuelled by ethanol", *Journal of Power Sources*, Vol. 102, No. 1, pp. 210–217, 2001.

42. Ortiz, A. L., R. P. Sámano, M. M. Zaragoza and V. Collins-Martínez, "Thermodynamic analysis and process simulation for the H_2 production by dry reforming of ethanol with $CaCO_3$", *International Journal of Hydrogen Energy*, Vol. 40, No. 48, pp. 17172–17179, 2015.

43. Kale, G. R. and B. D. Kulkarni, "Thermoneutral conditions in dry reforming of ethanol", *Asia-Pacific Journal of Chemical Engineering*, Vol. 9, No. 2, pp. 196–204, 2014.

44. Kale, G. R. and B. D. Kulkarni, "Thermoneutral point analysis of ethanol dry autothermal reforming", *Chemical Engineering Journal*, Vol. 165, No. 3, pp. 864–873, 2010.

45. Hu, X. and G. Lu, "Syngas production by CO_2 reforming of ethanol over Ni/Al_2O_3 catalyst", *Catalysis Communications*, Vol. 10, No. 13, pp. 1633–1637, 2009.

46. Zawadzki, A., J. Bellido, A. Lucredio and E. Assaf, "Dry reforming of ethanol over supported Ni catalysts prepared by impregnation with methanolic solution", *Fuel Processing Technology*, Vol. 128, pp. 432–440, 2014.

47. Bahari, M. B., B. C. Goo, T. L. Pham, T. J. Siang, H. T. Danh, N. Ainirazali and D.-V. N. Vo, "Hydrogen-rich Syngas Production from Ethanol Dry Reforming on La-doped Ni/Al_2O_3 Catalysts: Effect of Promoter Loading", *Procedia Engineering*, Vol. 148, pp. 654–661, 2016.

48. Bellido, J. D., E. Y. Tanabe and E. M. Assaf, "Carbon dioxide reforming of ethanol over Ni/Y_2O_3–ZrO_2 catalysts", *Applied Catalysis B: Environmental*, Vol. 90, No. 3, pp. 485–488, 2009.

49. Da Silva, A. M., K. R. De Souza, G. Jacobs, U. M. Graham, B. H. Davis, L. V. Mattos and F. B. Noronha, "Steam and CO_2 reforming of ethanol over Rh/CeO_2 catalyst", *Applied Catalysis B: Environmental*, Vol. 102, No. 1, pp. 94–109, 2011.

50. Tengfei, H., L. Yusheng, S. ZHANG, J. ZHANG and C. Weijie, "Ethanol dry reforming for syngas production over Ir/CeO_2 catalyst", *Journal of Rare Earths*, Vol. 33, No. 1, pp. 42–45, 2015.

51. Drif, A., N. Bion, R. Brahmi, S. Ojala, L. Pirault-Roy, E. Turpeinen, P. K. Seelam,

R. L. Keiski and F. Epron, "Study of the dry reforming of methane and ethanol using Rh catalysts supported on doped alumina", *Applied Catalysis A: General*, Vol. 504, pp. 576–584, 2015.

52. Oliveira-Vigier, D., N. Abatzoglou, F. Gitzhofer *et al.*, "Dry-Reforming of Ethanol in the Presence of a 316 Stainless Steel Catalyst", *The Canadian Journal of Chemical Engineering*, Vol. 83, No. 6, pp. 978–984, 2005.

53. Abatzoglou, N., J. Blanchard, H. Oudghiri-Hassani, S. Jankhah and F. Gitzhofer, "The use of catalytic reforming reactions for CO_2 sequestration as carbon nanotubes", *Proceedings of the 2006 IASME/WSEAS International Conference on Energy & Environmental Systems, Chalkida, Greece*, pp. 21–26, Citeseer, 2006.

54. Mortensen, P. M. and I. Dybkjær, "Industrial scale experience on steam reforming of CO_2-rich gas", *Applied Catalysis A: General*, Vol. 495, pp. 141–151, 2015.

55. Wang, W., "Thermodynamic analysis of glycerol partial oxidation for hydrogen production", *Fuel processing technology*, Vol. 91, No. 11, pp. 1401–1408, 2010.

56. Valliyappan, T., N. Bakhshi and A. Dalai, "Pyrolysis of glycerol for the production of hydrogen or syn gas", *Bioresource Technology*, Vol. 99, No. 10, pp. 4476–4483, 2008.

57. Kale, G. R. and B. D. Kulkarni, "Thermodynamic analysis of dry autothermal reforming of glycerol", *Fuel Processing Technology*, Vol. 91, No. 5, pp. 520–530, 2010.

58. Siew, K. W., H. C. Lee, M. R. Khan, J. Gimbun and C. K. Cheng, "CO_2 reforming of glycerol over La-Ni/Al_2O_3 catalyst: A longevity evaluative study", *Journal of Energy Chemistry*, Vol. 24, No. 3, pp. 366–373, 2015.

59. Lee, H. C., K. W. Siew, J. Gimbun and C. K. Cheng, "Synthesis and characterisation of cement clinker-supported nickel catalyst for glycerol dry reforming",

Chemical Engineering Journal, Vol. 255, pp. 245–256, 2014.

60. Lee, H. C., K. W. Siew, M. R. Khan, S. Y. Chin, J. Gimbun and C. K. Cheng, "Catalytic performance of cement clinker supported nickel catalyst in glycerol dry reforming", *Journal of Energy Chemistry*, Vol. 23, No. 5, pp. 645–656, 2014.

61. Arif, N. N. M., D.-V. N. Vo, M. T. Azizan and S. Z. Abidin, "Carbon Dioxide Dry Reforming of Glycerol for Hydrogen Production using Ni/ZrO_2 and Ni/CaO as Catalysts", *Bulletin of Chemical Reaction Engineering & Catalysis*, Vol. 11, No. 2, pp. 200–209, 2016.

62. Harun, N., J. Gimbun, M. T. Azizan and S. Z. Abidin, "Characterization of Ag-promoted Ni/SiO_2 Catalysts for Syngas Production via Carbon Dioxide (CO_2) Dry Reforming of Glycerol", *Bulletin of Chemical Reaction Engineering & Catalysis*, Vol. 11, No. 2, pp. 220–229, 2016.

63. Kumar, M. A., C. Venumadhav, T. Sagar, M. Surendar, N. Lingaiah, G. N. Rao and P. Prasad, "Catalytic tri-reforming of glycerol for hydrogen generation", *Indian Journal of Chemistry*, Vol. 53A, pp. 530–534, 2014.

64. Adhikari, S., S. D. Fernando, S. F. To, R. M. Bricka, P. H. Steele and A. Haryanto, "Conversion of glycerol to hydrogen via a steam reforming process over nickel catalysts", *Energy & Fuels*, Vol. 22, No. 2, pp. 1220–1226, 2008.

65. Nichele, V., M. Signoretto, F. Menegazzo, A. Gallo, V. Dal Santo, G. Cruciani and G. Cerrato, "Glycerol steam reforming for hydrogen production: Design of Ni supported catalysts", *Applied Catalysis B: Environmental*, Vol. 111, pp. 225–232, 2012.

66. Rossetti, I., A. Gallo, V. Dal Santo, C. L. Bianchi, V. Nichele, M. Signoretto, E. Finocchio, G. Ramis and A. Di Michele, "Nickel catalysts supported over TiO_2, SiO_2 and ZrO_2 for the steam reforming of glycerol", *ChemCatChem*, Vol. 5, No. 1, pp. 294–306, 2013.

67. Cheng, C. K., S. Y. Foo and A. A. Adesina, "H_2-rich synthesis gas production over Co/Al_2O_2 catalyst via glycerol steam reforming", *Catalysis Communications*, Vol. 12, No. 4, pp. 292–298, 2010.

68. Zhang, B., X. Tang, Y. Li, Y. Xu and W. Shen, "Hydrogen production from steam reforming of ethanol and glycerol over ceria-supported metal catalysts", *International Journal of Hydrogen Energy*, Vol. 32, No. 13, pp. 2367–2373, 2007.

69. Hirai, T., N.-o. Ikenaga, T. Miyake and T. Suzuki, "Production of hydrogen by steam reforming of glycerin on ruthenium catalyst", *Energy & Fuels*, Vol. 19, No. 4, pp. 1761–1762, 2005.

70. Chiodo, V., S. Freni, A. Galvagno, N. Mondello and F. Frusteri, "Catalytic features of Rh and Ni supported catalysts in the steam reforming of glycerol to produce hydrogen", *Applied Catalysis A: General*, Vol. 381, No. 1, pp. 1–7, 2010.

71. Karakaya, M., *Experimental and Quantitative Analysis of Multiphase Catalytic Reactions under Microfluidic Flow Conditions and Geometries*, Ph.D. Thesis, Bogazici University, 2014.

72. Koc, S., *Microchannel Enabled Reforming of Glycerol to Hydrogen Over Ni-Based Catalysts*, M.Sc. Thesis, Bogazici University, 2015.

73. Zheng, X., X. Zhang, X. Wang, S. Wang and S. Wu, "Preparation and characterization of CuO/CeO_2 catalysts and their applications in low-temperature CO oxidation", *Applied Catalysis A: General*, Vol. 295, No. 2, pp. 142–149, 2005.

74. Moulijn, J. A., A. Van Diepen and F. Kapteijn, "Catalyst deactivation: is it predictable?: What to do?", *Applied Catalysis A: General*, Vol. 212, No. 1, pp. 3–16, 2001.

75. Chung, W.-C. and M.-B. Chang, "Review of catalysis and plasma performance on dry reforming of CH_4 and possible synergistic effects", *Renewable and Sustainable*

Energy Reviews, Vol. 62, pp. 13–31, 2016.

76. Simsek, E., M. Karakaya, A. K. Avci and Z. I. Onsan, "Oxidative steam reforming of methane to synthesis gas in microchannel reactors", *International journal of hydrogen energy*, Vol. 38, No. 2, pp. 870–878, 2013.

77. Paksoy, A. I., B. S. Caglayan and A. E. Aksoylu, "A study on characterization and methane dry reforming performance of Co–Ce/ZrO_2 catalyst", *Applied Catalysis B: Environmental*, Vol. 168, pp. 164–174, 2015.

78. Bej, B., S. Bepari, N. C. Pradhan and S. Neogi, "Production of hydrogen by dry reforming of ethanol over alumina supported nano-NiO/SiO_2 catalyst", *Catalysis Today*, 2016.

79. Siew, K. W., H. C. Lee, J. Gimbun and C. K. Cheng, "Production of CO-rich hydrogen gas from glycerol dry reforming over La-promoted Ni/Al_2O_3 catalyst", *international journal of hydrogen energy*, Vol. 39, No. 13, pp. 6927–6936, 2014.

80. Ferreira-Aparicio, P., A. Guerrero-Ruiz and I. Rodrıguez-Ramos, "Comparative study at low and medium reaction temperatures of syngas production by methane reforming with carbon dioxide over silica and alumina supported catalysts", *Applied Catalysis A: General*, Vol. 170, No. 1, pp. 177–187, 1998.

81. Bitter, J., K. Seshan and J. Lercher, "On the contribution of X-ray absorption spectroscopy to explore structure and activity relations of Pt/ZrO_2 catalysts for CO_2/CH_4 reforming", *Topics in Catalysis*, Vol. 10, No. 3, pp. 295–305, 2000.

82. Guo, J., H. Lou, L. Mo and X. Zheng, "The reactivity of surface active carbonaceous species with CO_2 and its role on hydrocarbon conversion reactions", *Journal of Molecular Catalysis A: Chemical*, Vol. 316, No. 1, pp. 1–7, 2010.

83. Puolakka, K., S. Juutilainen and A. Krause, "Combined CO_2 reforming and partial oxidation of n-heptane on noble metal zirconia catalysts", *Catalysis today*, Vol. 115,

No. 1, pp. 217–221, 2006.

84. Liao, M.-S. and Q.-E. Zhang, "Dissociation of methane on different transition metals", *Journal of Molecular Catalysis A: Chemical*, Vol. 136, No. 2, pp. 185–194, 1998.

85. Bellido, J. D. and E. M. Assaf, "Effect of the Y_2O_3–ZrO_2 support composition on nickel catalyst evaluated in dry reforming of methane", *Applied Catalysis A: General*, Vol. 352, No. 1, pp. 179–187, 2009.

86. Djinović, P., J. Batista and A. Pintar, "Efficient catalytic abatement of greenhouse gases: methane reforming with CO_2 using a novel and thermally stable Rh–CeO_2 catalyst", *international journal of hydrogen energy*, Vol. 37, No. 3, pp. 2699–2707, 2012.

87. Pant, B. and S. M. Stagg-Williams, "Investigation of the stability of Pt/$LaCoO_3$ during high temperature reforming reactions", *Catalysis Communications*, Vol. 5, No. 6, pp. 305–309, 2004.

88. Zhao, H., J. Chen and Y. Sun, "Effect of calcination temperature on the performance of Co/ZrO_2 catalysts for Fischer-Tropsch synthesis", *Prepr. Pap.-Am. Chem. Soc., Div. Fuel Chem*, Vol. 48, No. 2, p. 733, 2003.

89. Eriksson, S., S. Rojas, M. Boutonnet and J. Fierro, "Effect of Ce-doping on Rh/ZrO_2 catalysts for partial oxidation of methane", *Applied Catalysis A: General*, Vol. 326, No. 1, pp. 8–16, 2007.

90. Campa, M., G. Ferraris, D. Gazzoli, I. Pettiti and D. Pietrogiacomi, "Rhodium supported on tetragonal or monoclinic ZrO_2 as catalyst for the partial oxidation of methane", *Applied Catalysis B: Environmental*, Vol. 142, pp. 423–431, 2013.

91. Xiong, H.-f., Y.-h. Zhang, J.-l. Li and Y.-y. Gu, "Effect of cobalt loading on reducibility, dispersion and crystallite size of Co/Al_2O_3 fischer-tropsch catalyst",

Journal of Central South University of Technology, Vol. 11, No. 4, pp. 414–418, 2004.

APPENDIX A: CALIBRATION CURVES OF MFCs

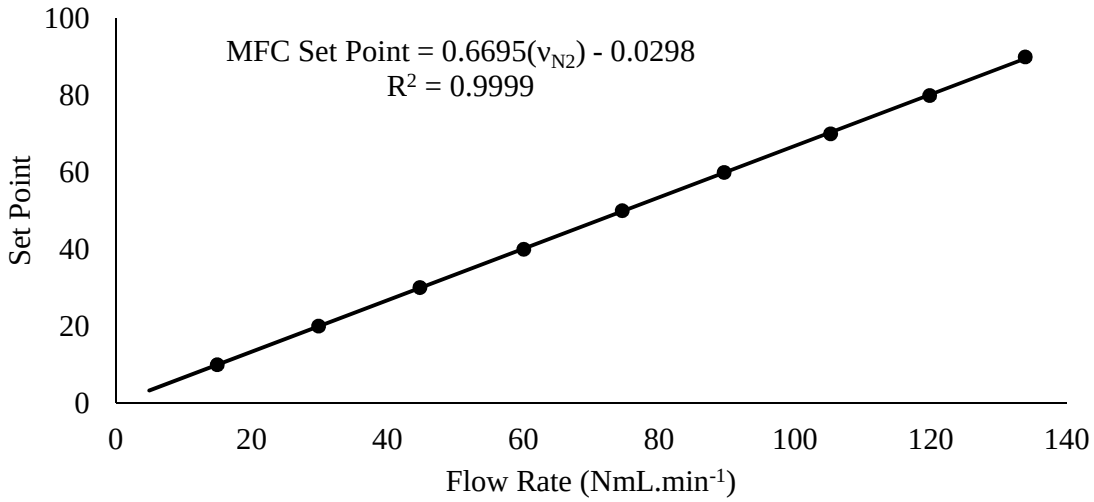

Figure A.1. MFC calibration curve for N_2.

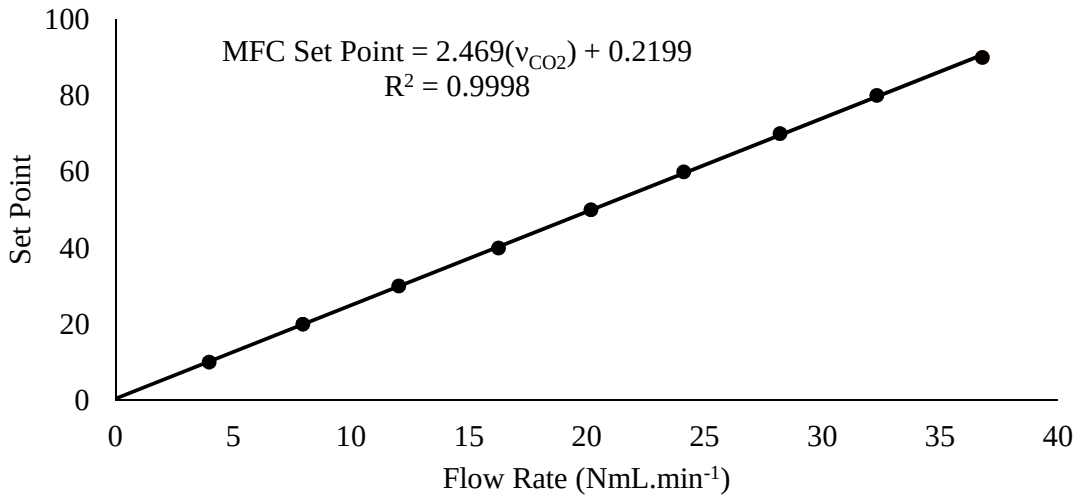

Figure A.2. MFC calibration curve for CO_2.

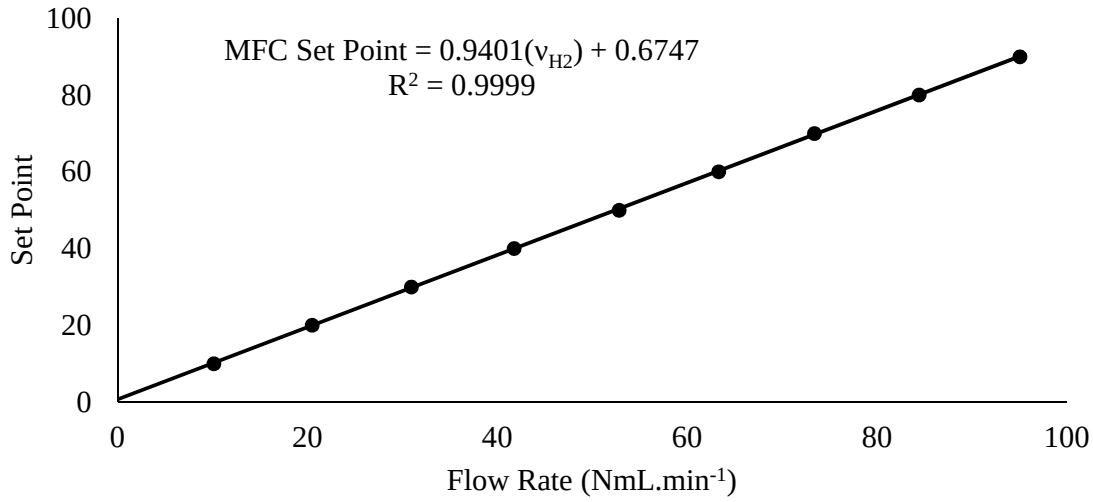

Figure A.3. MFC calibration curve for H_2.

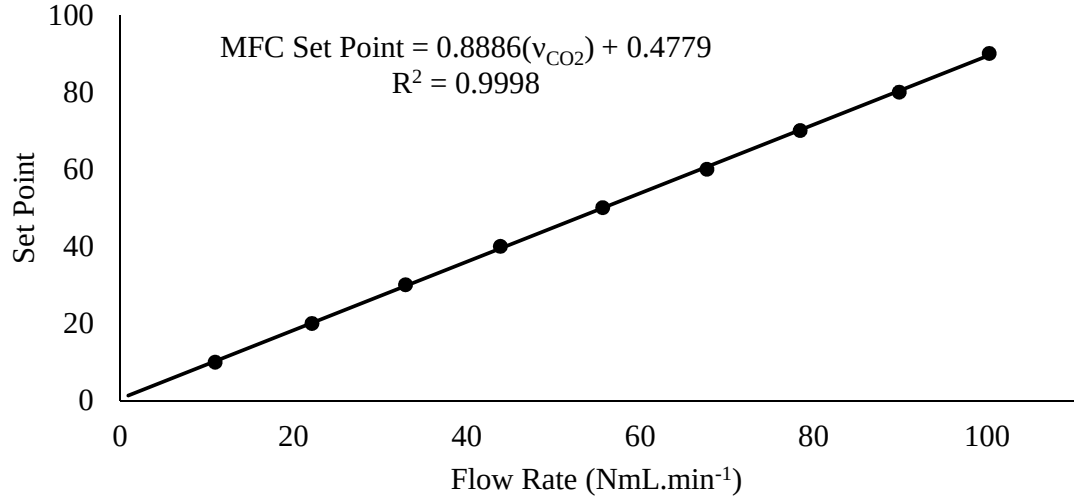

Figure A.4. MFC calibration curve for O_2.

APPENDIX B: CALIBRATION CURVES OF GCs

B.1. Calibration Curves for Shimadzu GC - 2014

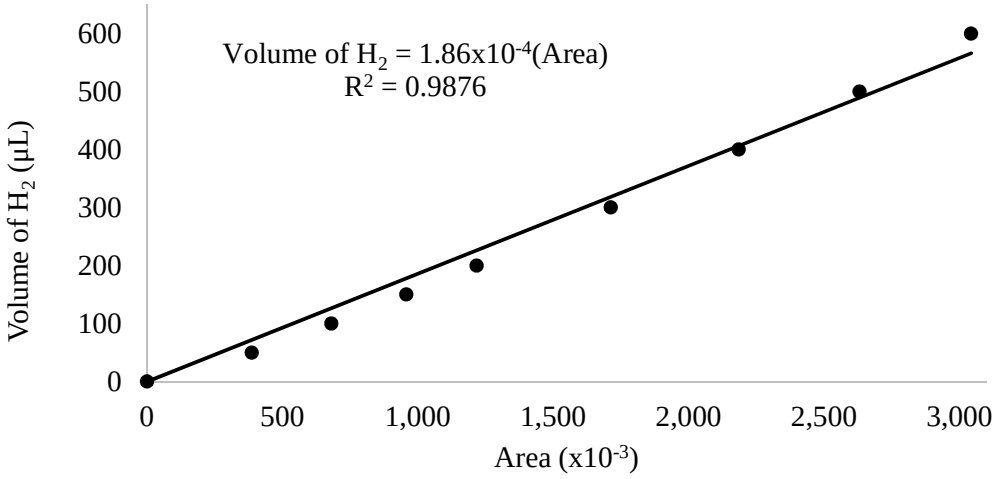

Figure B.1. GC calibration curve for hydrogen.

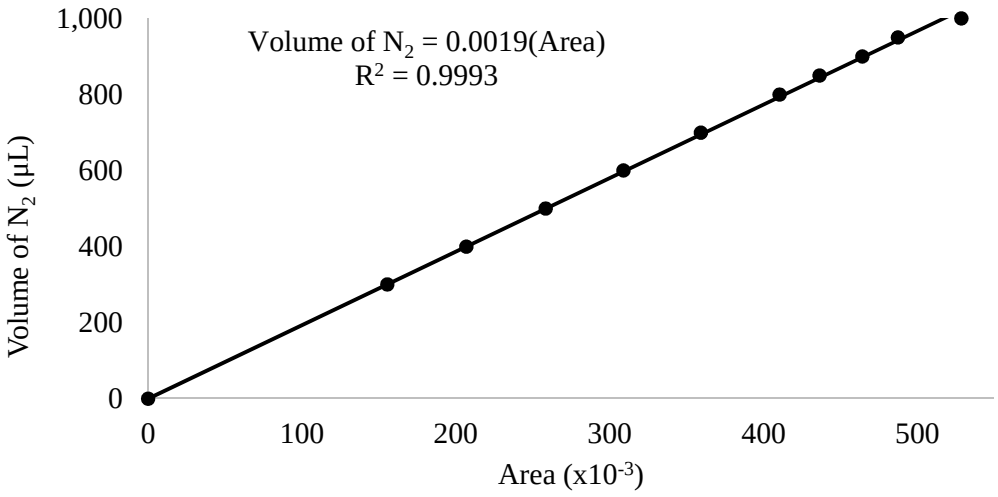

Figure B.2. GC calibration curve for nitrogen.

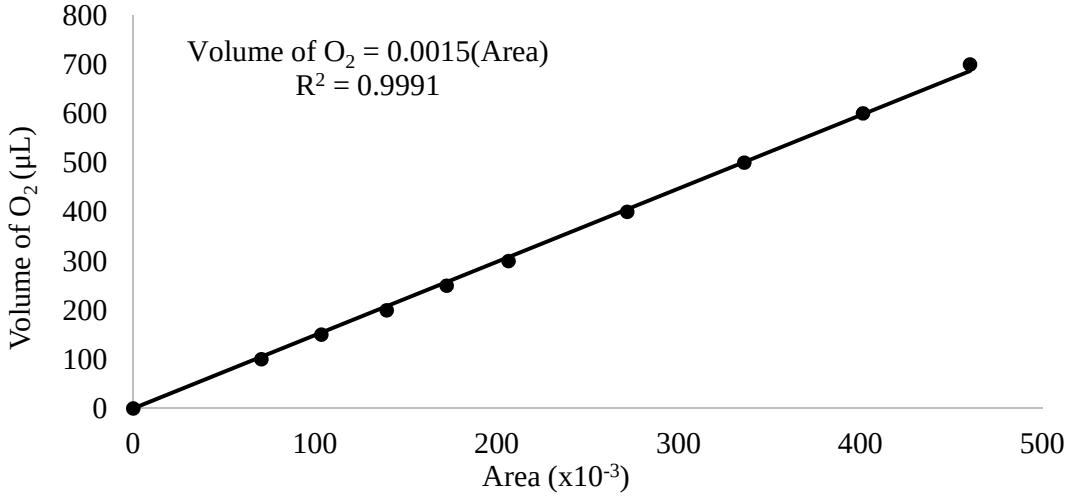

Figure B.3. GC calibration curve for oxygen.

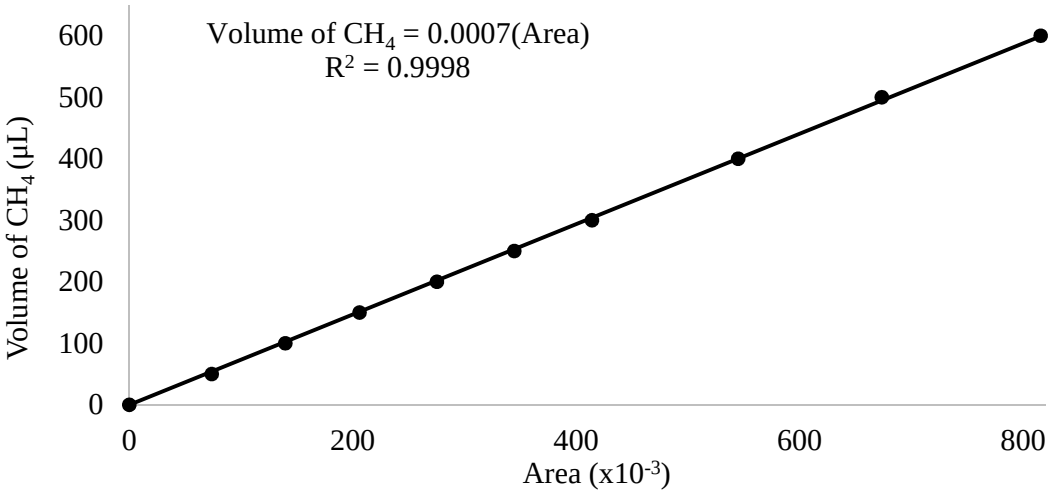

Figure B.4. GC calibration curve for methane.

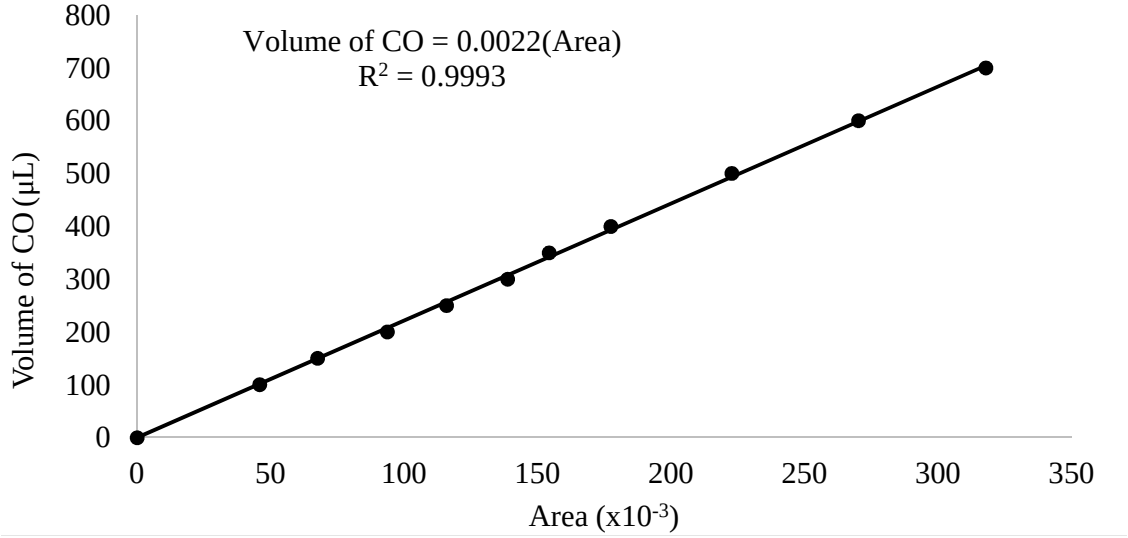

Figure B.5. GC calibration curve for carbon monoxide.

B.2. Calibration Curves for Agilent GC - 6850

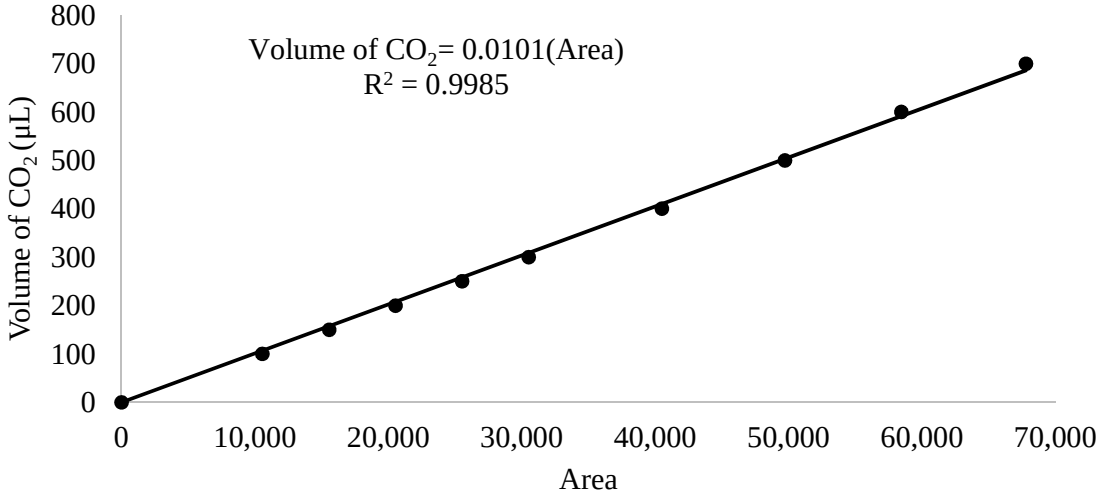

Figure B.6. GC calibration curve for carbon dioxide.

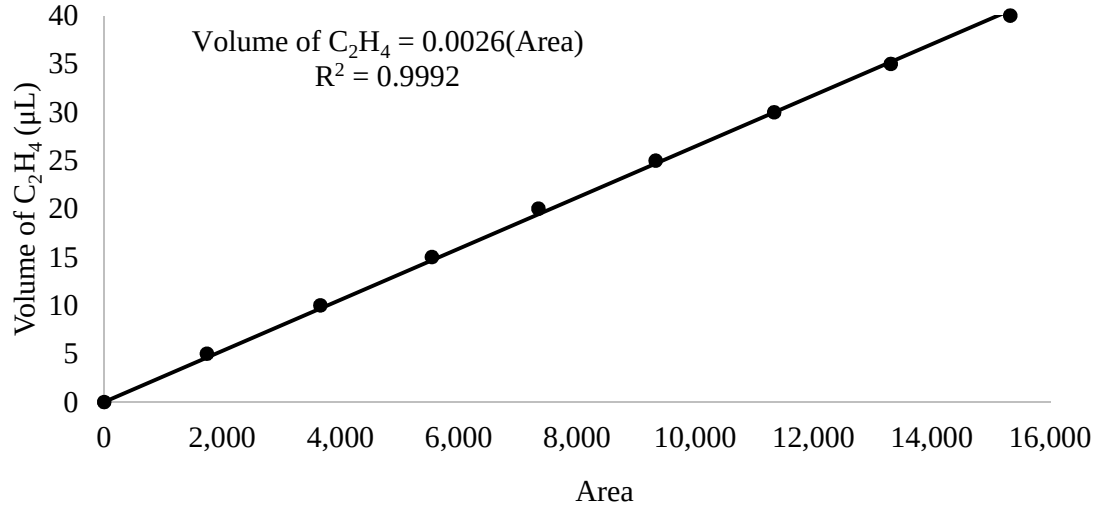

Figure B.7. GC calibration curve for ethylene.

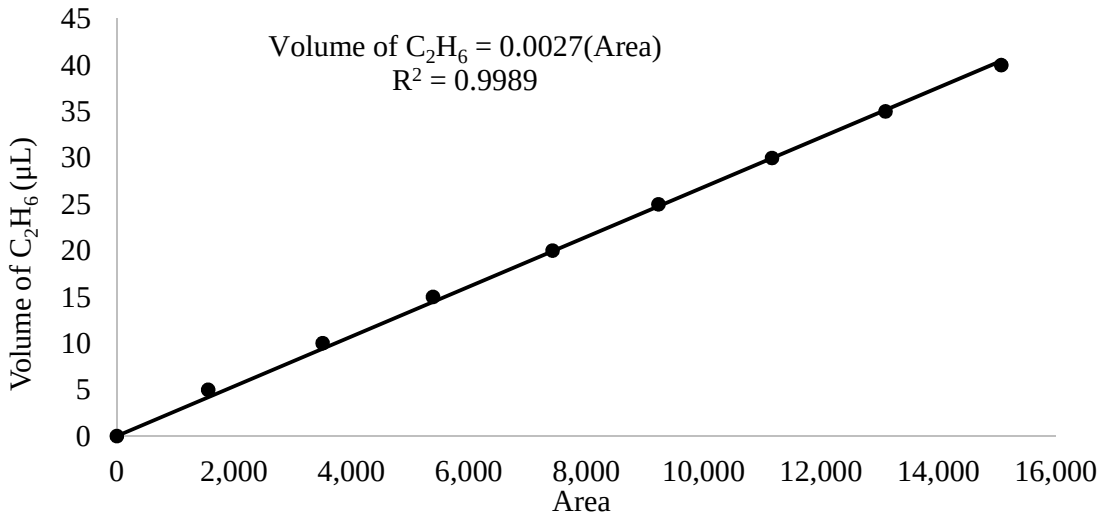

Figure B.8. GC calibration curve for ethane.